



**Bio-synthesised LytC protein kills bacteria and the  
study of protein dynamics in *B. subtilis***

INAUGURAL DISSERTATION

zur Erlangung der Doktorwürde der

Fachbereich Chemie

an der Philipps-Universität Marburg

vorgelegt von Mingle Cao (M. Sc.)

geboren in Henan, VR China

Marburg 2015

**(UMR= 1180)**

**Mingle Cao**

Geschwister-Scholl-Straße 7  
35309 Marburg

Datum: 04.11.2015

**An den Vorsitzenden  
des Promotionsausschusses des Fachbereichs Chemie**  
(die amtierende Dekanin/der amtierender Dekan)

Unter Überreichung meiner Dissertation: "Bio-synthesised LytC protein kills bacteria and the study of protein dynamics in *B. subtilis*" bitte ich um Zulassung zum Promotionsverfahren.

Betreuer meiner Arbeit war Prof. Dr. Peter Graumann.

Als Mitglieder der Prüfungskommission schlage ich vor (drei bis fünf Personen die drei unterschiedlichen Fachgebieten angehören müssen - §4 Promotionsordnung 28.04.2010):

Dekan: **Prof. Dr. Gerhard Hilt**

Erstgutachter und Betreuer der Arbeit: **Prof. Dr. Peter Graumann**

Zweitgutachter: **Dr. Gert Bange**

weitere Mitglieder Prüfungskommission:

**Prof. Dr. Norbert Hampp**

**Prof. Dr. Martin Thanbichler**

Einreichungstermin:

Prüfungstermin:

---

Unterschrift

## **Erklärung:**

Ich erkläre, dass eine Promotion noch an keiner anderen Hochschule als der Philipps-Universität Marburg, Fachbereich Chemie, versucht wurde.

Ich versichere, dass ich meine vorgelegte Dissertation

“Bio-synthesised LytC protein kills bacteria and the study of protein dynamics in *B. subtilis*”

selbst und ohne fremde Hilfe verfasst, nicht andere als die in ihr angegebenen Quellen oder Hilfsmittel benutzt, alle vollständig oder sinngemäß übernommenen Zitate als solche gekennzeichnet sowie die Dissertation in der vorliegenden oder einer ähnlichen Form noch bei keiner anderen in- oder ausländischen Hochschule anlässlich eines Promotionsgesuchs oder zu anderen Prüfungszwecken eingereicht habe.

---

Ort, Datum

---

Unterschrift (Vor- und Zuname)

# **Bio-synthesised LytC protein kills bacteria and the study of protein dynamics in *B. subtilis***

## **Zusammenfassung**

Eine Vielzahl von Antibiotika greifen in die Zellwandsynthese ein. Gegen fast alle gängigen Antibiotika existieren Resistenzen, die von einem Bakterium in das andere weitergegeben werden können. Daher wollten wir eine alternative Strategie verfolgen und Zellwand-degradierende Enzyme einsetzen, um Bakterien durch externe Zugabe zu lysieren. LytC ist in sogenanntes Autolysin von *Bacillus subtilis*, das in der Lage ist, Brüche in die Zellwand einzuführen, und ist ein Kandidat für unsere Strategie. Ich habe das *lytC* Gen kloniert und das Protein in *E. coli* Zellen überproduziert, und anschließend aufgereinigt. Um die Funktion der verschiedenen LytC Domänen zu untersuchen, haben wir unterschiedliche Konstrukte von LytC hergestellt. LytC besitzt eine "low complexity region" (LCR), vier Zellwand-Bindedomänen (CWB) und eine funktionale Hydrolase Domäne. Ich habe das Gram negative Bakterium *E. coli* und den Gram positiven Organismus *B. subtilis* verwendet, um zu untersuchen, ob extern zugegebenes LytC zur Zelllyse führen kann. Die Ergebnisse zeigten dass LytC effizient das Wachstum beider Organismen hemmen kann, wobei dieser Effekt nur in der exponentiellen Wachstumsphase zu beobachten war. Eine C-terminale Fusion von LytC mit einem Streptavidin-tag konnte effizient überproduziert und gereinigt werden, ein N-terminaler nicht. Die Überexpression von LytC führte zu einem schnellen Absinken der optischen Dichte, eine Stunde nach Induktion der Transkription. Das LytCF6 Konstrukt bestand nur aus der Hydrolase Domäne und konnte Zelllyse herbeiführen, was zeigt, dass die CWB und die LCR Domänen nicht essentiell für die Aktivität sind. Kontrollversuche mit BSA oder Elutionspuffer belegten, dass die Aktivität spezifisch für LytC ist. Eine Deletion von 22 Aminosäuren von C-Terminus der funktionalen Domäne führten zu einer starken Reduktion der lytischen Aktivität, was zusätzlich belegt, dass die wachstumshemmende Aktivität von LytCF2 stammt.

Im zweiten Teil der Arbeit wurden die Lokalisation und die Einzelmolekülbewegungen von Proteinen MreB, MreC, MreD, Pbp1A und RodZ, die



an der Zellmorphologie in vielen Bakterien beteiligt sind, und den Untereinheiten der Pyruvat-Dehydrogenase (PDH) und der Phosphofruktokinase (PfkA) als zytosolische Proteine untersucht. Die Morphologie-Proteine sind entweder Membran-integral, oder Membran-assoziiert, was die Lokalisation der fluoreszierenden Fusionsproteine bestätigte. MreB aus *B. subtilis* und aus *E. coli* bildete, wie zuvor beschrieben, filamentöse Strukturen an der Zellmembran aus. Eine Reduktion des Expressionsniveaus von MreB führte zur Ausbildung kurzer Filamente und diffuser Aggregate. MreC und MreD interagieren mit MreB und lokalisierten in punktuellen Mutsren innerhalb der Membran. Die PDH Untereinheiten PdhB, PdhC und die PfkA wiesen homogene Lokalisation in der Zelle auf, im Einklang mit einer zytosolischen Enzym-Funktion. Interessanterweise lokalisierte PdhA an nur einem Zellpol in zwei Dritteln der Zellen, und PdhD wies zwei Lokalisationsmuster auf, ein homogen zytosolisches, und eines, dass mit der Lokalisation der Chromosomen im Nukleoid überein stimmte. Dem entsprechend haben zwei der vier Untereinheiten der PDH eine spezifische Lokalisation in *B. subtilis* Zellen.

Durch Einzelmolekül-Fluoreszenzmikroskopie und automatisierter Molekülverfolgung konnte bestimmt werden, dass MreB Moleküle zwei Populationen ausbilden, eine eher immobile Population, die in den filamentösen Strukturen vorhanden ist, und eine bewegliche aus diffundierenden Molekülen. Die Mehrheit der MreB Moleküle ist immobil und damit in filamentöser Struktur. Auch MreC, MreD und RodZ, sowie Pbp1A und die PDH Untereinheiten wiesen eine statische und eine dynamische Population auf, nur PfkA zeigte zwei dynamische Populationen, die vermutlich aus einer Population langsamer und schnell diffundierender Proteine besteht. Die Diffusionsgeschwindigkeit der dynamischen MreB Moleküle ist deutlich niedriger als die der PfkA Moleküle, was vermuten lässt, dass MreB hauptsächlich entlang der Membran diffundiert, was die Diffusion verringert. Die E2 Untereinheit der PDH, PdhC, scheint die zentrale Untereinheit der PDH zu sein, da sie die geringste Diffusionskonstante der vier Untereinheiten aufwies, und daher die meisten PdhC Moleküle im Komplex gebunden sind, während die übrigen in höherem Masse zwischen freier und gebundener Form wechseln.

## Abstract

For many years, efforts for discovering new antibiotics were mainly focused on the inhibitors of the cell wall synthesis machinery. We set out to find other factors that target the cell wall by making use of the cell wall degradation enzymes, which lyse the cell wall and therefore potentially kill bacteria. LytC is an autolysin from *B. subtilis*, which is capable of degrading the bacterial cell wall and make it a potential candidate antibiotic. In this dissertation, I cloned the *B. subtilis* *lytC* gene and over-expressed LytC protein in *E. coli*. In order to characterize the function of different LytC regions, we designed different constructs of *lytC*. I used the Gram-negative bacterium *E. coli* and Gram-positive *B. subtilis* to test if LytC can degrade the cell wall components when used as an external additive in cell medium. Different constructs of purified LytC protein were used, the results showed that LytC constructs can efficiently and greatly inhibit the growth of *E. coli* and *B. subtilis*, yet it is only effective for exponentially growing cells. The cell wall of stationary cells was more resistant to LytC and cell lysis was not observed. I proved that the C-terminal fusion of LytC with a strep-tag can be successfully over-expressed and purified while the N-terminal fusion cannot. Overexpression of LytC leads to a fast drop in OD<sub>600</sub> after one hour induction with 0.5 mM IPTG. The construct of LytCF6 only contains the functional region and the purified protein can still function like full length protein, which means the four cell wall binding (CWB) and the „low complexity region“ (LCR) domains are not necessary for LytC activity. I used strep elution buffer with BSA (bovine serum albumin) as control to verify that it is the LytC protein that is responsible for cell growth inhibition. I deleted 22 amino acids from the C-terminus of the functional region, and protein activity of this partially deleted LytCF2R2 was compared with LytCF2 (which has the full length of functional region). As a result, LytCF2R2 lost almost half of the protein activity in comparison to LytCF2. This further demonstrates that LytCF2 contains the functional region and the deletion of it can result in loss of activity.

We reviewed the localization and the single molecule trajectories of proteins (MreBCD, Pbp1A, RodZ and PDH complex) in exponentially grown *B. subtilis* cells. Phosphofructokinase (PfkA), which is a fast moving protein, was used as a control for MreB in the single molecule tracking study. In the protein localization study, we

found that MreB, MreC, MreD, RodZ and Pbp1A are localized along the cell membrane and have a similar localization pattern. The results indicate that MreB, MreC, MreD, RodZ and Pbp1A are membrane proteins. We confirmed the phenomenon that MreB forms discontinuous filaments structure underneath the cell membrane, both in *B. subtilis* and in *E. coli*. Upon reduction in its expression level, MreB forms patchy and short filament structures in *B. subtilis*. MreC and MreD also form patchy spots structures besides the membrane staining pattern. From our calculation, two thirds cells have PdhA localized at one cell pole, one third of the cells does not contain PdhA spots. The localization studies of PdhB, PdhC and PfkA showed that they are all uniformly distributed within the cytoplasm of the cell, which indicates they are cytoplasmic proteins. PdhD has two localization patterns, one is the same as chromosome DNA staining, and the other one is uniformly distributed within the cytoplasm.

We found single molecules of MreB are composed of two populations. One is the immobile population that forms the filamentous structures. The other one is the mobile population that freely diffuses within the cell. The same conclusions apply to the Pbp1A and PDH subunits proteins, as well as for the MreB colocalized proteins (MreC, MreD and RodZ). The single molecules of the PfkA compose two mobile populations. The fraction and movement speed of MreB mobile single molecules are lower than those of PfkA. We also deduced that MreB is a membrane-associated protein and that PdhC (E2 subunit) is the core of PDH complex from our data analysis, because the fraction and diffusion coefficient of mobile PdhC single molecules are the slowest of the four PDH subunits.

# TABLE OF CONTENTS

<b>1 Introduction .....</b>	<b>1</b>
<b>1.1 Cell wall .....</b>	<b>1</b>
<b>1.2 Peptidoglycan (PG).....</b>	<b>2</b>
<b>1.3 LytC .....</b>	<b>4</b>
<b>1.4 Penicillin Binding Proteins (PBPs).....</b>	<b>7</b>
<b>1.5 MreB, RodZ, MreC and MreD .....</b>	<b>8</b>
Structure and localization of MreB .....	8
Function of MreB in cell wall synthesis .....	9
RodZ.....	12
<b>1.6 PfkA and PdhABCD.....</b>	<b>13</b>
<b>1.7 Aims of reserach .....</b>	<b>15</b>
<b>2 Materials and Methods .....</b>	<b>17</b>
<b>2.1 Chemicals .....</b>	<b>17</b>
<b>2.2 Solutions .....</b>	<b>17</b>
<b>2.3 Strains .....</b>	<b>18</b>
<b>2.4 Methods .....</b>	<b>21</b>
2.4.1 Growth condition .....	21
2.4.2 Genomic DNA Extraction of <i>B. subtilis</i> .....	21
2.4.3 PCR (Polymerase Chain Reaction) .....	21
2.4.4 Site Directed Mutagenesis.....	22
2.4.5 DNA Digestion, Ligation and Detection.....	22

2.4.6 <i>E. coli</i> competent cells preparation and transformation .....	23
2.4.7 Plasmid extraction .....	25
2.4.8 <i>B. subtilis</i> competence cell preparation and transformation .....	25
2.4.9 SDS Poly-acrylamide gel-electrophoresis (SDS-PAGE).....	27
2.4.10 Immunoblot analysis .....	27
2.4.11 Gibson Assembly .....	28
<b>2.5 Protein overexpression and purification .....</b>	<b>30</b>
2.5.1 Expression test .....	30
2.5.2 Expression and purification of Strep-tagged LytC in <i>E. coli</i> BL21 .....	30
Purification of LytC-strep recombinant protein .....	31
2.5.3 Expression and purification of His-tagged LytC in <i>E. coli</i> BL21 .....	31
2.5.4 Gel filtration .....	32
2.5.5 Concentration of proteins by Ultrafiltration.....	32
2.5.6 Bradford protein assay .....	33
<b>2.6 Fluorescence Microscopy .....</b>	<b>33</b>
2.6.1 Cell growth and sample preparation .....	33
2.6.2 Fluorescence microscopy stains .....	34
2.6.3 Image acquisition .....	34
<b>2.7 Single molecule microscopy .....</b>	<b>35</b>
2.7.1 Sample preparation for single molecule microscopy .....	36
2.7.2 Single molecule microscopy .....	36
2.7.3 Single molecule tracking and track analysis .....	37
2.7.4 Calculation of the diffusion constants (diffusion coefficient) by MSD .....	37

<b>3 Results .....</b>	<b>38</b>
<b>3.1 Inhibition study of different constructs of protein LytC <i>in vitro</i> .....</b>	<b>38</b>
3.1.1 Design of <i>lytC</i> gene constructs.....	38
3.1.2 Purification of constructed protein LytCF2 .....	40
LytC kills host <i>E. coli</i> strain during overexpression step .....	40
The optimization of host strain and growth condition.....	41
Protein purification of other LytC constructs. ....	42
3.1.3 The functional study of constructed LytC proteins.....	45
LytC inhibits the growth of bacteria in liquid culture .....	45
LytC inhibits the growth of bacteria on agar plate .....	50
Autolysin effect rather than the protein effect of LytC inhibits the growth of bacteria .....	50
<b>3.2 Site directed mutagenesis of LytC and functional region partial deletion.....</b>	<b>51</b>
3.2.1 Site directed mutagenesis.....	51
3.2.2 Partial deletion of the functional region.....	54
<b>3.3 Microscopy evidence that LytC degrades the cell wall .....</b>	<b>55</b>
<b>3.4 Localization studies of MreB, MreC, MreD, PfkA, Pbp1A, RodZ and subunits of PDH complex <i>in vivo</i> .....</b>	<b>57</b>
3.4.1 Localization studies of MreB, MreC and MreD <i>in vivo</i> .....	57
3.4.2 Localization studies of PDH complex in <i>B. subtilis</i> .....	60
3.4.3 Localization study of RodZ, PfkA, Pbp1A, RecX and YfhH in <i>B. subtilis</i> .....	61
<b>3.5 Single molecule microscopy .....</b>	<b>62</b>
3.5.1 Single molecule detection and identification .....	63
3.5.2 Tracking analysis of YFP-MreB and PfkA-YFP single molecules .....	65

3.5.3 Single molecule analysis of MreC, MreD, RodZ and Pbp1A .....	70
3.5.4 Single molecule analysis of pyruvate dehydrogenase (PDH) complex .....	73
<b>3.6 Conclusion .....</b>	<b>76</b>
<b>4 Discussion .....</b>	<b>78</b>
LytC kills host during incubation.....	78
LytC is not a monomer and is moderately stable .....	78
LytC keeps its function only by C-terminal fusion and kills bacteria during exponential growth .....	79
Functional region rather other domains work as bacteria inhibitor .....	80
Defect of LytC functional region causes activity loss .....	81
Localization study of proteins <i>in vivo</i> .....	81
Two distinct fractions of YFP-MreB single molecules.....	83
The movement pattern and fraction of MreC, MreD, RodZ and Pbp1A are similar to MreB .....	85
Single molecule data analysis indicate PdhC is the core of PDH complex .....	85
<b>5 Prospects of future study .....</b>	<b>87</b>
<b>References .....</b>	<b>90</b>
<b>Acknowledgements.....</b>	<b>101</b>
<b>Appendix .....</b>	<b>102</b>
<b>Curriculum Vitae .....</b>	<b>105</b>

## LIST OF ABBREVIATIONS

Abbreviation	Full name
LB	Luria Bertani
10×	Ten fold concentration
Amp <sup>R</sup>	Ampicillin resistance
APS	Ammonium persulphate
BSA	Bovine Serum Albumin
<i>B. subtilis</i>	<i>Bacillus subtilis</i>
CV	column bed volume
CWB	Cell wall binding
DAPI	4',6-diamidino-2-phenylindole
DMF	dimethylformamide
DNA	Deoxyribonucleic acid
<i>E. coli</i>	<i>Escherichia coli</i>
EDTA	Ethylenediaminetetraacetate
Exp.	Exponential
FP	Fluorescent protein
FRAP	Fluorescence recovery after photobleaching
GFP	Green fluorescent protein
IPTG	Isopropyl β-D-thiogalactopyranosid
LCR	Low complexity region
MMC	Mitomycin C
MreB	Protein product of murein cluster e, gene B
MSD	Mean square displacement
NA	Numeric aperture
OD <sub>600</sub>	Optical density at 600 nm



PAGE	Polyacrylamide gelelectrophoresis
PBS	Phosphate buffered saline
PBST	Phosphate buffered saline Tween
PCR	polymerase chain reaction
PDH	Pyruvate dehydrogenase
ROI	Region of interest
RPM	rounds per minute
RT	Room temperature
SDS	Sodium dodecylsulphate
Stat.	Stationary
TBS	Tris buffered saline
TIRF	Total internal reflection fluorescence
v/v	volume per volume
WT	wild type
w/v	weight per volume
Xyl	Xylose
YFP	Yellow fluorescent protein

# 1 Introduction

## 1.1 Cell wall

Bacteria have different cell shapes and sizes, the external cell wall plays an essential role in cell shape determination. A great number of bacterial species are cylindrical (or rod-shaped). In most cases, cell growth occurs along the longitudinal axis, while keeping a fixed diameter (usually 0.5-1.5  $\mu\text{m}$ ) [1]. The peptidoglycan (PG) cell wall is the major determinant of cell shape [2]. The composition of the cell wall is shown as Figure 1 [3].

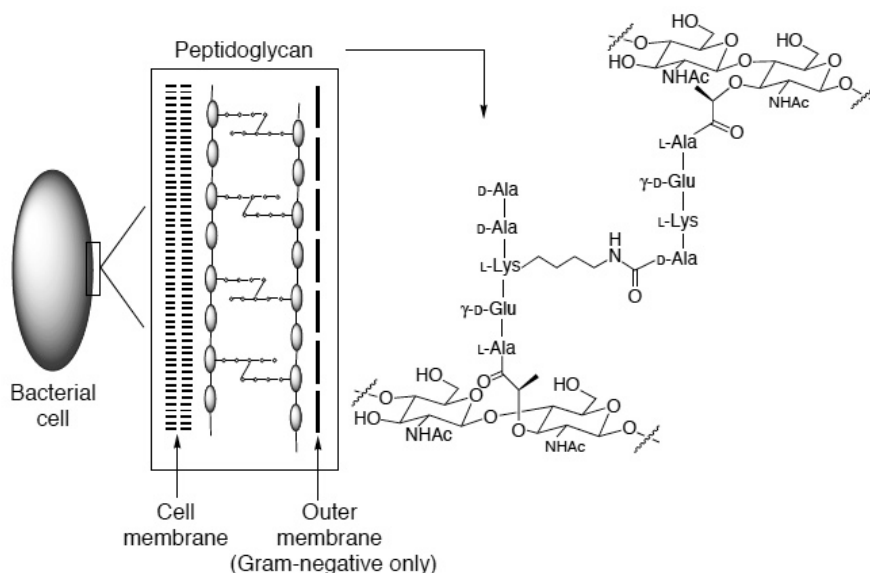


Figure 1. Schematic cartoon showing the composition and structure of peptidoglycan, which is a major component of the bacterial cell wall. Image was taken and modified from the work of Kristi Lazar and Suzanne Walker, 2002 [3].

The process of cell wall synthesis is a target for several antibiotics. The biosynthesis of the cell wall starts from the formation of soluble precursors which are produced by cytoplasmic reactions that are catalyzed by MurA-MurF [4]. This is followed by the production of lipid-linked precursors Lipid I and Lipid II that are catalyzed by MraY and membrane-associated protein MurG at the inner face of the cytoplasmic membrane. Lipid II is then translocated across the membrane and incorporated into the existing cell wall of the periplasm of Gram-negative bacteria or outside the membrane of Gram-positive bacteria [5]. Penicillin binding proteins (PBPs) catalyze

the reactions of transglycosylation (polymerization of the glycan strand) and transpeptidation (cross-linking between glycan chains) [6, 7]. In both rod-shaped and spherical bacteria, the synthesis of PG precursors, hydrolysis and insertion of PG require the coordination of several enzymes from multiple subcellular compartments. The new cell wall synthesis of spherical bacteria occurs during cell division while rod-shaped bacteria require an elongation growth phase between division circles [8].

## 1.2 Peptidoglycan (PG)

The peptidoglycan (PG or murein) of Gram-positive and Gram-negative bacteria has different amino acid composition and PG layer thickness [9, 10]. The main function of PG is to preserve cell integrity by withstanding the internal osmotic pressure [11]. During the cell division, PG components are inserted along the length of the cell, and the integrity of the cell wall is maintained by the simultaneous insertion of new glycan strands and hydrolysis of pre-existing ones [8]. PG synthesis occurs during two developmental phases: i) along the length of the cell during the cell elongation; ii) at the midcell during cell division. During the cell division of *C. crescentus*, MreB localizes to the midcell, indicating that MreB may be needed for the recruitment of PG synthesis enzymes at the site of division [8]. The PG sacculus forms a closed, bag-shaped structure that surrounds the cytoplasmic membrane [10]. Degradation of the PG or inhibition its biosynthesis during cell growth can cause cell lysis [10]. PG is also a key factor for cell shape maintenance and function as a scaffold for anchoring other cell envelope components such as proteins and teichoic acids [12, 13].

In the peptide stem, there are some variations between different bacterial species (e.g. glycan strands and the composition of interpeptide bridge). Even in the same species, different growth conditions can also cause variations in the structure of PG and cell wall [10]. Most variations of the PG are due to modes of cross-linkage or composition of the interpeptide bridge [10]. Generally, cross-linkage can be divided into two groups [14]. I) 3-4 cross-linkage group. II) 2-4 cross-linkage group, which is only found among coryneform bacteria. The cross-linking reactions were catalyzed by the transpeptidase domain of the penicillin-binding proteins (PBPs) [6].

The thickness of the PG layer is not dependent by the chain length of the glycan strands. Gram-negative bacteria (e.g. *E. coli*) have a single layer of PG while Gram-

positive bacteria (*B. subtilis*) have a multilayered PG and thick cell wall. For Gram-positive and negative species, some species have long glycan strands while some other species have short glycan strands. In Bacilli (*B. subtilis*, *B. licheniformis* and *B. cereus*), the average chain length of glycan strands is from 50 to 250 disaccharide units [15-17]. Gram-negative bacteria have different chain length, but usually the chain length varies from 20 to 40 disaccharide units [18-20]. In *E. coli*, the average chain length of glycan strands varies with different strains and growth conditions [21]. The thickness of Gram-negative bacteria PG layer varies from 1.5 to 15 nm [22-26]. The thickness of the inner wall zone (IWZ) or periplasmic space of *B. subtilis* is 22 nm. The outer wall zone (OWZ) thickness varies between different bacterial species and growth phase. The thickness of OWZ is between 15 to 30 nm in *S. aureus*, *B. subtilis*, *Streptococcus gordonii* and *Enterococcus gallinarum* [10]. Cells with less PG layer are more fragile to harming agents. However, cells with the ability of reducing PG content can deal with temporary inhibitions of cell wall biosynthesis, and have higher chances of survival [10, 27]. The architecture of the cell wall of Gram-positive cells is still poorly understood. The thick, multi-layered PG are linked to other major surface polymers [10].

The biosynthesis of PG is a complex process that involves around 20 reactions, which happens in cytoplasm (synthesis of nucleotide precursors), on the inner (synthesis of lipid-linked intermediates) and outer side (polymerization reactions) of the cytoplasmic membrane [4]. The stepwise assembly of the peptide stem of PG is ensured by Mur ligases (MurC, D, E and F) and Mpl [4]. PG synthesis involves both a cytoplasmic and an extracellular phase as shown in Figure 2 [3].

The enzymes that are responsible for PG synthesis are potential targets for antibiotic synthesis. However, the study of the enzymes is not well illustrated due to the lack of antibiotics that can inhibit the function of enzymes efficiently and specifically. Most of the PG synthesis inhibitors are not capable of crossing the cytoplasmic membrane [4]. The last generation of antibiotic mainly focuses on the inhibition of the enzymes of PG synthetic machinery. The inhibitors of each enzyme have been identified, although not all of them can be applied for clinical use [28]. However, a lot of these antimicrobial agents can be inactivated by the resistance mechanisms of bacteria [28]. Hereby, we provide a new approach for developing antibiotics. Instead of searching

new antibiotics that inhibit the biosynthetic machinery of PG, we investigated the possibility of using PG lytic enzymes that break down the cell wall.

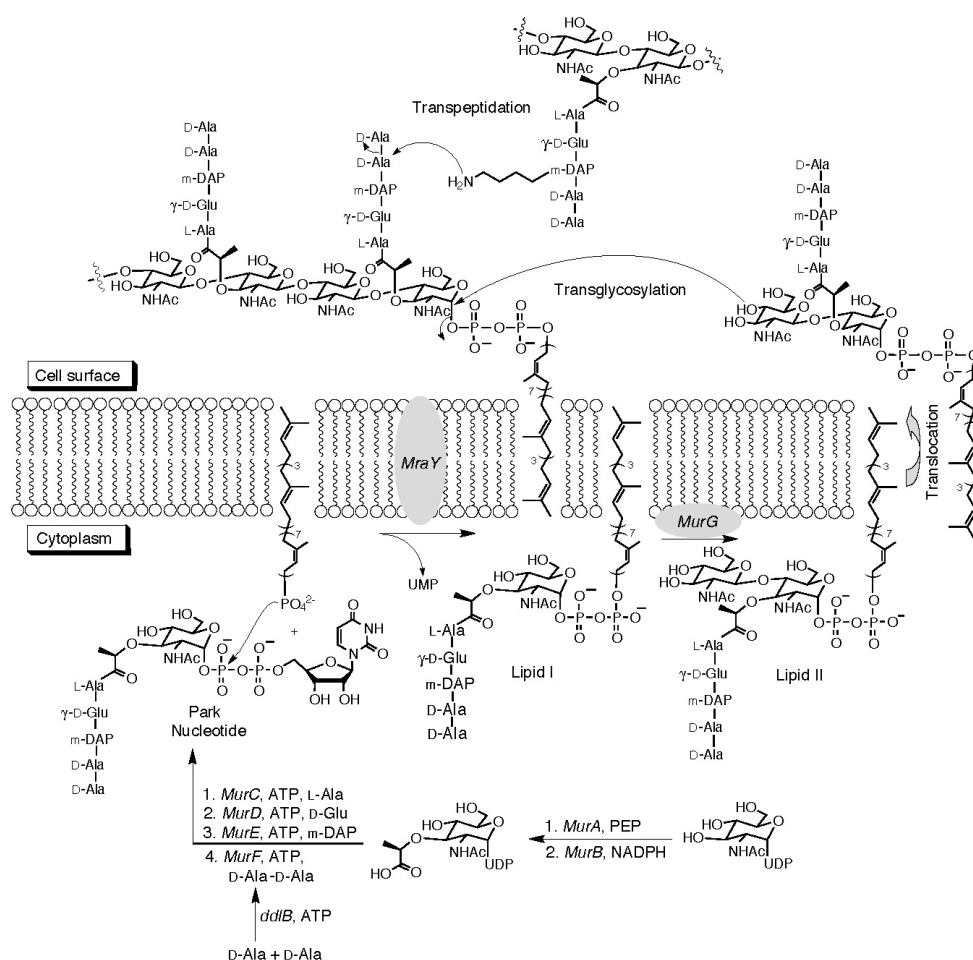


Figure 2. Model of PG biosynthesis. PG synthesis involves a cytoplasmic and an extracellular stages. The cytoplasmic steps can be divided into four sets of reactions [4]. The extracellular reactions of transglycosylation and transpeptidation are mediated by PBPs [6, 7]. Image was taken and modified from the work of Kristi Lazar and Suzanne Walker, 2002 [3].

### 1.3 LytC

PG hydrolases include LytC (CwlB), LytD (CwlG), LytE (CwlF), LytF (CwlE), LytG (YubE), CwlO (YvcE), CwlS (YojL) and CwlK (YcdD). These PG hydrolases mediate diverse functions such as cell growth, cell separation, cell wall turnover, cell mobility, sporulation and germination of bacterial cells [29-37]. LytC, LytD, LytG and LytE have been confirmed to mediate cell lysis [29, 33]. Autolysins can

hydrolyze the bacterial cell wall and remodel the PG, and are found in all bacteria that have PG.

In *B. subtilis* there are more than 30 autolysin genes, LytC, LytD and LytF have been implicated in vegetative cell separation and motility [29, 30, 32, 38, 39]. *lytD* and *lytF* genes are under control of  $\sigma^D$ , and 70% of LytC expression is under  $\sigma^D$  control [40-44]. Sigma D regulates expression of genes involved in motility, chemotaxis, autolysin production and cell separation [30, 45-47]. Depleting the expression of these three autolysins showed that *B. subtilis* does not form separated cells and grows continuously in chains [48]. Exponentially growing *B. subtilis* are heterogeneous in cell morphology, some of them grow as single cells that are motile and the other cells are grow in multicellular, nonmotile chains [49]. The flagellar filament assembly is also under the control of sigma factor D [49-51]. Cells that are ON for  $\sigma^D$  express both the autolysin and flagellar genes and grow as separate motile cells. However, cells that are OFF for  $\sigma^D$ , do not express the autolysins or late flagellar genes and grow as nonmotile chains [38]. The expression of LytF is ON in single cells and OFF in long chains. *B. subtilis* strains with *lytC* or *lytD* mutation grow as individual cells, but cells with *lytF* mutation grow as chains. Thus LytF is the only autolysin under  $\sigma^D$  control that is essential for cell separation [38]. In the undomesticated strain (*B. subtilis* 3610), mutation of *lytC* resulted in a reduction in swarming motility. Furthermore, double mutation of *lytC* with *lytD* or *lytF* and triple mutation resulted in total loss of swarming motility, indicating that LytC is required for swarming mobility [30, 38, 43, 52]. The  $\sigma^D$  dependent autolysins are required for swarming motility, but are not required for flagellum biosynthesis [53]. LytF was reported to localize at the septa during cell division. Moreover, LytE localizes at the cell poles of vegetative cells and LytC localizes uniformly [53]. LytC is also needed to lyse the mother cell wall at the end of sporulation [54]. There must be a balance between PG synthesis and disassembly during cell elongation and separation. During *B. subtilis* cell division, the cell wall divides the mother cell into two daughter cells and the autolysins are needed.

The major function of LytC is to hydrolyze the linkage of *N*-acetylmuramoyl-L-alanine in PG [53]. It has been shown that *lytC* mutation did not cause any cell separation defects, the knock-out of *lytC* gene can increase biomass and the product formation in the cell [55]. The structure of LytC is predicated to be composed of a

transmembrane region (a.a. 7-24), a „low complexity region“ (a.a. 197-214) and three CWB (cell wall binding) repeat regions at the N-terminal region of LytC, and a catalytic region (a.a. 380-492) at the C-terminal of LytC. The CWB domains of LytC are not similar to the N-terminal CWB domains of LytE and LytF [53]. The CWB domain of LytC has been used as a CWB anchor for two artificial fusion proteins and both had the enzyme activity and CWB activity [56-58]. Another major vegetative autolysin is a 90-kDa endo- $\beta$ -N-acetylglucosaminidase (LytD or CwlG), which works together with the amidase LytC on cell lysis. The glucosaminidase LytD and LytC account for around 95% of the autolytic activity of the cell [29]. LytE and LytF are cell separation enzymes. *lytG* encodes another minor PG hydrolases N-acetylglucosaminidase [33]. Single mutant of *lytE*, which encodes an endopeptidase, results in cell growth defect and lysis reduction, but has no significant effect on the degradation of isolated cell wall. LytE could aid the action of LytC [31]. Furthermore, a *lytE cwlO* double mutant causes synthetic lethality due to the defect in lateral cell wall metabolism and cell elongation [59, 60]. Some proteins can also enhance the autolysin activity of LytC, such as LytA and LytB (not autolysins). SpoIID may also affect the activity of autolysin, because of its homology to LytB and the cell wall binding domain of LytC [42, 61, 62].

*S. pneumoniae* LytC contains a N-terminal choline-binding module (CBW, composed of 11 repeats, p1-p11) and a C-terminal catalytic module (residues 268-468). Repeats p1-p9 are involved in choline binding (NI domain), p10 and p11 (NII domain) are involved in modular arrangement, p11 interacts with the catalytic module [63]. The model of *S. pneumoniae* LytC is depicted in Figure 3.

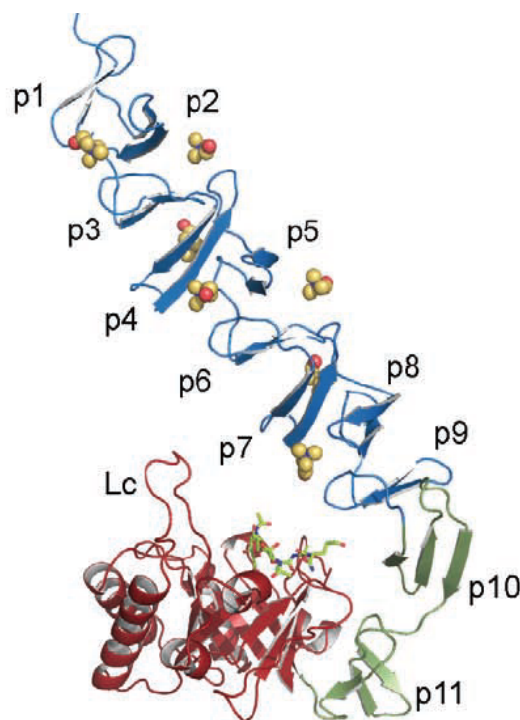


Figure 3. 3D structure of LytC-PG complex. A purified pneumococcal PG fragment (green sticks) is bound to the catalytic module (red) of LytC. Image taken from the work of Inmaculada Pérez-Dorado, et al., 2010 [63].

## 1.4 Penicillin Binding Proteins (PBPs)

PBPs (penicillin-binding proteins) catalyze the polymerization of Lipid II glycan chains and the cross-linking of stem peptides [28, 64, 65]. In *E. coli*, PBP1A and PBP1B play an important role in the final stage of PG biosynthesis, but deletion of one gene will not be lethal for the bacteria [6, 66, 67]. It has been found that  $\beta$ -lactam resistance is associated to alteration in PBPs, which makes them a well known target for  $\beta$ -lactam antibiotics [68-70]. The synthesis of the peptide bridges contains a transpeptidation reaction [70]. Many studies showed that penicillin can prevent the formation of cross-linkages by interfere with the transpeptidation reaction. Further research suggested that a stable penicilloyl derivative was formed at the active site of the transpeptidase, causing a permanent inactivation [71-73]. PBPs are classified into two groups, the high-molecular mass (HMM) PBPs and the low-molecular mass (LMM) PBPs [6]. The HMM proteins (PBPs1-3) are essential proteins for cell elongation, cell shape determination (PBP1A/PBP2) and cell septation (PBP1B/PBP3) [74-79]. The HMM-PBPs contain a penicillin-binding transpeptidase and a non-



penicillin-binding domain [6, 78]. LMM proteins (PBPs 4-7 and AmpH) can behave as DD-carboxypeptidases [70]. *E. coli* contains three class A PBPs (PBP1A, PBP1B and PBP1C) and two class B PBPs (PBP2 and PBP3), the major transglycosylase of *E. coli* is PBP1B [6]. PBP2 interacts with MreC and is the only murein synthase that is required for cylindrical growth of the sacculus. Depletion of PBPs and MreC proteins form spherical cells that eventually lyse [80-82]. *B. subtilis* has 16 PBPs, four belong to the class A. PBP1 is part of the cell division machinery and is required for the formation of the asymmetric sporulation at the septum. The other six PBPs belonged to class B [6, 83]. Transglycosylases are potential targets for new antibiotics. One reason is that they located on the outer surface of the bacterial membrane, which makes them accessible for antibiotics without the need to cross the membrane. There are several homologous of transglycosylases in each bacterial strain, so inhibitors that target one of these enzymes could act against several others [3]. Microorganisms produce a wide range of antibiotics that bind to Lipid II or other PG intermediates. This include glycopeptide antibiotics such as vancomycin and teicoplanin, which inhibit the last steps of PG synthesis [84, 85].

## 1.5 MreB, RodZ, MreC and MreD

### Structure and localization of MreB

MreB structures were depicted as extended, helical filaments that localize underneath the inner membrane in live cells and exhibit fast remodeling due to a high turnover rate. MreB was described as actin-like cytoskeletal element in bacteria based on the filamentous structures. However, recent studies showed that MreB is more likely to form discontinuous filaments that are localized along the lateral membrane [86-88]. These results suggested that MreB proteins might have an actin-like cytoskeletal role in bacteria, hence MreB filaments would play a role in cell wall synthetic, cell shape maintenance and other subcellular processes of rod-shaped bacteria (Figure 4) [89-92]. *mreB* genes are widely distributed in most rod-shaped or non-spherical bacteria, which contains at least one *mreB* homologue, while spherical bacteria lack *mreB* genes [93, 94]. These observations led to the idea that MreB functions during cell wall growth.

The early MreB localization experiments showed that MreB can form helix-like filamentous structures, peripheral spots and tilted bands [89, 93]. Several other reports

confirmed similar structures of MreB in different organisms [1, 95]. A great number of proteins that are involved in cell envelope synthesis are associated with MreB proteins and mostly have a similar helical localization pattern [96-98]. MreB in *E. coli* was described to localize as heterogeneous patchy [88]. The model of MreB localization had changed from helical filaments to one of protein patches. In which the filaments are short, and in a highly dynamic state that driven by (or at least dependent on) PG synthesis [1]. MreB can also form filaments *in vitro* [99].

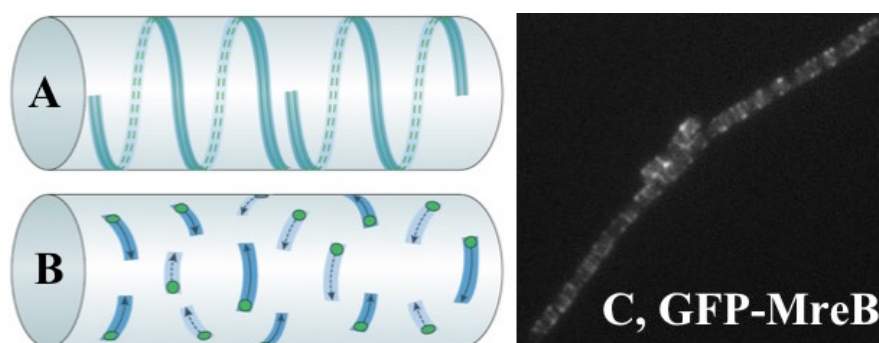


Figure 4. Models for MreB localization. (A) Early work indicated that MreB formed the helical elongated filaments (green solid and dashed lines) that along the rim of inner cell membrane. It was assumed that the helical filaments of MreB directed a helical pattern of new PG (blue shading) insertion. (B) MreB was recently depicted as discontinuous patches (green), which rotated circumferentially and around the long axis of cell (shown as arrows) and might driven by PG synthesis (blue shading). (C) Localization of GFP-MreB in a chain of exponentially growing *B. subtilis* cells. Images A and B are from the work of Jeff Errington, 2015 [1]. Image C taken from the work of Soufo, H.J.D., et al., 2010 [100].

### Function of MreB in cell wall synthesis

MreB involves the determination and maintenance of cell shape and PG synthesis. However, the functions proteins MreC, MreD and RodZ in cell shape maintenance remain to be elucidated [101-105]. MreB is thought to act in organization of these complexes. MreB also interacts with the division machinery in some organisms such as *E. coli* [106, 107]. *B. subtilis* has three MreB homologues, MreB, Mbl, and MreBH, and mutations of these genes have different effects on cell shape [92, 108-112]. MreB holds structural homology with eukaryotic actins, and purified MreB shows actin like properties of polymerization, ATP binding and hydrolysis [113-115].

Cell shape is assumed to depend on MreB filament dynamics as reported previously [116, 117]. Cells with un-flat surface tend to have shorter MreB filaments but the length of filaments could increase when the cell approaches a smooth shape [1]. MreB was shown to interact with different components of the cell wall synthetic machinery. MreB filaments recruit multiple synthetic complexes and move in the direction of glycan-strand insertion, and a PG synthesis process moves MreB filaments. MreB regulation of new PG insertion results in the elongation of the existing cylindrical sacculus [1, 118]. By interacting with the membrane and cell wall synthesis complex, MreB may function as a stabilizing factor (Figure 5). MreB may act to stabilize the location and precise movement of PG synthesis in *E. coli* [88].

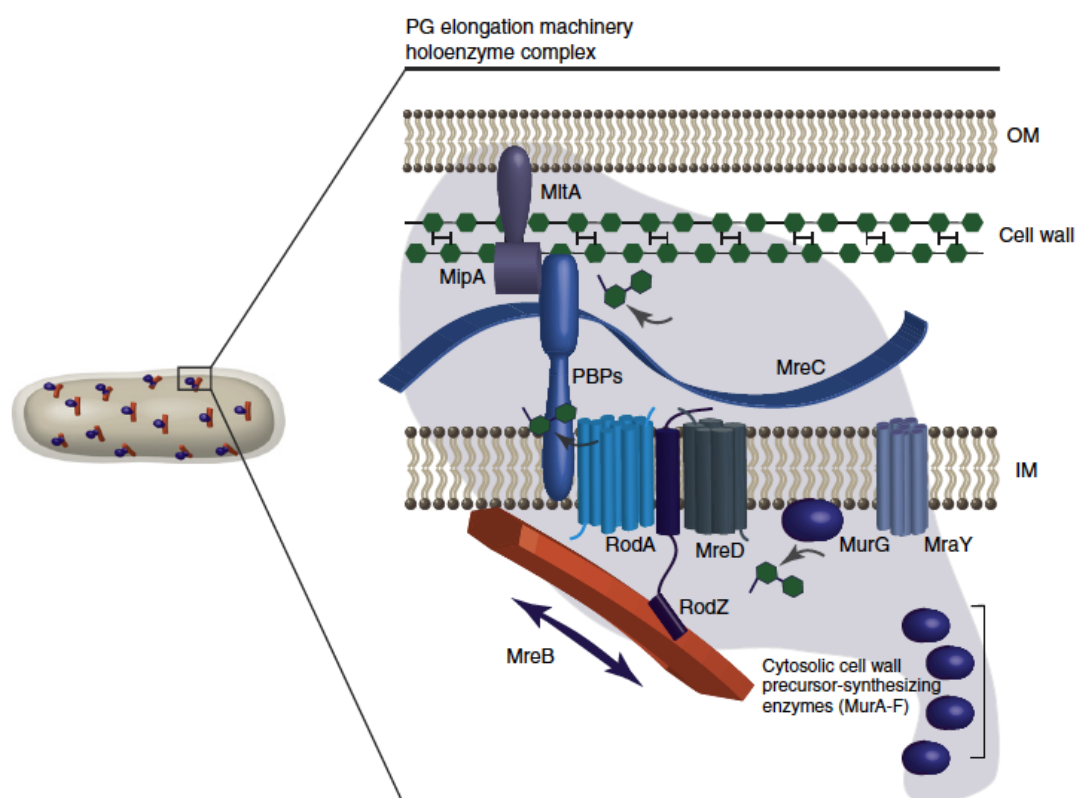


Figure 5. Model of PG synthesis, which can be divided into three steps: i) synthesis of cell wall precursor in the cytosol (MurA-F); ii) MraY and MurG complete the synthesis of PG precursor (Lipid II) in the cytoplasm that faces the inner membrane; iii) Lipid II is translocated into the periplasm and incorporated into pre-existing PG (dark green), which is accomplished by PBPs and lytic transglycosylases. During the cell wall synthesis, MreC functions in the periplasm, MreD, RodA and RodZ function in the inner membrane, and MreB might act as a scaffold. The entire elongation machinery is shown in shades of blue. IM, inner membrane; OM, outer membrane. Image taken from the work of Courtney L. White and James W. Gober, 2012 [8].

MreC, MreD and RodZ are required for the function of MreB and cell wall synthesis [1]. MreD is an integral bitopic membrane protein with short stretches of amino acids exposed to the cytoplasm. MreC has a larger periplasmic domain and an N-terminal tail protruding into the cytoplasm [82]. In rod-shaped bacteria, cells lacking *mreB* or its neighboring genes such as *mreC* and *mreD* result in morphology defects. Site-specific mutagenesis of MreB also causes some morphological defects [103, 119]. Moreover, when MreB is depleted in the cells, the downstream PBP mislocalize and the PG synthesis is abrogated [120]. MreB localization pattern *in vivo* is similar to that of PBPs [121-123]. The role of MreB in cell elongation has been confirmed in several model organisms (*E. coli*, *B. subtilis* and *Caulobacter crescentus*). MreB may play a key role in the similar helical localization patterns for several cell shape proteins, such as cytoplasmic precursor synthesizing enzymes (MurB, MurC, MurE and MurF), inner membrane proteins (MreD, MraY and RodA), and proteins with large domains outside the inner membrane (PBPs and MreC) [124-126]. Total internal reflection fluorescence (TIRF) microscopy was used to track the movement of GFP-MreB and its paralogs Mbl and MreBH in *B. subtilis*. The GFP tagged MreB proteins was shown to move perpendicular to the cell length in both direction [8]. In these studies, patches of MreB were discontinuous and often exhibited some reversals in direction or crossed over one another. Movements of MreC, MreD, RodA and various PBPs have a similar speed and pattern as MreB and PbpH [8]. The deletion of RodA, RodZ and a PBP result in a gradual decrease of MreB movement, indicating that these three proteins may play as the driving force of MreB movement [87]. The antibiotics that target the PG synthesis also slowdown the movement of MreB, Mbl and PBP. This movement can be restored by removing the antibiotics, implicating that PG synthesis is required to move the PG elongation holoenzyme [86, 88].

PG precursor synthesizing proteins (MurA-MurG and MraY) could form cytosolic complexes with MreB [124]. MreD is essential for lateral PG synthesis in *C. crescentus*, which interacts with the precursor synthesizing enzymes MurG and MraY. MreD is dependent on MreB localization along the cell length [124]. In periplasm, MreC of *C. crescentus* plays a key role in enzymes organization such as lytic transglycosylase MltA and the scaffolding proteins MipA and PBPs, which are required for PG assembly and breakdown [101, 127]. In *C. crescentus*, MltA and MipA have a similar helical localization pattern, which is dependent on MreC. MreC

form the center of a periplasmic interaction network with various PBPs and lytic transglycosylases [101, 124]. MreC of both *B. subtilis* and *E. coli* can also form polymers *in vitro* [8, 80, 128]. RodZ, MreD and RodA might function as a connect bridge for MreB to form interactions with proteins on the outside of the membrane. Therefore, the PG synthesis inside the cell is connected to the outside of the cell or to the periplasm [8]. In *B. subtilis*, there is a strong interaction between MreC and MreD. MreB may stabilize interactions with other membrane proteins and promote the activity of PBPs and directly binds to several PBPs [80, 96, 99, 129].

### **RodZ**

RodZ colocalizes with MreB, which is dependent on the cytoplasmic region of RodZ, and this colocalization is independent from MreC, MreD, PBP2 and RodA [130, 131]. RodZ has an N-terminal cytoplasmic region and a periplasmic C-terminal tail. The crystal structure of both MreB and RodZ showed that RodZ is involved in the MreB-coordinated network where RodZ is sandwiched between two MreB molecules [8]. Proper assembly of the actin cytoskeleton requires RodZ [82, 132]. It has been shown that the cytoplasmic domain of RodZ is required for its helical organisation *in vivo* [130, 132]. RodZ domains on both sides of the membrane play an role in cell shape maintenance [131]. The cytoplasmic and periplasmic domains of RodZ interact with other cell shape proteins at both sides of the membrane independently. There is a direct interaction between RodZ and MreB in its monomeric and filamentous form [82]. Mutations that influence this interaction causes morphological defects in *E. coli* and mislocalization of RodZ [82]. The model of RodZ interaction with MreB is shown as Figure 6 [82].

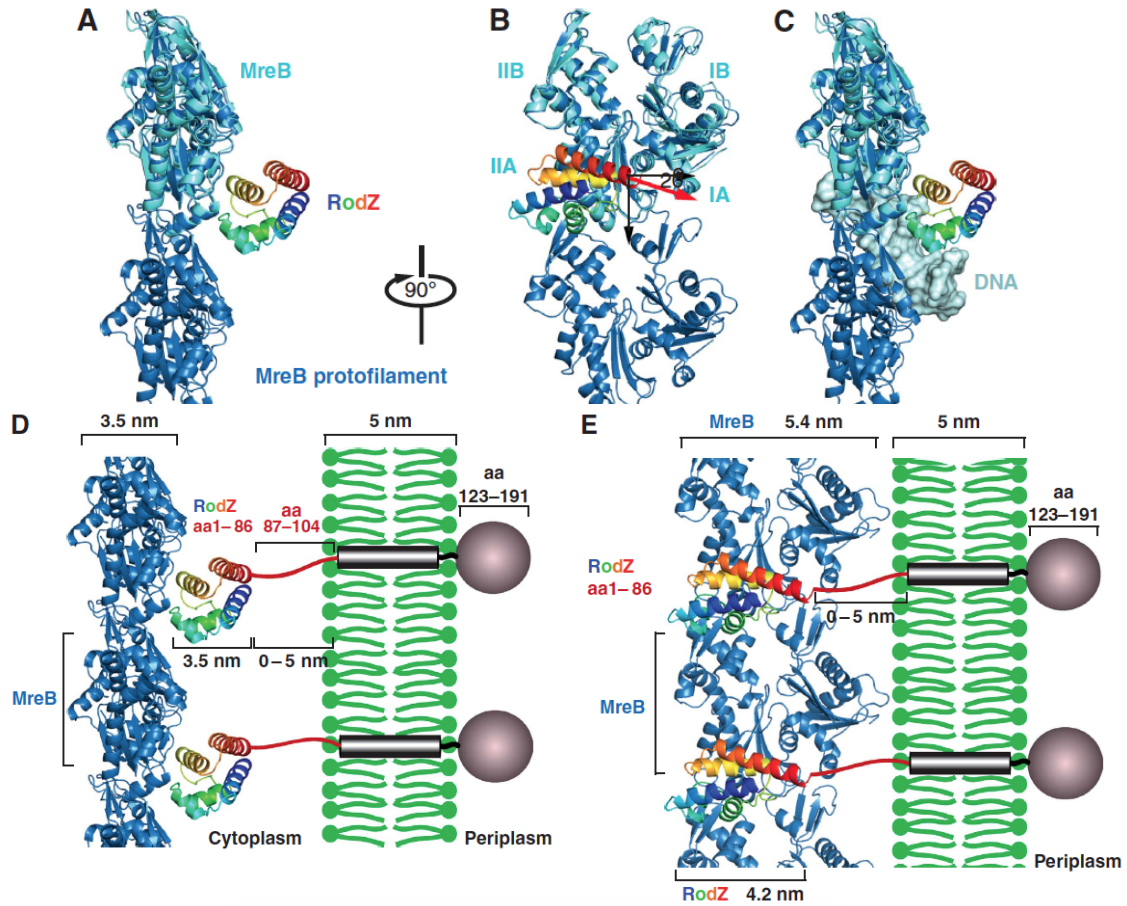


Figure 6. Colocalization model of RodZ and MreB. (A, B and C) 3D structure of RodZ (rainbow) in complex with MreB (blue). Grey color stands for the double-stranded DNA. (D, E) RodZ might anchor MreB in the membrane, RodZ localizes between MreB and the membrane. (D) The side-view. (E) Front-end view. Image taken from the work of Fusinita van den Ent, et al., 2010 [82].

## 1.6 PfkA and PdhABCD

6-phosphofructokinase (PfkA) phosphorylates fructose 6-phosphate to fructose-1,6-bisphosphate in glycolysis by transferring a phosphoryl group from ATP [133]. PFK has a homotetramer in bacteria and an octomer in yeast, and has two similar ( $\alpha/\beta$ ) lobes. The first lobe is involved in ATP binding and the other is housing both the substrate-binding site and the allosteric site. The tetramer subunits have 2 different conformations: i)'closed' state, the bound magnesium (Mg) ion bridges the phosphoryl groups of the enzyme products (ADP and fructose-1,6-bisphosphate); ii)'open' state, the Mg iron binds only the ADP [134-137].

The *pdhABCD* operon of *B. subtilis* encodes the pyruvate dehydrogenase multienzyme complex of E1 (pyruvate decarboxylase,  $\alpha$  subunit), E1 (pyruvate decarboxylase,  $\beta$  subunit), E2 subunit (dihydrolipoamide acetyltransferase) and E3 subunit (lipoamide dehydrogenase), respectively. Pyruvate dehydrogenase (PDH) can catalyze the conversion of pyruvate into acetyl coenzyme A (acetylCoA) that produce one NADH and links glycolysis to diverse pathways such as Krebs, overflow metabolism, fatty acid biosynthesis and fermentation pathways [138]. Expression of the *pdhABCD* operon is activated by glucose, which enhances the induction of the operon by three folds. This indicates that glucose induction may be necessary to avoid pyruvate accumulation [139]. The expression of the PDH complex is increased in the presence of the organic acids. The *pdhABCD* operon is negatively regulated upon decoyinine treatment. The guanines located at position 1 of the transcription initiation sites of *pdhABCD* is essential for the CodY-independent negative stringent control [140, 141]. This operon is transcribed as a 5.2-kb transcript from the promoter located upstream of *pdhA*. It was shown that the strict negative control of newly assigned *pdhABCD* promoter was independent of CodY and likely is mediated by the decrease in the GTP levels, which is resulting from lysine starvation and decoyinine addition [141].

There are two promoters in the *pdhABCD* operon. The first promoter is for the entire operon and the other promoter is located in front of the *pdhC* gene, which may function to ensure enough expression of E2 and E3 subunits because these subunits are needed in bigger amounts than E1 $\alpha$  and E1 $\beta$  [142]. The PDH complex of Gram-negative bacteria is composed of a core of 24 E2 subunits and 12 E1 and 6 E3 subunits [143]. PDH complex of Gram-positive bacteria consists a core of 60 E2 subunits. The E1 of Gram-negative bacteria is a homodimer, while the E1 from Gram-positive bacteria is a heterotetramer (E1 $\alpha$ <sub>2</sub>E1 $\beta$ <sub>2</sub>). The PDH complex of Gram-positive bacteria is encoded by genes *pdhA* (E1 $\alpha$ ), *pdhB* (E1 $\beta$ ), *pdhC* (E2) and *pdhD* (E3) [142, 144]. The *pdhA* gene is an essential gene for *B. subtilis*. Moreover, *pdhC* gene was not found to be essential for growth, and the inactivation of either *pdhB* or *pdhC* gene resulted in the inhibition of sporulation [142].

## 1.7 Aims of reserach

The misuse of antibiotics and the evolution of bacteria resistance to antibiotics have become a severe problem in the last decades. One of the resistance mechanisms is that bacteria can pump the antibiotics out of cell. Another mechanism is that bacteria can degrade the antibiotics inside or outside cells. For many years people try to find new antibiotics by studying the inhibitors of cell wall biosynthesis enzymes. In this dissertation, our way to find new antibiotics is different than the common way. Our goal is to develop an antibacterial agent that can hydrolyze the cell wall directly instead of inhibiting the function of cell wall synthesis enzymes. LytC is an autolysin (amidase) that can hydrolyze the linkage in PG. LytC can function in the extracellular space of bacteria. This will reduce the chance of developing antibiotic resistance in bacteria. While most traditional antibiotics inhibit the cell wall synthetic machinery, most traditional antibiotics cannot kill bacteria at stationary phase because the cell wall synthesis process has stopped.

The cytoskeletal actin-like element MreB in *B. subtilis* has obtained intense research interest since its discovery. It is well known that MreB plays an important role in cell shape maintenance in rod-shaped bacteria. MreB also forms helical filaments that localize underneath the cell membrane in *B. subtilis* and other bacterial cells. However, the structure of MreB polymerization *in vivo* is still in debate and the dynamic behavior of MreB at the single molecule level *in vivo* is still poorly understood. In this dissertation, our main aim was to characterize the localization and movement pattern of MreB *in vivo* at the single molecule level. This includes the single molecule movement tracking, diffusion constant (or diffusion coefficient) calculation, and comparison of diffusion constants between MreB and other proteins (MreC, MreD, RodZ, Pbp1A, PdhABCD, PfkA) in *B. subtilis*. We performed these experiments to gain more insight into the localization pattern and dynamics of MreB in live cells of *B. subtilis* and *E. coli*. Single molecule microscopy was used to record the movement of MreB. The movement of proteins (RodZ, MreC and MreD) associated to MreB *in vivo* is also one of the main interests of this study. MreB is also colocalize with the cell wall synthesis enzymes (Pbp1A). Therefore, the study of Pbp1A can help us to further understand the cell wall biosynthesis and maintenance.



RodZ also plays an important role in cell shape determination and cell wall synthesis, and it colocalizes with MreB [130, 131]. However, the function of RodZ in cell wall synthesis has not been clearly verified. In the future, we want to characterize RodZ in *B. subtilis*, including its localization pattern and dynamics within the membrane and investigate its connection to the actin-like cytoskeleton and its function in cell wall synthesis.

## 2 Materials and Methods

### 2.1 Chemicals

All the chemicals were purchased from Sigma, Roth, AppliChem, GE Healthcare or Difco. Gibson assembly (GA) mixtures, endonucleases, PCR-reagents, ligase, buffers and enzymes were purchased from NEB (New England Biolabs). Gel extraction of linear DNA fragments Kit, plasmid purification Kit, PCR purification Kit and chromosomal DNA extraction Kit were purchased from Qiagen, Sigma, QIAGEN and AnalytikJena, respectively.

### 2.2 Solutions

S7<sub>50</sub> Medium (100 ml): 10 ml 10× S7<sub>50</sub> Salts, 1 ml 100× Metals, 2 ml 50% Glucose/Fructose, 1 ml 5 mM 10% Glutamate, 0.4 ml 1% Casaminoacids, 1 ml 50% Xylose (with Fructose), 84.6 ml H<sub>2</sub>O (with Xylose). The completed medium was sterilized by filtration.

10× S7<sub>50</sub> Salts (100 ml): 10.47 g MOPS, 1.32 g (NH<sub>4</sub>)<sub>2</sub>SO<sub>4</sub>, 0.68 g KH<sub>2</sub>PO<sub>4</sub>. Adjust the pH to 7.0 with 1 M KOH. The salts were sterilized by filtration.

100× Metals: 0.2 mM MgCl<sub>2</sub>, 0.07 mM CaCl<sub>2</sub>, 0.1 mM ZnCl<sub>2</sub>, 0.005 mM MnCl<sub>2</sub>, 0.002 mM HCl, 0.5 mM FeCl<sub>3</sub>, 0.1 mg/ml Thiamine-HCl. Iron was added at last to prevent precipitation. The metals were sterile filtered and then wrapped in aluminum foil to prevent contact with light and subsequent oxidization.

LB Medium (1 L): 10 g Tryptone, 5 g Yeast Extract, 10 g NaCl, 15 g Agar (for solid medium). Adjust pH to 7.4 by 1 mM NaOH. Use the corresponding antibiotics. Sterilized by autoclaved.

Antibiotics and other additives (final concentration): 100 µg/ml Ampicillin sodium salt (dissolved in ddH<sub>2</sub>O), 5 µg/ml Chloramphenicol (dissolved in ethanol), 100 µg/ml Spectinomycin dihydrochloride (dissolved in 50% ethanol, v/v), 0.5% (w/v) Xylose, 0.25 mM to 1 mM Isopropyl β-D-thiogalactopyranosid (IPTG).

## 2.3 Strains

Plasmids were constructed and then amplified in the *E. coli* strain XL-1 Blue (Stratagene). *E. coli* BL21(DE3) (Invitrogen) was used for *B. subtilis* heterologous proteins overexpression. All constructed strains of *B. subtilis* in this dissertation are derivatives of the prototroph wild type strain PY79. All other used bacterial strains are listed in Table 1.

Name	Strain	Genotype
PG1	PY79	<i>Bacillus subtilis</i> wild type[145]
PG105	DH5 $\alpha$	<i>fhuA2</i> $\Delta$ ( <i>argF-lacZ</i> )U169 <i>phoA glnV44</i> $\Phi$ 80 $\Delta$ ( <i>lacZ</i> )M15 <i>gyrA96 recA1 relA1 endA1 thi-1 hsdR17</i>
PG156	BL21(DE3)	<i>E. coli</i> F <sup>-</sup> <i>ompT gal dcm lon hsdS<sub>B</sub>(r<sub>B</sub><sup>-</sup> m<sub>B</sub><sup>-</sup>)</i> $\lambda$ (DE3 [ <i>lacI lacUV5-T7 gene 1 ind1 sam7 nin5</i> ])
PG145	XL1-Blue	<i>endA1 gyrA96(nal<sup>R</sup>) thi-1 recA1 relA1 lac glnV44</i> F' [::Tn10 <i>proAB<sup>+</sup> lacI<sup>q</sup> <math>\Delta</math>(lacZ)M15]</i> <i>hsdR17(r<sub>K</sub><sup>-</sup> m<sub>K</sub><sup>+</sup>)</i>
PG950	DH5 $\alpha$	pPR-IBA101, Amp <sup>R</sup>
PG575	DH5 $\alpha$	pET-Dute-1, Amp <sup>R</sup>
PG450	Rosetta 2 (DE3) pLysS	F- <i>ompT hsdS<sub>B</sub>(R<sub>B</sub>-m<sub>B</sub>-)</i> <i>gal dcm</i> $\lambda$ (DE3) [ <i>lacI lacUV5-T7 gene 1 ind1 sam7 nin5</i> ] pLysSRARE(CamR)
PG2001	DH5 $\alpha$	pSG1164-NLMV <i>amp, cm</i> pSG1164-New Linker-MonomericVenus-yfp expression vector, Pxyl
PG2276	DH5 $\alpha$	linker-mVenus <i>amp</i> pSG1729-linker mVenus-yfp <i>amy-locus</i> , Pxyl
PG2658	<i>Bacillus subtilis</i> PY79	Pxyl-yfp-pbp1A::amyE spec
PG2659	<i>Bacillus subtilis</i> PY79	P <sub>xyl</sub> -yfp-pbp1A (original locus) Cm
PG2664	pfkA-yfp (original locus)	pfkA-yfp (original locus)-1164
PG1375	RecX-YFP	recX-yfp-1164
PG2984	ymfM-yfp	pSG 1164, ymfM-yfp, Amp <sup>R</sup> , Cm <sup>R</sup> +Xylose
PG3007	ymfM-yfp	pSG1729@amyE, yfp-ymfM, Spec <sup>R</sup>
PG1461	yfp-mreB	Pxyl-yfp-mreB::amyE, Spec, Xylose (pSG1729)
PG1444	gfp-mreC	Pxyl-gfp-mreC::amy
PG1445	gfp-mreD	Pxyl-gfp-mreD::amy
PG1463	yfp-mreC	Pxyl-yfp-mreC::amy
PG1464	yfp-mreD	Pxyl-yfp-mreD::amy
PG2658	yfp-pbp1A	Pxyl-yfp-pbp1A::amyE, Spec, Xylose (pSG1729)
PG2659	yfp-pbp1A (original locus)	Pxyl-yfp-pbp1A (original locus), Cm, pHJDS

PG3087	GFP-MreB	St.GFP(MreB fusion)
PG3088	GFP-MreB	St.GFP-pS2131 (St GFP-MreB sandwich under PLAC)
MC1	lytCF1-Strep	lytCF1-Strep-pPR-IBA101 (P <sub>T7</sub> , Amp <sup>R</sup> )
MC2	lytCF2-Strep	lytCF2-Strep-pPR-IBA101 (P <sub>T7</sub> , Amp <sup>R</sup> )
MC3	lytCF3-Strep	lytCF3-Strep-pPR-IBA101 (P <sub>T7</sub> , Amp <sup>R</sup> )
MC4	lytCF4-Strep	lytCF4-Strep-pPR-IBA101 (P <sub>T7</sub> , Amp <sup>R</sup> )
MC5	lytCF5-Strep	lytCF5-Strep-pPR-IBA101 (P <sub>T7</sub> , Amp <sup>R</sup> )
MC6	lytCF6-Strep	lytCF6-Strep-pPR-IBA101 (P <sub>T7</sub> , Amp <sup>R</sup> )
MC7	GST-His-lytCF1	GST-His-lytCF1-pGAT3
MC8	GST-His-lytCF2	GST-His-lytCF2-pGAT3
MC9	GST-His-lytCF3	GST-His-lytCF3-pGAT3
MC10	GST-His-lytCF4	GST-His-lytCF4-pGAT3
MC11	GST-His-lytCF5	GST-His-lytCF5-pGAT3
MC12	GST-His-lytCF6	GST-His-lytCF6-pGAT3
MC13	pdhA-yfp	pdhA-yfp (original locus)-1164
MC14	pdhB-yfp	pdhB-yfp (original locus)-1164
MC15	pdhC-yfp	pdhC-yfp (original locus)-1164
MC16	pdhD-yfp	pdhD-yfp (original locus)-1164
MC17	yfp-pdhA	Pxyl-yfp-pdhA::amyE, Spec, Xylose (pSG1729)
MC18	yfp-pdhB	Pxyl-yfp-pdhB::amyE, Spec, Xylose (pSG1729)
MC19	yfp-pdhC	Pxyl-yfp-pdhC::amyE, Spec, Xylose (pSG1729)
MC20	yfp-pdhD	Pxyl-yfp-pdhD::amyE, Spec, Xylose (pSG1729)
MC21	yfp-yfhH	yfp-yfhH-pHJDS (original locus)

Table 1. Strains used in this research.

## Primers:

All the primers used in this dissertation are listed in Table 2.

LytCEcoRIF1	CATGAATTCGTTGGGGGAAGCAATAGATAC
LytCEcoRIF2	CATGAATTCCTACAAGAATTAGCGGTTCA
LytCSacIIF3	CATCCGCGGACGGTATACAACAAGTTACCT
LytCSacIIF4	CAT CCGCGGGATAACTCAGTGAAAAGAGTT
LytCSacIIF5	CATCCGCGGGGTGAAACAATCTTTATTGATC
LytC EcoRIF6	CATGAATTCATGCAGGAGAGAGTAAATAAAGCA
LytCXhoIR	CATCTCGAGTCTGTAATAAGATACTGTGCC
GST-F1	GCCCATGGGCCACCATCACCATCACCATGTTGGGGGAAGCAATAGATAC
GST-F2	GCCCATGGGCCACCATCACCATCACCATCCTACAAGAATTAGCGGTTCA
GST-F3	GCCCATGGGCCACCATCACCATCACCATACGGTATACAACAAGTTACCT
GST-F4	GCCCATGGGCCACCATCACCATCACCATGATAACTCAGTGAAAAGAGTTG
GST-F5	GCCCATGGGCCACCATCACCATCACCATGGTGAAACAATCTTTATTGATC
GST-F6	GCCCATGGGCCACCATCACCATCACCATCAGGAGAGAGTAAATAAAGCA
GST-R	GATCTCGAGTTATCTGTAATAAGATACTGTGCC
lytE342QF	GGCAATGGACTCCTTCAGAAAGAAGTCAACCTTGAT
lytE342QR	ATCAAGGTTGACTTCTTTCTGAAGGAGTCCATTGCC
lytE461QF	GCCGAGTGTTTTAGTTCAAAGTGCCTTTATCACTAAT
lytE461QR	ATTAGTGATAAAGGCAGTTTGAAGTAAACACTCGGC
LytCecoriCF	CATGAATTCATGTTG CGTTCTTATATAAAAGTC
LytCxhoiCR	CATCTCGAGTCTCTCCTGTAAAGAATAAAA
lytexhoiR2	CATCTCGAGATCTGATGCATTAGTGATAAA
pdhAFP	CCTAGGATGGGTACCGGGCCCATGGCTGCAAAAACGAAAAAA
pdhARP	TGGCGCATACTGCAGGAATTCTTACTTCGACTCCTTCTGTGTATA
pdhBFP	CCTAGGATGGGTACCGGGCCCATGGCGCAAATGACAATGATT
pdhBRP	TGGCGCATACTGCAGGAATTCTTAAATTCAGCACTTTTCTTGC
pdhCFP	CCTAGGATGGGTACCGGGCCCGTGGCATTGGAATTTAAACTT
pdhCRP	TGGCGCATACTGCAGGAATTCTTACGCCTCCATTAAATTAATTG
pdhDFP	CCTAGGATGGGTACCGGGCCCATGGTAGTAGGAGATTTCCCT
pdhDRP	TGGCGCATACTGCAGGAATTCTTATTTTACGATGTGAATCGGACT
pdhAFP2	GATTCCTAGGATGGGTACCGGAATGGCTGCAAAAACGAAAAAA
pdhARP2	CAGGCCAGATAGGCCGGGCCCCCTTCGACTCCTTCTGTGTATA
pdhBFP2	GATTCCTAGGATGGGTACCGGAATGGCGCAAATGACAATGATT
pdhBRP2	CAGGCCAGATAGGCCGGGCCCCAAATTCAGCACTTTTCTTGC
pdhCFP2	GATTCCTAGGATGGGTACCGGAGTGGCATTGGAATTTAAACTT

pdhCRP2	CAGGCCAGATAGGCCGGGCCCCGCCTCCATTAAAAATTAATTG
pdhDFP2	GATTCCTAGGATGGGTACCGGAATGGTAGTAGGAGATTTCCCT
pdhDRP2	CAGGCCAGATAGGCCGGGCCCCCTTTACGATGTGAATCGGACT
yfhHSalIF1	CATGTCGACATGGAGAAACGATACAGTCAA
yfhHEcoRIR1-198	CATGAATTCTTACAAATCAGAAGAACAAATATAAT

Table 2. Primer collection.

## 2.4 Methods

### 2.4.1 Growth condition

All the *E. coli* strains were grown in Luria-Bertani (LB) liquid medium or on solid LB agar plates with the appropriate antibiotics. The cells for protein overexpression were incubated on a shaking platform (INFORS-HT Multitron) with 200 rpm (rounds per minute) for small scale flasks or 150 rpm for 1 L culture at 37°C. All the strains used for microscopy were cultivated in S7<sub>50</sub> minimal medium because it provides a very low background of fluorescence. If not mentioned, all the *B. subtilis* strains were grown at 30°C in LB medium or S7<sub>50</sub> medium with appropriate antibiotics. The bacterial optical density (OD) was measured at 600 nm.

### 2.4.2 Genomic DNA Extraction of *B. subtilis*

Genomic DNA of *B. subtilis* was extracted by following the instructions of innuPREP Bacteria DNA Kit (analytic jena).

### 2.4.3 PCR (Polymerase Chain Reaction)

PCR was performed to amplify the desired DNA fragments. A standard PCR mixture is: 1 µl template DNA (genomic/plasmid1:100), 1 µl dNTPs (10 mM), 2 µl Forward Primer (12 mM), 2 µl Reverse Primer (12 mM), 10 µl Buffer HF (5×), 0.5 µl Phusion DNA polymerase, 1 µl DMSO, 32.5 µl ddH<sub>2</sub>O.

The PCR reactions were performed in a thermocycler (Eppendorf, Mastercycler personal) with a standard PCR procedure as Table 3. The annealing temperature of Primers (forward and reverse) are dependent on the length and the melting temperature of oligonucleotides. The temperature was calculated as:  $2 \times n(A/T) +$

4×n(G/C). The elongation time of DNA at 72°C is decided by the length of aimed DNA fragment, which is usually 1 min for 1 kb DNA.

1	95 °C	5 min	
2	95 °C	30 sec	×10 cycles
3	55 °C	30 sec	
4	72 °C	1 min (1 min/1 kb)	
5	95 °C	30 sec	×25 cycles
6	61 °C	30 sec	
7	72 °C	1 min (1 min/1 kb)	
8	72 °C	10 min	
9	16 °C	∞	

Table 3. PCR program.

#### 2.4.4 Site Directed Mutagenesis

Single site mutation at desired position in a gene sequence is performed by site directed mutagenesis. The gene to be mutated was first cloned into the pPR-IBA101 vector (IBA Bio TAGnology). The desired mutation was performed by using two complementary primers that also bear complementarity regions to the shuttle vector. The mutation site was included within both primers' sequences, and the template plasmid was amplified with the PCR program: 95°C 2 min, 25 cycles (95°C 30 s, 50-55°C 30 s, 72°C 5-8 min), 72°C 10 min. The machine was programmed to store the amplified products at 16°C till they were subsequently removed and frozen or used.

The amplified plasmids were purified by using a PCR purification Kit (OMEGA) and then transformed into *E. coli* XL1-Blue for propagation. The plasmid was then purified from an overnight culture of XL1-Blue, and finally transformed into BL21 for overexpression and subsequent protein purification.

#### 2.4.5 DNA Digestion, Ligation and Detection

Restriction enzymes and buffers from New England Biolabs (NEB) were used for the digestion of plasmid or linear DNA. Procedures were performed according to the protocol of NEB. The mixture of the digestion reaction was as follows: 20 µl plasmid, 5 µl NEB Buffer, 5 µl 1×BSA, 1 µl endonuclease. The reaction volume was

completed to 50  $\mu$ l with ddH<sub>2</sub>O. Digested DNA was purified with Cycle Pure Kit (OMEGA) according to the manufacturer's protocol. For a ligation, the vector and the insert were added in a molar ratio of around 1:4. The concentration of DNA was either accurately measured by a Nanophotometer (Implem GmbH), or visually estimated by running an agarose gel. The ligation reaction contained: 6  $\mu$ l insert DNA, 2  $\mu$ l vector, 1  $\mu$ l 10 $\times$  Ligation Buffer, 1  $\mu$ l T4 Ligase. After the standard ligation mix was performed, the mixture was incubated at 16°C overnight. The ligation products were transformed into XL1-Blue competent cells and incubated on LB agar plates, the colonies were inoculated into liquid LB for plasmids extraction.

After purification of the constructed plasmid, a test digestion was performed to check if the insert was correctly incorporated into the vector. A standard test digestion mixture consisted of: 3  $\mu$ l plasmid, 1  $\mu$ l NEB Buffer, 1  $\mu$ l 1 $\times$  BSA, and 0.2  $\mu$ l endonuclease. The volume was completed to 10  $\mu$ l with ddH<sub>2</sub>O, and incubated for 2 hours at the adequate digestion temperatures of the enzymes indicated by NEB. Linear or circular DNA were separated according to their sizes (bp) and conformation by agarose gel electrophoresis. 1% (w/v) of agarose gel was dissolved in 1 $\times$ TB buffer in a microwave oven. The gel was poured into a cast and left to polymerize. The DNA samples were mixed with 6 $\times$  Loading Dye (1:5) prior to loading into the lanes of the gel, and the electrophoresis was performed at 130 V for 30 min. The DNA bands were visualized under UV light (UVP, UV transilluminator) and the linear DNA corresponding to a correct band size on the gel was extracted by using Cycle Pure Kit (OMEGA).

TB Buffer: 48 mM Tris (hydroxymethyl) aminomethane, 38 mM Glycin, 0.035% (w/v) Sodium dodecylsulphate, 20% Methanol. 6 $\times$ DNA Loading Dye: 20% (v/v) Glycerin, 6 $\times$ TB Buffer, 0.001% (w/v) Bromophenol blue, 1:60000 GelRed<sup>TM</sup> Nucleic Acid Gel stain.

#### **2.4.6 *E. coli* competent cells preparation and transformation**

##### **Electro-competent cells preparation:**

A single colony of *E. coli* XL1-Blue was inoculated from fresh plate into 15 ml liquid LB medium (50 ml flask) containing tetracycline, and the culture was incubated at 37°C on a 200 rpm shaking platform overnight. 1% culture was re-inoculated into 1 L



LB medium (2 L flask), incubate at 37°C until an OD<sub>600</sub> 0.5~0.7 was reached. The culture was incubated on ice for 30 min before pelleting down by centrifugation at 4,500 rpm for 15 min at 4°C (BECKMAN COULTER Avanti J-26 XP centrifuge, JLA 9,1000 rotor). The supernatant were discarded, and the pellet was re-suspended in 300 ml Mops solution (15%(w/v) Glycerol, 1 mM Mops). A second centrifugation was carried out at 4,000 rpm, at 4°C for 20 min (BECKMAN COULTER Allegra X-15R). The cells were washed a second time in 30 ml Mops solution and then re-suspended again in 6 ml Mops solution. 50 µl aliquots were made and stored in a -80°C deep freezer.

#### **Transformation of electro-competent *E. coli*:**

The ligations were dialyzed (Millipore, pore-size 0.025 µm, MF-membrane filters) for 20 min before being used for electro transformation. Dialyzed DNA was added to an aliquot of electro-competent cells that has been thawed on ice for 10 min. The mixed DNA with cells were transferred into an electroporation cuvette (Eurogentech) and shocked at 2500 V (Equibio, Easyject prima). The shocked products were re-suspended by 1 ml LB medium and incubated on a 200 rpm shaker at 37°C for 1 h. The cells were then pelleted down, re-suspended in 50 µl LB medium, and then streaked on an LB agar plate with the corresponding antibiotic, and incubated at 37°C overnight.

#### **Preparation of chemical competent *E. coli* cells:**

1% overnight incubated pre-culture of cells were transferred into 1 L LB medium (2 L flask) and incubated at 37°C with low shaking speed (150 rpm) until the OD<sub>600</sub> reached 0.5-0.7 (usually in 1.5-2 h). The culture was incubated on ice for 30 min before centrifugation at 4°C with 4500 rpm for 20 min. The supernatant was discarded and the pellet was re-suspended with 6.75 ml cold CaCl<sub>2</sub> solution (0.1 M) followed by mixing with 5.75 ml cold glycerine (50% (w/v)). The cells were split into aliquots of 250 µl in sterilized Eppendorf tubes and then shock-frozen in liquid nitrogen before being stored in a -80°C freezer.

#### **Transformation of chemical competent cells:**

An aliquot tube of competent cells was thawed on ice for 10 min and 1 µl of plasmid was added before an incubation on ice for 20 min. This step facilitates the attachment of plasmids to the cells. The tube containing the competent cells and the plasmids

mixture was heat shocked at 42°C for 1-2 min, which serves for the taking-in of plasmids into the cells. The tube was again incubated on ice for 10 min to recover the cells after the heat shock. 1 ml LB medium was added into the mixture which was then incubated on a shaker (200 rpm) at 37°C for 1 h. The cells were pelleted down by centrifugation for 30 sec at 8000 rpm, and the pellet was re-suspended with 150 µl LB medium. The cells were streaked on an LB agar plate with the corresponding antibiotic(s), and then incubated overnight at 37°C.

#### **2.4.7 Plasmid extraction**

Purification of plasmids from *E. coli* was performed either with the Plasmid DNA Mini Kit I (OMEGA) according to the standard protocol (for sequence) or with the quick and dirty plasmid extraction protocol. The sequence of DNA was determined by the sequencing service of Eurofins. Quick and dirty protocol is as following:

2 ml overnight culture was pelleted down in an Eppendorf tube by centrifugation at 8000 rpm at room temperature (RT) for 1 min. The pellet was re-suspended in 300 µl P1 and vortexed to assure its complete dissolution, followed by adding 300 µl P2 then gently mixing till the solution became homogenous, and finally 300 µl P3 were also mixed in gently. The mixture was incubated on ice for 5 min and then centrifuged at 4°C, 13.000 rpm for 15 min. The supernatant was next transferred (~900µl) to a new Eppendorf tube and 600 µl isopropanol were added, followed by a centrifugation at RT, 13000 rpm for 30~45 min. The supernatant was discarded, and the pellet was washed with 500 µl 70% ethanol (2-4 times, 10 min, 13.000 rpm and RT centrifuge). The ethanol was completely discarded with a pipette and the pellet was dried and then re-suspended in 35 µl ddH<sub>2</sub>O and stored in a -20°C freezer. P1: 5 ml Tris-HCl (pH 8, 50 mM), 1 ml EDTA (1 M), 10 mg RNase A, the volume was completed with ddH<sub>2</sub>O to a total volume of 94 ml. P2: 10 ml SDS (10% w/v), 20 ml NaOH (1 M), 70 ml ddH<sub>2</sub>O. P3: 60 ml (5 M) KC<sub>2</sub>H<sub>3</sub>O, 11.5 ml Actic Acid, 28,5 ml ddH<sub>2</sub>O.

#### **2.4.8 *B. subtilis* competence cell preparation and transformation**

##### **Preparation of competent *B. subtilis* cells:**

*B. subtilis* is naturally competent during the early stationary phase of its growth, which allows it to take up exogenous DNA. If the exogenous DNA bears homology to regions on the chromosome, it can get incorporated into the genome via homologous

recombination [146, 147]. The *B. subtilis* strain to be driven to competence was streaked on LB agar plate with the corresponding antibiotic(s) at 30°C overnight. Fresh SpC medium with the adequate antibiotic(s) was prepared and inoculated from *B. subtilis* plate and then incubated in a shaking platform at 37°C. After 3 hours of growth, the OD<sub>600</sub> was measured every 30 min until a steady read from two subsequent time intervals was reached indicating the entry of cells in the stationary phase (OD<sub>600</sub>=3~6). The culture was then transferred into 50 ml SpII and incubated at 37°C for 90 min in a 200 rpm shaking incubator. Afterwards, the culture was centrifuged at 4500 rpm for 20 min at RT to pellet down the cells. 4.5 ml of the supernatant were collected in a separate falcon tube while the rest of the volume was discarded. The pellet was re-suspended in the saved 4.5 ml supernatant mixed with 0.5 ml 50% (v/v) glycerol, and then 500 µl aliquots were transferred into sterile Eppi-Tubes (Eppendorf) that were subsequently shock-frozen in liquid nitrogen before being stored in a -80°C freezer.

#### **Transformation of competent *B. subtilis* cells:**

500 µl aliquots of competent *B. subtilis* cells were thawed at RT. Out of the 500 µl, 125 µl of cells were aliquoted into 3 sterile Eppendorf tubes. The first tube was used as a control without plasmid DNA. 3 µl plasmid DNA were added (or 0.2 µl chromosomal DNA) to the second tube, and 6 µl plasmid DNA (or 0.4 µl chromosomal DNA) were added to the third tube. The three tubes were incubated at 37°C for 30 min on a shaking incubator. Afterwards, the cells were plated on LB agar plates with the appropriate antibiotic(s). The plates were incubated at 30°C overnight or 2 days. T-Base Buffer (10×): 20 g (NH<sub>4</sub>)<sub>2</sub>SO<sub>4</sub>, 182 g K<sub>2</sub>HPO<sub>4</sub>·3 H<sub>2</sub>O, 60 g KH<sub>2</sub>PO<sub>4</sub>, 10 g Trisodium citrate·2 H<sub>2</sub>O. The volume was completed with ddH<sub>2</sub>O to 1 L. SpC (to be prepared fresh): 4 ml 10×T-Base, 0.4 ml 50% (w/v) Glucose, 0.6 ml 1.2% MgSO<sub>4</sub>·7 H<sub>2</sub>O, 1 ml 1% Casamino acids, 0.8 ml 10% Bacto Yeast extract. The volume was completed with ddH<sub>2</sub>O to 40 ml. SpII (to be prepared fresh): 10 ml 10×T-Base, 1 ml 50% (w/v) Glucose, 7 ml 1.2% MgSO<sub>4</sub>·7 H<sub>2</sub>O, 1 ml 1% Casamino acids, 1 ml 10% Bacto Yeast extract, 0.5 ml 0.1 M CaCl<sub>2</sub>. The volume was completed with ddH<sub>2</sub>O to 100 ml.

#### **2.4.9 SDS Poly-acrylamide gel-electrophoresis (SDS-PAGE)**

Proteins were denatured and separated according to their molecular weight by SDS-PAGE, which can also determine the purity of proteins. Discontinuous gels were prepared according to the protocol of Laemmli [148]. The thickness of the running Gel used was dependent on the molecular weight of protein: 12% acrylamide was used for bigger proteins and 15% for the smaller proteins. The stacking gel used was standard with 4% of acrylamide. The gels were prepared with PerfectBlue Dual Gel System casts. Protein samples were mixed with 2×SDS Loading Buffer and heated at 97°C for 10 min before loading into the lanes of SDS-PAGE gel. The electrophoresis was done in 1×SDS running buffer with a constant voltage of 180 V.

SDS-PAGE Running Buffer: 25 mM Tris (hydroxymethyl) aminomethane, 250 mM Glycine, 0.1% (w/v) Sodium dodecylsulphate. The pH was adjusted to 8.3 by HCl.

2×Loading Buffer: 50 mM Tris (hydroxymethyl) aminomethane, 5% (v/v) Glycine, 1% (w/v) Sodium dodecylsulphate (SDS), 1.5% (v/v) β-mercaptoethanol, 0.05% (w/v) Bromophenol blue. The pH was adjusted to 6.8 by HCl. Running Gel (12%, 10 ml): 3.3 ml ddH<sub>2</sub>O, 4.0 ml Rotiphorese Gel 30 (30% Acrylamid (w/v), 0.8% *N-N'*-Methylenbisacrylamid), 2.5 ml Tris (hydroxymethyl) aminomethane pH 8.8 (1.5 M), 0.1 ml 10% (w/v) SDS, 0.1 ml 10% (w/v) APS, 0.004 ml TEMED. Stacking gel (5%, 4 ml): 2.7 ml ddH<sub>2</sub>O, 0.67 ml Rotiphorese Gel 30 (30% Acrylamid (w/v), 0.8% *N-N'*-Methylenbisacrylamid), 0.5 ml Tris (hydroxymethyl) aminomethane pH 6.8 (1 M), 0.04 ml 10% (w/v) SDS, 0.04 ml 10% (w/v) APS, 0.004 ml TEMED. The SDS-PAGE gels were stained by Coomassie Brilliant Blue in staining solution at room temperature for 1 h on a rotating platform. Stained gels were then incubated in destaining solution until the unbound dye was removed. The gels were then imaged with an imaging system (Biorad). Staining Solution: 0.1% Coomassie Brilliant Blue R250, 40% Methanol, 10% Acetic Acid. Staining was done for 1-2 h or overnight. De-Staining Solution: 10% Methanol, 10% Acetic acid. Destaining was done for 3-10 h. The solution was exchanged with a fresh one until the protein bands were clear enough to be visualized by eye.

#### **2.4.10 Immunoblot analysis**

Specific proteins can be more precisely detected by protein immuno-staining. After proteins were separated by size on SDS-PAGE gel, they were transferred to a

nitrocellulose membrane (Immobilon-P, Millipore) by using the semi-dry-blot method. Three layers of Whatman papers were placed on the cathode of Bio-Rads Trans-Blot SD semi-dry transfer cell after soaking them in transfer buffer. A nitrocellulose membrane was activated in MilliQ water and placed on three layers of Whatman papers. The SDS-PAGE gel was placed on top of the nitrocellulose membrane, and the other three layers of soaked Whatman papers were placed on the gel. After the air bubbles were removed, the proteins were transferred at 25 V for 30 min. After blotting, the un-specific sites on the membrane were blocked by incubating overnight in 5% (w/v) skimmed milk in PBST buffer on a shaking platform. This step is crucial for preventing the unspecific interactions between membrane and antibody. Primary antibody pre-mixed with 5% milk in PBST buffer was added to the membrane and incubated on a shaking platform for 1 h. The membrane was washed three times (each time for 10 min) in PBST buffer to get rid of the excessive antibody. The second antibody mixed with 5% milk in PBST buffer was added to the membrane and incubated for 1 h. The membrane was washed again three times by PBST buffer. Then the membrane was developed by incubating with the mixture of solution 1 and solution 2 for 2 min. After the oxidation of luminol by hydrogen peroxide with an emission of low intensity X-ray light, the chemiluminescence was detected with a UV imaging system (Molecular Imager ChemiDoc XRS System, Biorad). For the strep-tagged proteins, only one antibody was used, and the skimmed milk was replaced by 3% (w/v) BSA (Bovine Serum Albumin), the rest steps and chemicals were the same.

1×PBST Buffer: 3.45 g  $\text{Na}_2\text{HPO}_4$ , 9 g  $\text{NaH}_2\text{PO}_4$ , 17.5 g  $\text{NaCl}$ , 3 ml Tween 20. Volume was completed to 3 L with distilled water. Transfer Buffer: 5.81 g Tris (hydroxymethyl) aminomethane (48 mM), 2.98 g Glycin (39 mM), 0.35 g SDS (1.3 mM), 200 ml Ethanol (20%). Volume was completed with ddH<sub>2</sub>O to 1 L, there was no need to adjust pH and the final pH is 9.8. Solution 1: 8.85 ml ddH<sub>2</sub>O, 1 ml Tris (hydroxymethyl) aminomethane (1 M, pH 8.5), 100 µl Luminol (250 mM), 40 µl Coumaric acid (90 mM). Solution 2: 9 ml ddH<sub>2</sub>O, 1 ml Tris (hydroxymethyl) aminomethane (1 M, pH 8.5), 6 µl H<sub>2</sub>O<sub>2</sub> (30%).

#### **2.4.11 Gibson Assembly**

GA (Gibson Assembly) is capable of multiple DNA fragments assembly regardless of fragment length and end compatibility. Multiple overlapping of DNA fragments can

be done in a single tube isothermal reaction. The vector we used for GA was pSG1164-NLMV. Genomic DNA of *B. subtilis* PY79 was used as template, and the primers were designed to contain homologous overhangs to the vector. The PCR was performed as in Table 4. PCR products were purified with PCR purification Kit (Sigma), and the concentration of DNA was measured by Nanodrop or agarose gel electrophoresis.

PCR mixture system		PCR program		
Template DNA	1.0 $\mu$ l	98°C	30 s	×29
dNTPs (20mM)	1.0 $\mu$ l	98°C	10 s	
Forward primer(10 $\mu$ M)	2.5 $\mu$ l	Tm	30 s	
Reverse Primer (10 $\mu$ M)	2.5 $\mu$ l	72°C	1 min	
HF Buffer (5x)	10 $\mu$ l	72°C	10 min	
Phusion	0.5 $\mu$ l	16°C	$\infty$	
ddH <sub>2</sub> O	32.5 $\mu$ l			

Table 4. PCR system and program of Gibson Assembly.

500 ng-1  $\mu$ g of plasmid pSG1164-NLMV was digested with restriction enzymes *Apa*I and *Eco*RI-HF. The reaction mixture used was: 500 ng-1  $\mu$ g plasmid, 5  $\mu$ l NEB Buffer 4, 5  $\mu$ l BSA (1×), 1.5  $\mu$ l *Apa*I, 1.5  $\mu$ l *Eco*RI-HF, completed with ddH<sub>2</sub>O to a volume of 50  $\mu$ l. The mixture was incubated in a thermocycler at 25°C for 1.5 h and then at 37°C for another 1.5 h. The digested linear plasmid was purified after separation on 1% agarose gel with a gel extraction Kit. DNA was eluted into 30-50  $\mu$ l ddH<sub>2</sub>O and the concentrations was measured by the Nanodrop. The linear plasmid was used for the GA. The GA reaction mixture was as follows: 150 ng plasmid, 50 ng insert, 5  $\mu$ l Gibson Master Mix (2x), completed with ddH<sub>2</sub>O to 10  $\mu$ l. The volume of plasmid and insert was 5  $\mu$ l. The final mixture was incubated in a thermocycler at 50°C for 60 min. Following the incubation, the assembly products were transformed into competent *E. coli* cells and the transformed plasmids were purified, performed test digest and sequenced. The success of the procedure and the integration of the insert were verified with a test digest and positive digestion products were sequenced.

## 2.5 Protein overexpression and purification

### 2.5.1 Expression test

The C-terminal of *B. subtilis* *lytC* was cloned in pPR-IBA101 (IBA Bio-TAGnology) upstream of the One-Strep-tag. The construct was transformed into competent *E. coli* BL21 for protein overexpression. The N-terminal fusion of His-*lytC* tag was ligated with pGAT3 vector downstream of the GST tag. To test if LytC protein was successfully expressed by the *E. coli* host, 4 ml of LB culture with Amp were used for the incubation of the desired strain and the culture was incubated on a shaking incubator with 200 rpm at 37°C until the OD<sub>600</sub> reached a value between 0.5 and 0.8. The cells were then induced with 0.5 mM IPTG and further incubated for another 2 h. Following the incubation period, 2 ml of cell culture were pelleted down, re-suspended in 50 µl ddH<sub>2</sub>O, and mixed with 2×SDS loading dye. The samples were then heated at 97°C for 10 min. 15 µl of each sample were loaded into an SDS-PAGE gel, and the results were analyzed by western blot membrane.

### 2.5.2 Expression and purification of Strep-tagged LytC in *E. coli* BL21

The strep-tag purification system is based on the highly selective binding of engineered streptavidin, which allows purification of recombinant proteins *in vitro* while preserving their biological activities. This is mainly due to the fact that the small size of the strep-tag makes its effects on the tagged protein in terms of structure and folding small or even negligible. The *E. coli* BL21 strain containing the cloned construct that was verified in the above mentioned expression test was inoculated in a 2 L Erlenmeyer flask containing 1 L LB medium and Amp. Cells were incubated at 37°C on 150 rpm shaking incubator. When cells reached exponential phase (OD<sub>600</sub> 0.5~0.8), they were induced with 0.5 mM IPTG and then moved to 30°C, 150 rpm. Cells were harvested after 60 min of incubation by centrifugation for 20 min at 4,500 rpm, 4°C (BECKMAN COULTER Avanti J-26 XP centrifuge, JLA 9,1000 rotor). The pellet was re-suspended in 1×PBS buffer, and then the cells were pelleted down again by centrifugation (BECKMAN COULTER Allegra X-15R) at 4,000 rpm, 4°C for 20 min. The collected pellet was stored at -80°C or -20°C for further use. On the day the experiments were resumed, the pellet was thawed on ice and cells were re-suspended in 20 ml strep wash buffer with added protease inhibitor (Complete, Roche). Cells were then lysed by French-Press by two passes at 20,000 psi, and the

lysate was centrifuged at 4°C and 16000 rpm for 30 min (JA-25.50 rotor). The supernatant was filtered through a 0.20 µm membrane filter and the filtrate was kept on ice for later loading on the affinity chromatography column. PBS Buffer (10×Phosphate buffered saline): 16.2 mM Disodium hydrogen phosphate, 50 mM Sodium dihydrogen phosphate, 100 mM Sodium chloride.

### **Purification of LytC-strep recombinant protein**

Strep-tagged LytC was purified by affinity chromatography using gravity flow columns with 1 ml of strep tacin sepharose (IBA). Columns were equilibrated by applying 10 CV (column bed volume) strep-tag washing buffer (100 mM Tris HCl, 150 mM NaCl, 1 mM EDTA, pH 8.0). 0.5 to 10 CV of the clear filtered lysate were then loaded on the equilibrated columns. Once all the lysate has passed through the columns, unspecific bound proteins were washed away with 10 CV strep-tag washing buffer. The column bound strep-tag proteins were then eluted with 3 ml of strep-tag elution buffer (100 mM Tris-Hcl, 150 mM NaCl, 1 mM EDTA, 2.5 mM D-desthiobiotin, pH 8.0) and collected in 0.5 ml fractions. Columns were regenerated by 15 CV of strep-tag regeneration buffer (100 mM Tris-HCl pH 8.0, 150 mM NaCl, 1 mM EDTA, 1 mM HABA, hydroxy-azophenyl-benzoic acid), HABA was then removed and columns were equilibrated by adding 10 CV washing buffer. The columns were then stored at 4°C overlaid with 2 ml washing buffer. All the above steps were performed at 4°C, the elution fractions will be analyzed by SDS-PAGE and western-blotting and for further analysis.

### **2.5.3 Expression and purification of His-tagged LytC in *E. coli* BL21**

The pGAT3 with the GST-His-LytC N-terminal fusion was cloned in *E. coli* BL21 and an expression test was made as described above for the C-terminal fusion. The subsequent steps of incubation and lysate preparation were identical to those described for the strep-tagged LytC construct. His-tag columns were used for purification of Histidine-tagged recombinant proteins by immobilized metal ion affinity chromatography (IMAC). The high-performance matrix of the Ni-sepharose medium provides a convenient way in protein separation since it has a low nickel ( $\text{Ni}^{2+}$ ) ion leakage and is compatible with a wide range of additives used in protein purification. His-LytC was purified by IMAC using gravity flow columns with 1 ml of Ni-sepharose bed (GE Healthcare). Columns were first washed by at least 5



column volumes of distilled water or binding buffer. The filtered lysate was then applied to the column, washed with 10-15 CV binding buffer, and finally eluted with at least 10 fractions of 0.5 ml elution buffer. Fractions were either stored for further usage or immediately used for other experiments. The used columns were stripped by washing with at least 5-10 CV of stripping buffer, followed by 5-10 CV of binding buffer and 10 CV of distilled water. The stripped column were then recharged by loading 0.5 ml of 0.1 M NiSO<sub>4</sub> in distilled water, and finally washed with 5 CV distilled water and 5 CV binding buffer (to adjust the pH) and stored in 20% ethanol at 4°C. Binding buffer: 20 mM sodium phosphate, 0.5 M NaCl, 20 mM imidazole. Elution buffer: 20 mM sodium phosphate, 0.5 M NaCl, 500 mM imidazole. Stripping buffer: 20 mM sodium phosphate, 0.5 M NaCl, 50 mM EDTA. pH7.4.

#### **2.5.4 Gel filtration**

Gel filtration chromatography separates proteins on the basis of their sizes. Protein molecules pass through a bed of porous beads, enter into the beads. Smaller protein molecules enter further into the pores of the beads and thus move slowly to pass through the bed, while larger protein molecules enter less or not at all into the pores of the beads and therefore move quicker to pass through the bed. Both molecular weight and 3-dimensional shape determine the degree of retention. To remove unspecific proteins from purified samples, gel filtration was carried out by affinity chromatography using an ÄKTApurifier (GE Healthcare) and a gel filtration column (Superdex 200 10/300 GL, GE Healthcare). The column was equilibrated with strep-tag washing buffer prior to loading the protein samples. The column was then flushed with the same buffer at a flow rate of 2.0 ml/min at 4°C and the fractionation was programmed to collect 30 fractions of 1 ml volume. The fractions were then tested for purity by SDS-PAGE and the identity of the protein was confirmed by western-blot.

#### **2.5.5 Concentration of proteins by Ultrafiltration**

Ultrafiltration was used in order to concentrate proteins by passing the purified protein samples through concentrator columns (Sartorius Stedim Biotech, 50 kDa, 30 kDa, 10 kDa MWCO PES). A total of 6 ml of proteins in buffer were added to the columns, followed by centrifugation at 4000 rpm, 4°C until a volume of only 1 ml was retained above the filter.

### 2.5.6 Bradford protein assay

Protein concentration was measured by Bradford with BSA (Bovine Serum Albumin) as a standard. Gradient concentrations of BSA (from 2.5-100 µg/ml) and different dilutions of tested protein samples were prepared. Protein samples were mixed with 5×Bradford solution to a volume of 200 µl and then with ddH<sub>2</sub>O to a final volume of 1 ml. The mixture was incubated at room temperature for 30 min and the absorption of the control containing BSA alone and of protein samples were measured. The absorption values of BSA dilutions were plotted against the respective concentration and the curve was used to calculate the concentration of desired proteins. 5×Bradford Solution composition: 100 mg/l Coomassie Blue, 5% (v/v) Ethanol, 10% (v/v) H<sub>3</sub>PO<sub>4</sub>.

## 2.6 Fluorescence Microscopy

The genetically-encoded fluorescent proteins (FPs) were used as reporter dye molecules for *in vivo* fluorescence microscopy imaging, which is a powerful and well characterized experimental method for inquiring biological processes in intact cells [149]. The naturally green fluorescent protein (GFP) was first discovered in 1962 and produced by the marine jellyfish, *Aequorea victoria* [150]. The natural form of GFP has an excitation wavelength of ~395 nm. Cloning of this gene in 1992 was a milestone in the laboratory applications of GFP [151, 152]. The successful expression of GFP in several foreign hosts (eukaryotes and prokaryotes) demonstrated that for the luminescence there is no need for jellyfish specific biological catalysts [153, 154]. Controlled mutation of *gfp* gene by molecular biology can produce brighter, faster mature proteins than the natural GFP, mutated GFP can be excited with visible light over a wide range of wavelengths [155]. The GFP variant genes can be fused as fluorescent tags to unrelated proteins in a foreign organism. The use of the GFP family as molecular dyes in living cells has increased tremendously over the last decade and became widely used to investigate biological processes [156-158]. The GFP tag can be excited and the fluorescence of single molecules visualized in functional living organisms with advanced microscopy techniques [159-161].

### 2.6.1 Cell growth and sample preparation

All *B. subtilis* and *E. coli* strains used for fluorescence microscopy were grown at 30°C in S7<sub>50</sub> minimal medium, which was complemented with 0.002% casamino

acids and necessary antibiotics. For the strains that have a xylose promoter, the glucose in S7<sub>50</sub> was exchanged for 0.5% fructose, and 0.5% xylose was added for induction. If the cultures needed to be incubated overnight, it was done at 25°C. The cells were then diluted into fresh medium with a ratio of 1:100, and incubated on a 200 rpm rotary shaker at 30°C until they were ready to use (usually exponential phase). 3.5 µl cells were transferred to a glass slide (Roth, Microscope slides standard) coated with an agarose layer and then covered with an objective slip (Roth, Cover slips). The slide agarose was made by dissolving 1% agar in S7<sub>50</sub> minimal medium (10 mg/ml molecular standard agarose).

### **2.6.2 Fluorescence microscopy stains**

The fluorescence microscopy and conventional light microscopy were performed by using the Zeiss TIRF microscope with an oil immersion objective (1.45 numerical aperture, 100×magnification) and a CCD camera. If necessary, DNA were stained with 0.2 ng/ml blue fluorescent dye DAPI (4'6-diamidino-2-phenylidole) in cell culture and incubated for 2 min at RT. DAPI preferentially binds AT clusters in the minor groove of double stranded DNA and can be used in living cells due to its ability to pass through the membrane. DAPI stain was excited with 358 nm wavelength and visualized at 460 nm. Cell membranes were stained by FM4-64 (which is a non-toxic lipophilic styryl compound) with a final concentration of 2.5 mg/ml and excited at 515 nm and observed at an emission of 640 nm in the red range.

### **2.6.3 Image acquisition**

Fluorescence microscopy images were obtained with the digital camera (EM-CCD camera, Photometric Cascade). The microscopy was controlled and recorded with the Metamorph 7.5.5.0 program (Molecular Devices, Sunnyvale, USA). The program can also be used to calibrate the intensity of fluorescence and specify the cell length according to pixel size. The filter setup used was as follows: yellow 475-525 nm (excitation wavelength) and 505-565 nm (emission wavelength); red 534-558 nm (excitation wavelength) and 575-640 nm (emission wavelength). All fluorescence microscopy and bright-field photos were processed by the ImageJ program (by Wayne Rasband at National Institutes of Health) with corresponding plugins.

## 2.7 Single molecule microscopy

Fluorescence microscopy offers a minimally perturbative approach to probe biology *in vivo*, but the traditional techniques are limited in sensitivity and resolution. Many biological processes happen on a timescale of milliseconds, and it is hard to study the proteins function at single molecule level. A new imaging system that can detect and quantify fluorescent proteins at the single molecule level has been developed. In this system, the microscopy is customized with a illumination mode called 'slimfield'. The excitation intensities of slimfield is  $\sim 100$  times greater than the wide-field, slimfield is also a cheap and simple approach, which allow single-molecule detection at high speed [149]. Slimfield facilitates millisecond time scale imaging of single molecule, and the time scale is fast enough to catch the diffusional motion and molecular transitions in the cytoplasm [162].

A laser with appropriate intensity is used to excite the single fluorescent molecule and the emitted light is captured by a high-sensitivity video camera [163]. In the heterogeneous solvated environment of the living cell, a major task of single-molecule-microscopy is to reduce the background noise to produce an contrast that is sufficient to detect the single-molecule-signal [149]. An optimized low background epifluorescence microscopy (LBEFM) is used to visualize the movement of single fluorophores [164, 165]. Total internal reflection microscopy (TIRF) is another high-contrast mode of fluorescence illumination, which can be used with slimfield to visualize single fluorescence proteins in or near the membrane [165, 166]. However, this method cannot monitor processes occurring in cytoplasm [149]. Other illumination modes can be used for imaging the cytoplasm of cells, confocal fluorescence microscopy offers a high resolution for functional biological imaging [167, 168]. Resolution improvements in deep *in vivo* can be achieved by using multi-photon excitation, this technique has been used at single-molecule level to visualize organic dye molecules [149, 169]. An expanded illustration of the slimfield mode is shown in Figure 7.

The fluorescence excitation field is reduced to encompass only a single cell in slimfield microscopy. Slimfield creates a relatively compact Gaussian laser excitation field ( $\sim 30 \mu\text{m}^2$ ) compared to widefield epifluorescence microscopy. The fluorescence

emission intensity is then higher than the readout and dark noise of the camera detector, which is suitable for single-molecule detection and with high signal intensity [149, 170]. In the excited area, most of the fluorescence protein signals are fast bleached until only a few non-bleached molecules are left to be tracked. A stream of images is captured by the camera to record the trajectory of single molecules.

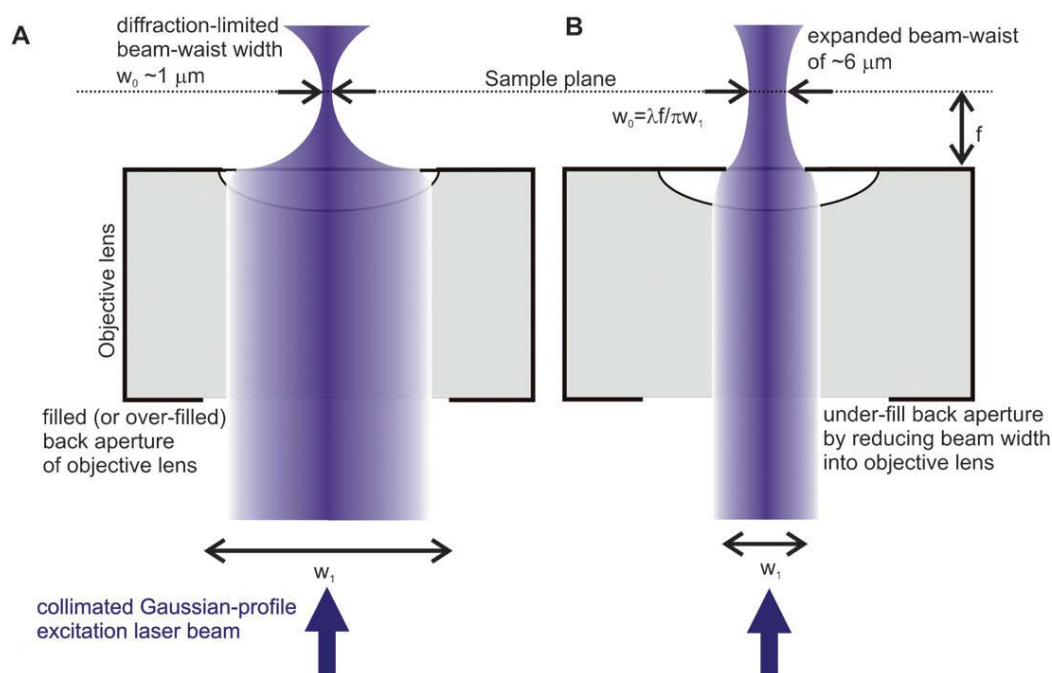


Figure 7. Cartoon depicts the excitation modes of confocal and slimfield. A is the conventional confocal microscopy, B is the slimfield illumination mode. Image taken from the work of Michael Plank, 2009 [149].

### 2.7.1 Sample preparation for single molecule microscopy

The objective slips were washed ultrasonically cleaned in 2% Hellmanex III solution for 10 min and subsequently dried by Elix Clean 720 GAS, then 3.5  $\mu\text{l}$  fresh cell culture were transferred onto the slide and covered with an agar-pad (1% high molecular grade agar dissolved in S7<sub>50</sub>).

### 2.7.2 Single molecule microscopy

Single molecule microscopy was performed in order to gain insights on proteins dynamic and movement in living *B. subtilis* cells. All the proteins were tagged with a yellow fluorescent protein (YFP). Cells were imaged with a NIKON microscope equipped with a back-illuminated EM-CCD camera and modified to have a slimfield setup. The objective used has a 1.45 light aperture. The excitation laser was focused

onto the back focal plane of the objective to increase the illumination, 10 mW of laser power were used at the sample plane within a square of  $25 \times 25 \mu\text{m}$  and the time interval used was 10 ms. The intensity of fluorescence in the stream decreased from the center of the imaged area to the edges and the number of single molecules dropped with time because of bleaching. The movies were between 1000 and 5000 frames long. If not mentioned otherwise, all the constructs in *B. subtilis* used for single molecule microscopy were expressed under the xylose promoter.

### **2.7.3 Single molecule tracking and track analysis**

The tracking analysis of single molecule data was done with plugins of MTrackJ/TrackMate on ImageJ, or by u-track-2.3.1 that was specifically written for MatLab. The obtained tracking data were analyzed by msd-analyzer in MatLab. Only the desired area of the recorded movies was cropped and the format was converted from RAW to TIFF through ImageJ. Trajectories that consist more than 5 frames were considered as a track and be used for further analysis.

### **2.7.4 Calculation of the diffusion constants (diffusion coefficient) by MSD**

Mean square displacement (MSD) analysis is a commonly used technique in biophysics study to determine the displacement mode (freely diffusing, transported, bound) of particles over time. And MSD analysis can also help to determine the diffusion coefficient of the particles movement. Msd-analyzer is a MATLAB tool that use for performing MSD analysis. The plot of MSD value can describe the diffusing movement of the particle. The MSD was calculated for each individual trajectory, and its log-log representation was fitted with a linear function. The slope of MSD line gives us the diffusion coefficient. The MSD for each single particle is also taken as a mean value. By default, the fit is only made on the first 25% of the curve and automatically calculated by msd-analyzer.

## 3 Results

### 3.1 Inhibition study of different constructs of protein LytC *in vitro*

#### 3.1.1 Design of *lytC* gene constructs

C-terminal strep-tag fusion of *lytC* constructs were cloned into pPR-IBA101 vector and further expressed in *E. coli* BL21(DE3) cells. The products of each recombinant fusion protein were measured by SDS-PAGE and immunoblot analysis. We predicted LytC structure with the SMART tool from Heidelberg University. The predicted LytC protein structure has a trans-membrane domain at the N-terminus (a.a. 7-24). Since we need to purify LytC in a soluble state, therefore, we removed the trans-membrane domain. In the middle of LytC, there is one low-complexity-region (LCR, a.a. 197-214) and three cell-wall-binding (CWB) domains. The functional region (a.a. 380-492) of catalytic domain is located at the C-terminus of LytC. In order to narrow down the N-terminal region that is important for lyse activity of LytC, regions in front of functional region were truncated into fragments of decreasing length and the lyse activity was measured respectively. To study the roles of these domains in LytC, we designed 6 constructs (Figure 8).

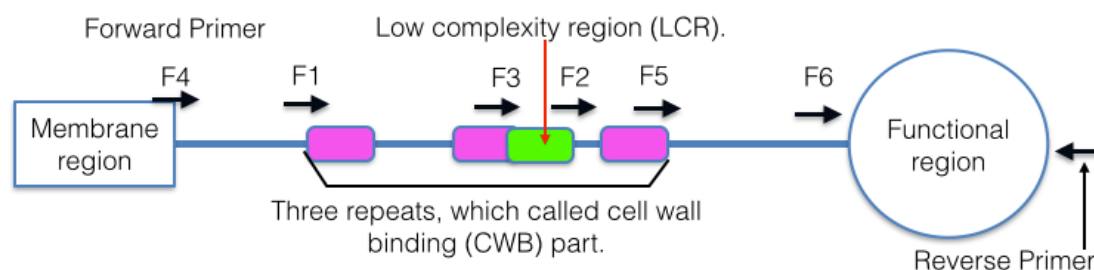


Figure 8. Schematic of LytC structure and *lytC* constructs. The rectangle stands for the trans-membrane domain, we removed this part since we want to purify soluble proteins. The round circle is the functional domain that catalyzes the cleavage of cell wall component PG. The small purple rectangle represents cell-wall-binding domains in LytC protein, which help LytC to bind with cell wall. The small green rectangle is the low-complexity-region. F1-F6 are the forward primers (I named each of my constructs by *lytC*+forward primer, e.g. *lytCF2* means the construct with F2 as forward primer, all the constructs have the same reverse primer), the black arrows stand for the start sites of each primer.

Table below is a brief summary of all the LytC constructs and feedback. The detail of each construct and the inhibition test results were displayed in the following chapters.

Name	Primers	Domains	Results
LytCF1	LytCEcoRIF1/LytC XhoIR	Two CWB, the LCR and the FR.	Purification failed.
LytCF2	LytCEcoRIF2/LytC XhoIR	One CWB and the full length of FR.	Inhibition tests on <i>E. coli</i> and <i>B. subtilis</i> were positive (Figure 15).
LytCF2R2	LytCEcoRIF2/lytc xhoi R2	One CWB and 22 a.a. deleted FR.	Inhibition tests on <i>E. coli</i> and <i>B. subtilis</i> were positive but the activity was much lower than LytCF2 (Figure 24).
LytCF3	LytCSacIIF3/LytC XhoIR	Half LCR, one CWB and the FR.	Inhibition test on <i>E. coli</i> was positive (Figure 15 D).
LytCF4	LytCSacIIF4/LytC XhoIR	Three CWB, the LCR and the FR.	Inhibition test on <i>E. coli</i> was positive (Figure 16 A).
LytCF5	LytCSacIIF5/LytC XhoIR	Region after CWB and FR.	Inhibition tests on <i>E. coli</i> and <i>B. subtilis</i> were positive (Figure 17 and Figure 18).
LytCF5-E342Q	lytcE342F/lytcE342R	Region after CWB with E342Q mutation.	Inhibition tests on <i>E. coli</i> and <i>B. subtilis</i> were positive (Figure 22).
LytCF5-E461Q	lytcE461F/lytcE461R	Region after CWB with E461Q mutation.	Inhibition tests on <i>E. coli</i> and <i>B. subtilis</i> were positive (Figure 22).
LytCF5-E342Q-E461Q	LytCecoriCF/LytC xhoiCR	Region after CWB with E342Q and E461Q mutation.	Inhibition test on <i>E. coli</i> was positive (Figure 23).
LytCF6	LytCEcoRIF6/LytC XhoIR	The FR domain.	Inhibition test on <i>E. coli</i> was positive (Figure 16 B).
GST-His-LytCF1	GST-F1/GST-R	Same as LytCF1	Purification failed.
GST-His-LytCF2	GST- F2/GST-R	Same as LytCF2	Purification failed.
GST-His-LytCF3	GST- F3/GST-R	Same as LytCF3	Purification failed.
GST-His-LytCF4	GST- F4/GST-R	Same as LytCF4	Purification failed.
GST-His-LytCF5	GST- F5/GST-R	Same as LytCF5	Purification failed.
GST-His-LytCF6	GST- F6/GST-R	Same as LytCF6	Inhibition test on <i>E. coli</i> was positive (Figure 16 C), but the activity was much lower than LytCF6.



Table 5. Summary of *lytC* constructs and the inhibition results. The trans-membrane domain was removed in all *lytC* constructs. LytC remains the catalytic activity as long as the full length of FR kept. Two amino acids mutation in FR domain does not reduce the activity of LytC, which means E342 and E461 amino acids are not important for LytC. 22 amino acids deletion of C-terminus of FR domain can reduce the lyse activity of LytC greatly, indicating that LytCF2 contains the full length of FR and the FR domain remains the lyse activity. All the LytC constructs without His label were fused to strep-tag at the C-terminus. CWB: cell-wall-binding domain. LCR: low-complexity-region. FR: functional region.

### **3.1.2 Purification of constructed protein LytCF2**

*E. coli* cells with recombinant proteins were pelleted down by centrifugation, and further lysed by French-Press. The supernatants that contain the recombinant proteins were purified through affinity chromatography strep-tactin columns. The expression and purification of each LytC constructs was confirmed by SDS-PAGE and Immunoblot analysis. In the Immunoblot analysis, the band that corresponds to the strep-tagged proteins should be detected according to the corresponding molecular weight (MW). Before the purification of LytC, test overexpression of each construct was confirmed by SDS-PAGE and western-blot. Since LytCF2 is the first positive construct we obtained, we chose LytCF2 for the selection of host strain and the optimization of growth condition. The selected host strain, growth condition were used for the remaining LytC protein overexpression.

#### **LytC kills host *E. coli* strain during overexpression step**

During the incubation process of protein overexpression, we found that LytCF2 is toxic and can inhibit the growth of *E. coli* BL21 cells. After inducing with 0.5 mM IPTG, the OD<sub>600</sub> of *E. coli* dropped dramatically within 1 hour (e.g. from 0.7 to 0.33) (Figure 9). However, if the cells were induced with 1 mM IPTG, the cells grew normally (data not shown). We used both 0.5 mM IPTG and 1 mM IPTG for LytCF2 overexpression and purification. According to the SDS-PAGE staining and followed immunoblot analysis, much less protein was obtained from the culture induced with 1 mM IPTG than the one with 0.5 mM IPTG (data not showed), thus we used 0.5 mM IPTG for the remaining experiments.

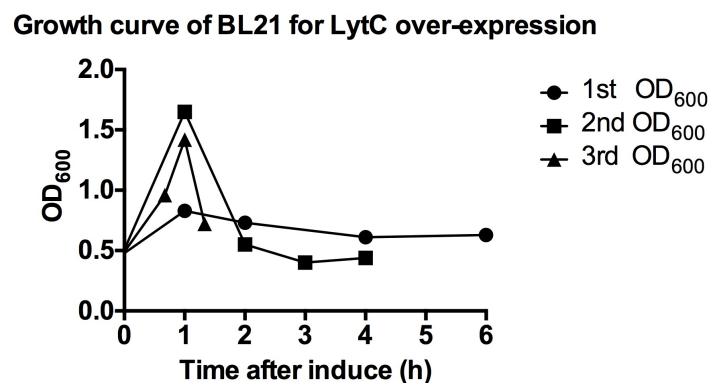


Figure 9. Growth curve of BL21 during LytCF2 overexpression, culture were induced with 0.5 mM IPTG. The time interval is 40 min. In all three times experiments, we observed the OD<sub>600</sub> start to drop after 1 hour incubation. For the 2nd experiment, the OD<sub>600</sub> continue increasing in 40 min but dropped in 1 hour after induction. 1st, the first experiment. 2nd, the second experiment. 3rd, the third experiment.

### The optimization of host strain and growth condition

At the beginning, we used *E. coli* BL21 (DE3) and Rosetta 2 (DE3) for the test overexpression of LytCF2. After cells lysed, the remaining LytCF2 in Rosetta pellet was much larger than the BL21 pellet (Figure 10 C). Therefore, BL21 was used as host for the remaining LytC protein overexpression experiments. LytCF2 has a molecular weight of around 36 kDa, the purity of purified LytCF2 was tested by SDS-PAGE and western-blot (Figure 10 A and B). The bigger bands (the white ellipses of Figure 10 A) above LytCF2 were confirmed to be chaperones by MS-SPEC measurement. The bands that smaller than LytCF2 band might be the un-correct folded or lysed protein. The expression level of LytCF2 did not fulfill our expectation, and the low temperature overexpression is usually used for low expression protein. Therefore we perform the low temperature overexpression for LytCF2. However, production level of low temperature was not increased in comparison with 30°C overexpression (data not shown). Thereby, overexpression of all LytC proteins were performed at 30°C.

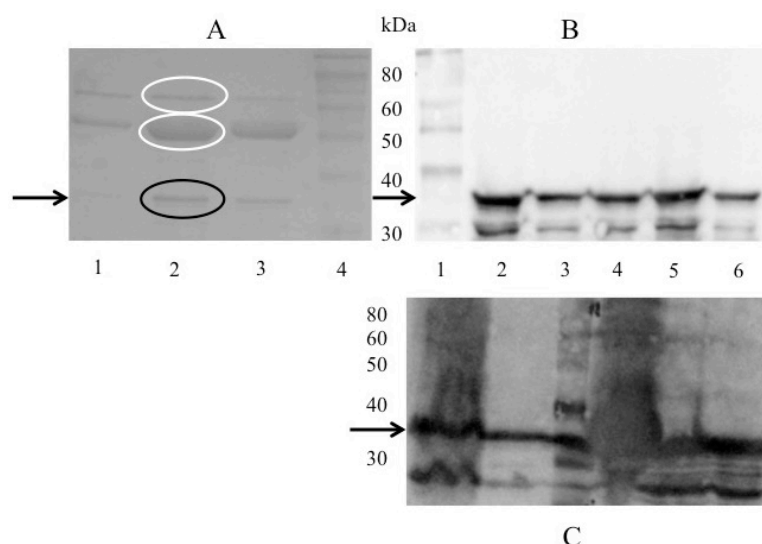


Figure 10. SDS-PAGE and western-blot results of purified LytCF2. (A): The SDS-PAGE image of purified LytCF2, lanes 1, 2 and 3 stand for different fractions of LytCF2 after purification by strep-tactin column, lane 4 represents prestained protein ladder (NEB). (B) Western-blot image: 1 is protein ladder, 2, 3, 4, 5 and 6 are different fractions of purified LytCF2. (C) Western-blot image: 1 is the BL21 pellet after cell lysis, 2 is the purified LytCF2 with BL21 as host, 3 is prestained protein ladder, 4 is the pellet after cell lysis using Rosetta 2(DE3) as host, 5 and 6 are two fractions of purified LytCF2 using Rosetta 2(DE3) as host. The black arrows and the black ellipse show the position of strep-tagged LytCF2, the white ellipse shows the bands of chaperones. Strep antibody was used in the western-blot detection.

### Protein purification of other LytC constructs.

After we purified the LytCF2 construct protein successfully, we tried to purify the construct of LytCF1 protein (a.a. 31-496, 50 kDa). Unfortunately, the purification of LytCF1 protein was not successful. We cannot detect LytCF1 in the strep elution fractions but in the cell pellet (Figure 11 D). LytCF3 (a.a. 210-496) has a molecular weight of about 32 kDa. The LytCF3 protein was first purified by affinity chromatography using strep-tactin column, yet the purity degree was too low. Therefore, a further purification step by gel filtration is necessary. After the gel filtration, the purity of LytCF3 protein increased even though a impurity band at 55 kDa remains with LytCF3. The impurity band turned out to be a chaperone of LytC by MS-SPEC analysis (Figure 11 A, B and C).

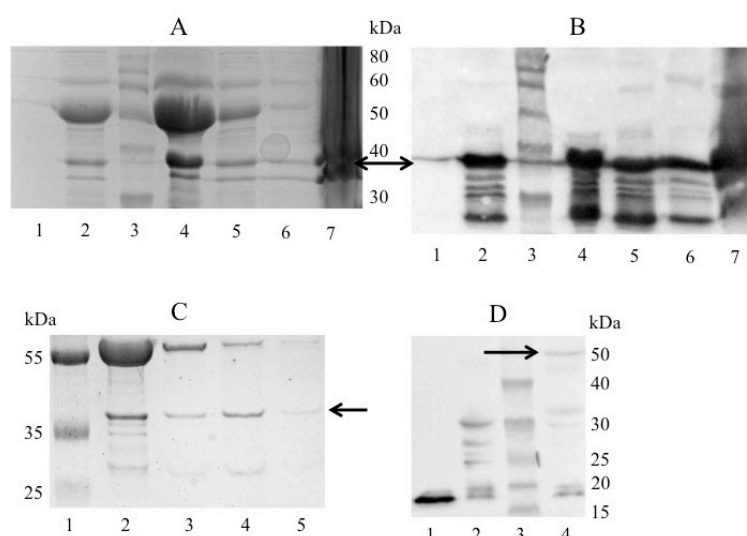


Figure 11. LytCF1 and purified LytCF3. (A) SDS-PAGE image of purified LytCF3. (B) Western-blot image of purified LytCF3 (strep antibody was used). Double head black arrow shows the position of LytCF3. Lanes 1, 2, 4, 5 and 6 are the different fractions of purified LytCF3, lane 3 is the prestained protein ladder (NEB), lane 7 is the cell pellet after lysis. (C) SDS-PAGE image of LytCF3 after gel filtration. Lane 1 is the prestained protein ladder, lane 2 to 5 are different elution fractions of gel filtration. Black arrow shows the position of LytCF3. (D) Western-blot image of LytCF1, lane 2 represents the supernatant after cell lysis, lane 3 stands for prestained protein ladder, lane 4 represents the pellet after cell lysis, lane 1 stands for the elution fraction of purified LytCF1. Black arrow shows the position of LytCF1.

LytCF4 (a.a. 25-496) and LytCF6 (a.a. 377-496) have a molecular weight of 57 kDa and 10 kDa, respectively. The purity of purified LytCF4 and LytCF6 were detected by SDS-PAGE and Western-blot (Figure 12). LytCF6 was concentrated with ultrafiltration columns, LytCF6 can be concentrated with 30 and 50 kDa MWCO PES columns with a molecular weight of 10 kDa. This phenomenon proves that LytC is not a monomeric protein.

LytCF5 (a.a. 319-496) has a molecular weight of about 25 kDa. A test overexpression was performed before the purification of LytCF5. LytCF5 was first purified by strep column and second by gel filtration, we obtained pure LytCF5 after the two steps of purification (Figure 13 C). there is a undesired band of around 50 kDa after the first strep purification (Figure 13 A and B) but this band was removed after the second gel filtration. The purified LytCF5 was concentrated by ultrafiltration (Sartorius Stedim Biotech) with concentrator columns, I discovered that LytCF5 can be concentrated

with 30 and 50 kDa MWCO PES columns even though LytCF5 has a molecular weight of 25 kDa. This phenomenon indicates that LytCF5 is not a monomer.

We also tried to produce an N-terminal fusion of GST-His tagged LytC with the same construct regions as the Strep-tag. Unfortunately, none of the fusion (From GST-His-LytCF1 to GST-His-LytCF5) worked except for GST-His-LytCF6, and the purified GST-His-LytCF6 is shown in Figure 14.

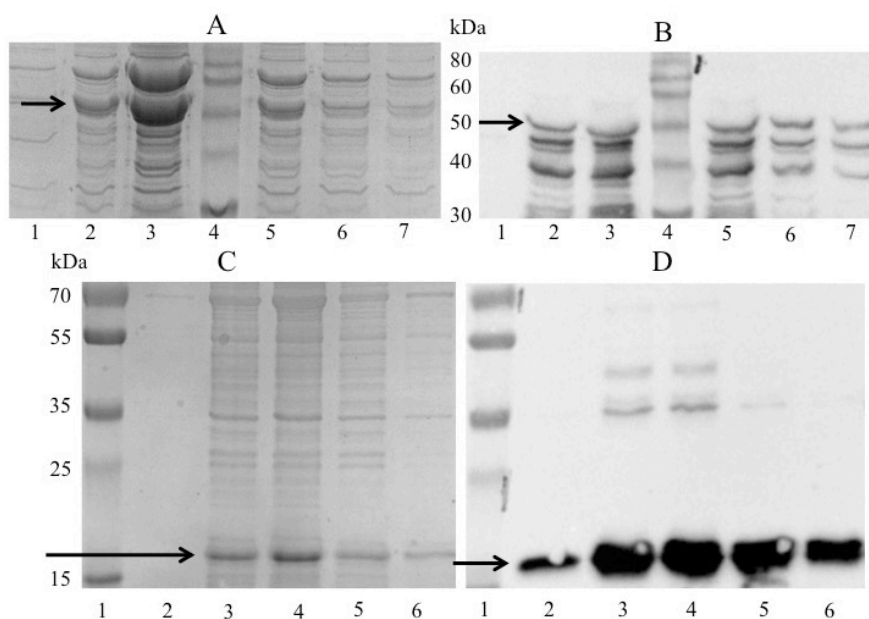


Figure 12. Purified LytCF4 and LytCF6. (A) SDS-PAGE image of purified LytCF4. (B) Western-blot image of purified LytCF4. In A and B, black arrow shows the position of LytCF4. Lanes 1, 2, 3, 5, 6 and 7 are the different elution fractions of purified LytCF4, lane 4 is the prestained protein ladder (NEB). The black arrows show the position of LytCF4 on SDS-PAGE and Western-blot images. C and D are the SDS-PAGE and Western-blot images of LytCF6. In C and D, lane 1 stands for prestained protein ladder (Thermo), lanes 2-6 are different elution fractions of purified LytCF6 products. The black arrows of C and D show the position of the LytCF6 protein. Strep antibody was used in immunoblot experiments.

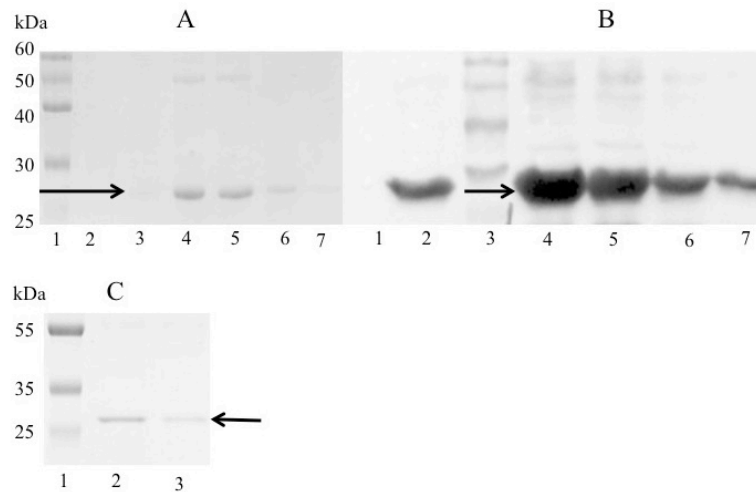


Figure 13. Purified LytCF5. (A) SDS-PAGE of purified LytCF5. Lane 1 represents prestained protein ladder (NEB), 2-7 are different fractions of purified products. (B) Western-blot image of purified LytCF5. Lane 3 is protein ladder (NEB), lane 1, 2, 4, 5, 6, 7 are different fractions of purified products. (C) SDS-PAGE of LytCF5 after gel filtration. Lane 1 is prestained protein ladder (Thermo), 2 and 3 are examples of 2 purified fractions. The black arrow shows the position of LytCF5.

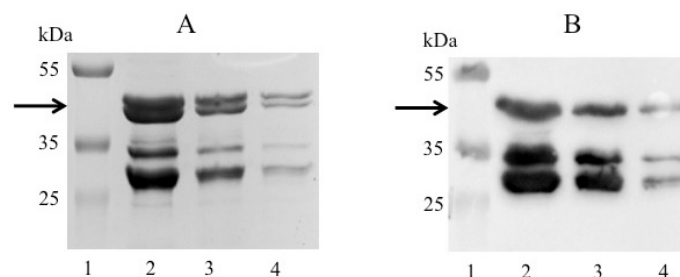


Figure 14. Purified GST-His-LytCF6. (A) SDS-PAGE image of purified GST-His-LytCF6. Lane 1 represents prestained protein ladder (Thermo), lanes 2, 3 and 4, represent different elution fractions of purified His-tag products; (B) SDS-PAGE image of purified GST-His-LytCF6. Lane 1 represents protein ladder, lanes 2, 3 and 4 represent different elution fractions of purified His-tag products. The black arrows show the position of GST-His-LytCF6 in images, the GST tag is 25 kDa, so the fused LytCF6 is around 39 kDa.

### 3.1.3 The functional study of constructed LytC proteins

#### LytC inhibits the growth of bacteria in liquid culture

In our study, we first found that LytCF2 can inhibit the growth of *E. coli* XL1 and BL21 with a final concentration of as little as 7.6 mM. Overnight incubated *E. coli* and *B. subtilis* cultures were inoculated into fresh LB medium containing strep elution

buffer or purified LytCF2 protein. The OD<sub>600</sub> of *E. coli* was measured after 3 and 5 hours of incubation, and the OD<sub>600</sub> of *B. subtilis* was measured after 2, 3, 5 and 6 hours of incubation. The growth difference between the control and samples started to appear after 3 hours incubation (Figure 15). With a concentration of 17 mM, LytCF2 inhibited the growth of *B. subtilis*, the growth difference between the control and treated samples was subtle after 2 hours of incubation. After incubated for 3 hours, the difference could be observed and increased strongly with time and the treated sample also grew but much slower in comparison with the control (Figure 15 C). To test the stability of LytCF2, LytCF2 stored at room temperature (over 24 hours), 4°C (over one week), -20°C and -80°C were used to treat *E. coli* and *B. subtilis*. The activity of LytC was mostly kept in comparison with the fresh LytCF2, so LytCF2 is relatively stable (data not shown). For test the inhibition effect, the purified LytCF3 after gel filtration was used to treat *E. coli*. An overnight culture was inoculated into 500 µl fresh LB rich medium, the control was treated with 150 µl strep elution buffer and the test samples were treated with 150 µl purified LytCF3. LytCF3 produces a strong inhibition on the growth of *E. coli* after 3 hours of incubation (Figure 15 D). I chose *E. coli* BL21 as object to test the inhibition ability of LytCF4. My results showed that LytCF4 is able to inhibit the growth of BL21 ( Figure 16 A) with a final concentration of 10.2 mM. The concentration of LytCF4 that needed to degrade cell wall is higher than other constructs, the reason could be because there is a high amount of chaperone proteins in the purified LytCF4 and the actual concentration should be much lower. *E. coli* XL1 and BL21 were used to test the inhibition activity of LytCF6. The results showed LytCF6 inhibits the growth of *E. coli*, which means that LytC can function as bacteria growth inhibitor as long as the functional region remained (Figure 16 B). I also further concluded that the deletion of CWB and LCR will not cause the activity lost of LytC, the same applies to the trans-membrane region. Treatment of bacteria with GST-His-LytCF6 showed that the fused protein has a minor effect on the growth of *E. coli* and no effect on *B. subtilis* (Figure 16 C), the reason could be that the N-terminal fusion or the GST-His affected the correct folding of LytC and therefore inhibited the activity of LytC. My results showed that LytC cannot maintain the function with His-tag fused at its N-terminal.

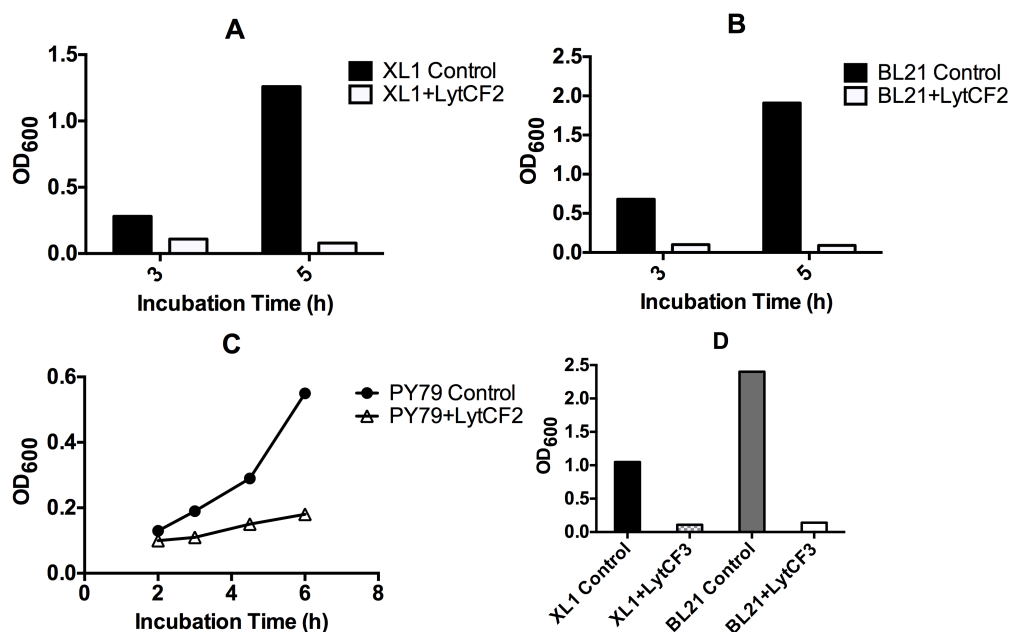


Figure 15. LytCF2 inhibits the growth of Gram-negative bacteria *E. coli* (A and B) and Gram-positive bacteria *B. subtilis* (C). In A and B, the final concentration of LytCF2 was 7.6 mM. In C, the final concentration of LytCF2 was 17 mM. (D) LytCF3 inhibits the growth of *E. coli* with a final concentration of 3.1 mM. Control was treated with strep elution buffer.

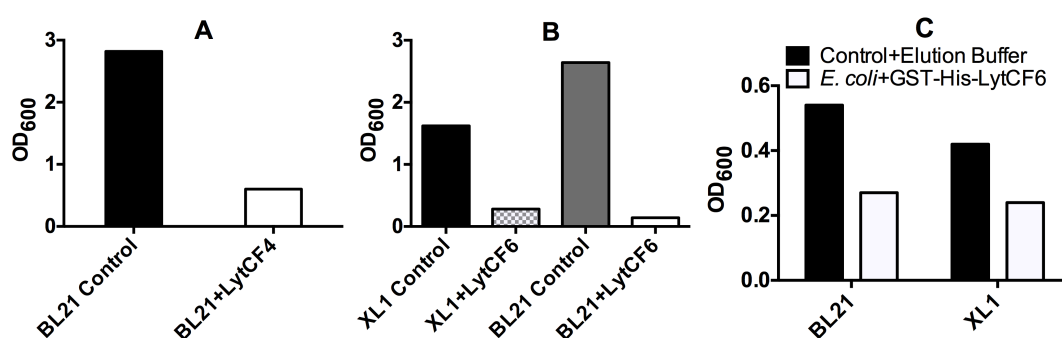


Figure 16. (A) LytCF4 inhibits the growth of *E. coli* BL21. (B) LytCF6 inhibits the growth of *E. coli* with a final concentration of 1.3 mM. (C) *E. coli* treated with GST-His-LytCF6, which has a final concentration of 1.8 mM.

To test the inhibition activity of LytCF5 in *E. coli* and *B. subtilis*, 500  $\mu$ l cultures were used to be treated with different volumes of LytCF5. Two LytCF5 samples were used in this experiment, both were frozen in  $-80^{\circ}\text{C}$  before used. One sample was frozen ( $-80^{\circ}\text{C}$ ) and melted twice, which has a concentration of 125 mM. The other sample was frozen ( $-80^{\circ}\text{C}$ ) and melted only once, which has a concentration of 87 mM. The test results are shown in Figure 17 B, the activity of LytF5 was lost after two times of freeze and melt, even though the final concentration of the twice frozen sample (20.8 mM for the one that treated with 100  $\mu$ l LytCF5) is higher than the once



frozen sample (14.5 mM for the one that treated with 100  $\mu$ l LytCF5). We concluded that the activity of LytCF5 should be partially kept with once frozen, but twice frozen will destroy the structure of LytCF5, which cause the activity lost. Therefore, LytCF5 is moderate stable. The results of LytCF5 inhibits the growth of *E. coli* are shown in Figure 17 A, C and D. From Figure 17 A, when the concentration of LytCF5 reaches 4.8 mM (final concentration), it can inhibits the growth of *E. coli* efficiently. The second experiment confirmed (Figure 17 C and D) that LytCF5 inhibits the growth of *E. coli*. We noticed that the OD<sub>600</sub> of control (from X axis 2, 3.7 to 6.3 mM) also decreased with increased strep elution buffer, the reason could be the salts in elution buffer can inhibit the growth of bacteria. The control of 6.3 mM LytCF5 (200  $\mu$ l) was added more elution buffer than the control of 3.7 mM LytCF5 (100  $\mu$ l) and 2 mM LytCF5 (50  $\mu$ l).

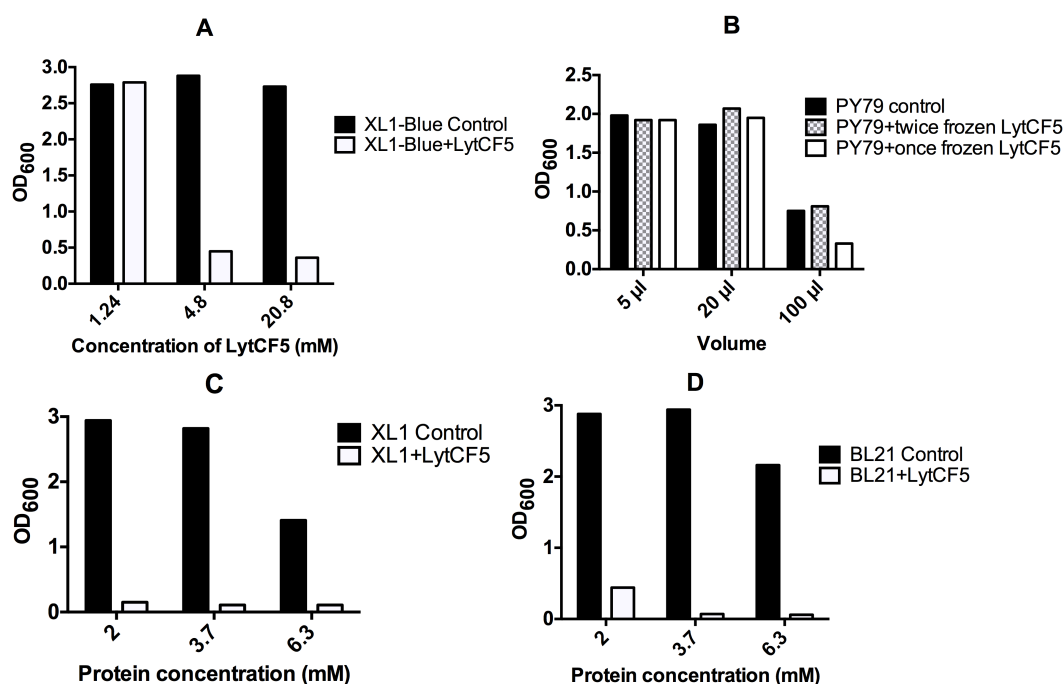


Figure 17. (A) LytCF5 inhibits the growth of *E. coli*. The black bars stand for XL1-Blue treated with strep elution buffer as a control. The white bars represent XL1-Blue treated with different concentrations of LytCF5. (B) LytCF5 inhibits the growth of *B. subtilis* PY79. The black bars stand for PY79 treated with elution buffer as control,. The lattice bars stand for PY79 treated with twice frozen LytCF5 (125 mM). The white bars stand for PY79 treated with once frozen LytCF5 (87 mM). All the original cultures were 500  $\mu$ l. C and D are confirmation of LytCF5 inhibits the growth of *E. coli*. (C) Gradient concentration test of LytCF5 on XL1-Blue. (D) Gradient concentration test of LytCF5 on BL21. LytCF5 can greatly inhibit the growth of *E. coli* when the final concentration of LytCF5 reaches 2 mM.

LytCF5 inhibits the growth of *E. coli* and *B. subtilis* with time course was observed. I recorded the OD<sub>600</sub> after 3 hours of incubation for *E. coli* and 1 hour incubation for *B. subtilis*. For *E. coli*, the control grew normally while the treated sample stayed the same. BL21 treated sample started to grow slowly after 5 hours of incubation. The reason could be the catalytic activity of LytCF5 exhausted after lysis the cell wall for 5 hours. For *B. subtilis*, the control grew much faster than the treated sample, which started to grow after 3 hours of incubation but very slowly. We suppose the reason could be that *B. subtilis* has thicker PG layer than *E. coli* so the activity of LytCF5 for *B. subtilis* exhausted faster than the one of *E. coli* even with a higher concentration of LytCF5.

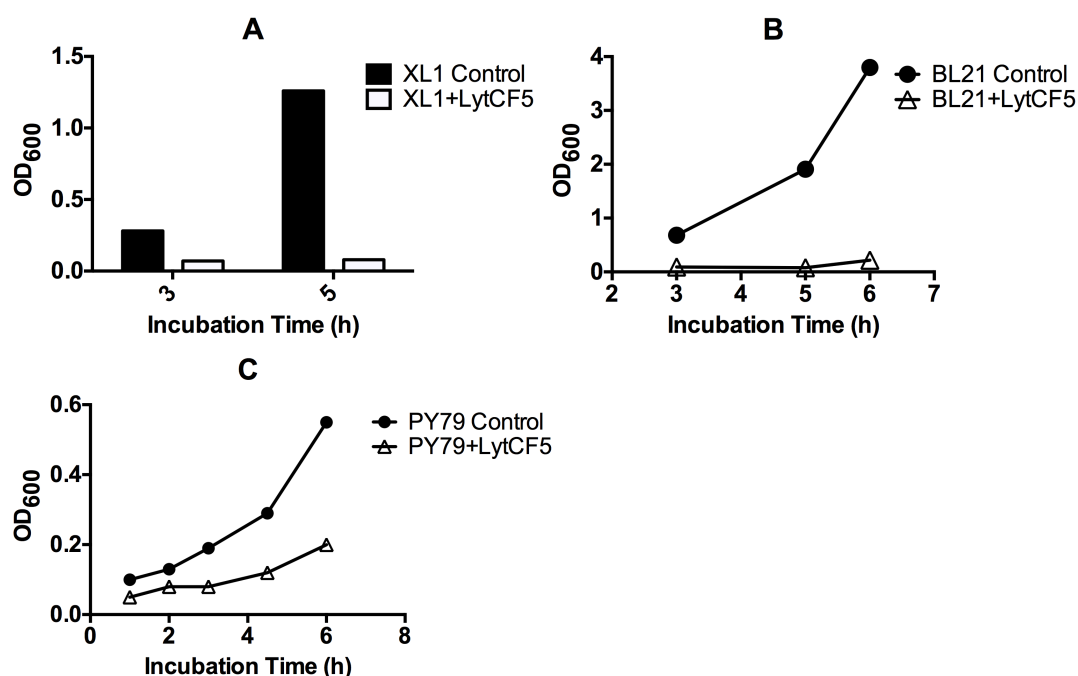


Figure 18. Time course of LytCF5 inhibiting the growth of *E. coli* and *B. subtilis*. In images A and B, the final concentration of LytCF5 was 3.7 mM, for image C the final concentration of LytCF5 was 8.3 mM. The black bar (A) represents XL1 cells treated with strep elution buffer as control. The empty white bar (A) represents XL1 cells treated with LytCF5. In B, the black circle represents control of BL21 cells treated with strep elution buffer, the empty white triangle represents BL21 treated with LytCF5. In C, the black circle represents PY79 cells control that treated with strep elution buffer, the empty white triangle represents PY79 cells treated with LytCF5.

### **LytC inhibits the growth of bacteria on agar plate**

LytCF2 can also inhibit the growth of *B. subtilis* and *E. coli* on agar plates (Figure 19 A, B and C). LytCF2 has the best inhibition effect on XL1, followed by BL21 and PY79. The reason that LytCF2 has weak inhibition on PY79 could be because *B. subtilis* grows slower than *E. coli*, and the LytCF2 might more easily be degraded by the secreted protease and the Gram-positive *B. subtilis* has thicker peptidoglycan than the Gram-negative *E. coli*. I wanted to figure out if LytCF3 can also inhibit the growth of *B. subtilis* on agar plate by applying LytCF3 on agar plate. When PY79 was treated with LytCF3 a big degradation halo was formed while the control that treated with elution buffer did not form the degradation halo (Figure 19 D).

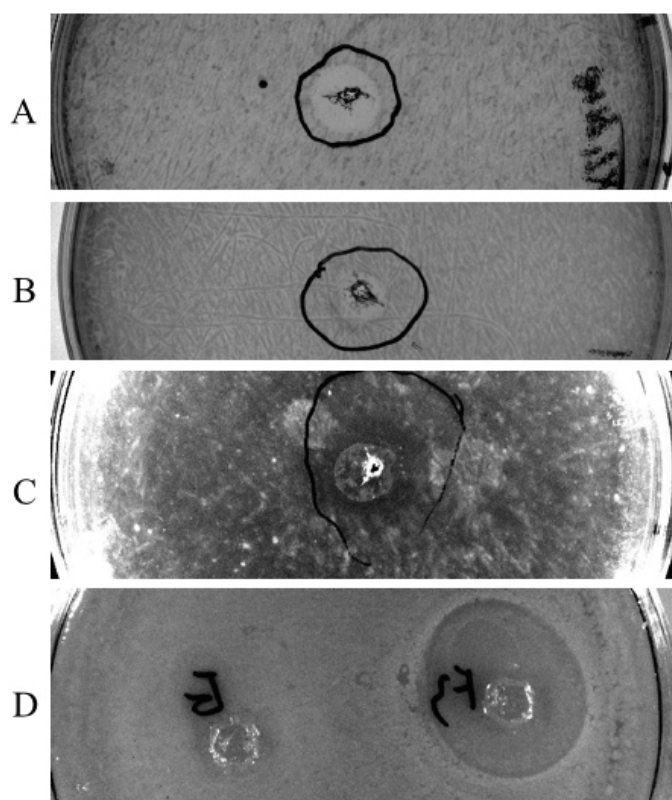


Figure 19. LytCF2 and LytCF3 inhibit the growth of bacteria on agar plates. (A) LytCF2 inhibits the growth of XL1-Blue. (B) LytCF2 inhibits the growth of BL21. (C) LytCF2 inhibits the growth of PY79. (D) LytCF3 inhibits the growth of PY79 on agar plate.

### **Autolysin effect rather than the protein effect of LytC inhibits the growth of bacteria**

To elucidate if the inhibition of bacteria growth is because of LytC activity or just the effect of common protein. We designed another experiment which used bovine serum

albumin (BSA) as control to compare with the one in which elution buffer was used, and the samples were treated with LytCF3. We performed the experiment of *E. coli* treated with BSA as control to see if other proteins can also inhibit the growth of bacteria when dissolved in elution buffer. Our results showed LytCF3 indeed inhibits the growth of *E. coli* while BSA does not, and an interesting phenomenon is that BSA can even promote the growth of *E. coli* (Figure 20 A). The experiment of using LytCF5 to treat *E. coli* (Figure 20 B) also showed that BSA does not inhibit the growth of *E. coli* so we conclude that the LytCF5 is responsible for the growth inhibition. *E. coli* might use BSA as source of protein nutrition which promotes the growth. Hereby we can conclude that the *E. coli* growth inhibition is not the effect of common proteins but the specifically of the cell wall breakdown protein LytC.

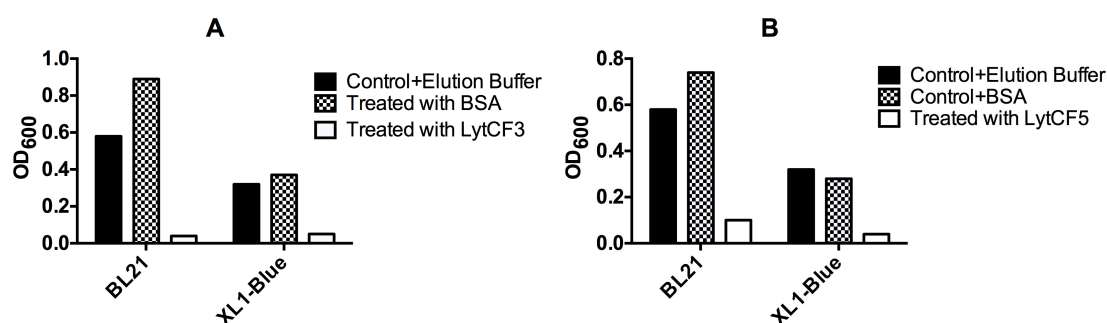


Figure 20. BSA does not inhibits the growth of *E. coli*. (A) The final concentration of BSA is 0.5 mg/ml, and LytCF3 is 6.6 mM. The grey bars represent the *E. coli* control that treated with strep elution buffer. The black bars stand for the *E. coli* treated with BSA, which was dissolved in strep elution buffer. The empty bars stand for *E. coli* treated with LytCF3. (B) BSA (with a final concentration of 5 mg/ml) was dissolved in strep elution buffer. The final concentration of LytCF5 was 1.8 mM. The black bars represent control cells treated with elution buffer. The lattice bar represent control cells were treated with BSA. The empty white bars represent cells were treated with LytCF5. All the original cultures were 500  $\mu$ l.

## 3.2 Site directed mutagenesis of LytC and functional region partial deletion

### 3.2.1 Site directed mutagenesis

To test if the inhibition activity was caused by the functional region of LytC, or just any region of LytC can lyse the cell wall. I chose LytCF5 as control to perform a site-directed mutagenesis. From the former work I found two amino acid sites that could

be the key sites for the activity of LytC (a.a. 342 and 461) [171]. LytCF5 mutants have the same molecular weight as LytCF5. The purified LytCF5 mutants are shown in Figure 21.

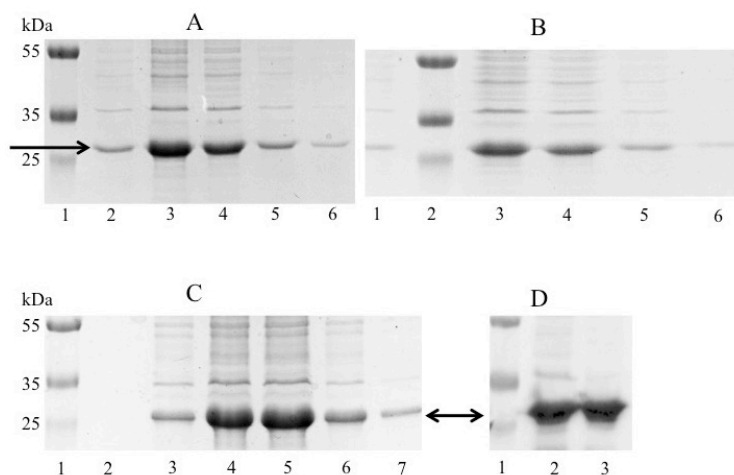


Figure 21. Images of mutated LytCF5. (A) SDS-PAGE image of LytCF5-E342Q, lane 1 represents prestained protein ladder (Thermo), lanes 2-6 represent different strep elution fractions of purified LytCF5-E342Q. (B) SDS-PAGE image of LytCF5-E461Q, lane 2 represents the protein ladder, lanes 1, 3, 4, 5 and 6 stand for elution fractions of purified LytCF5-E461Q. (C) SDS-PAGE image of LytCF5-E342Q-E461Q. Lane 1 represents the protein ladder, 2-7 are fractions of purified LytCF5-E342Q-E461Q. (D) Western-blot (with strep antibody) image of LytCF5-E342Q-E461Q, lane 1 represents the protein ladder, lanes 2 and 3 are LytCF5 double mutation products. Black arrows show the position of purified LytCF5 mutant proteins.

After the construction of LytC single mutants (E342Q or E461Q), the inhibition activities of LytCF5 mutants were tested. *E. coli* cultures were treated with 30  $\mu$ l of purified proteins and *B. subtilis* cultures were treated with 100  $\mu$ l of purified proteins. The inhibition activity test showed no significant difference between the mutants and LytCF5 (Figure 22), the site mutagenesis does not affect the activity of LytC. The reason is probably the mutation sites are not the key sites for the function of LytC. Since the activity of LytCF5 (E342Q or E461Q) single mutants were not reduced in comparison with LytCF5. We constructed the double mutant LytCF5 (E342Q and E461Q). And the inhibition ability was tested. The double mutation also did not affect the activity of LytC, therefore, the mutation sites are not the key sites for the activity of LytC.

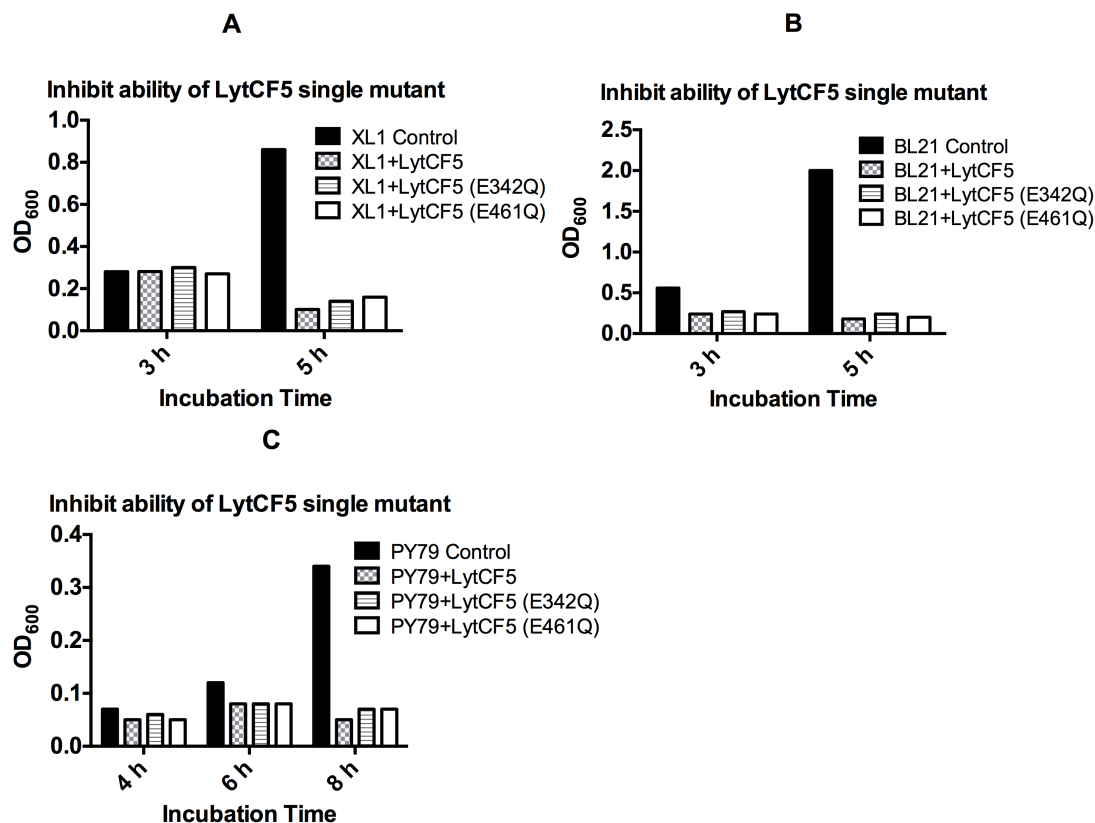


Figure 22. The inhibition test of LytCF5 single mutants (E342Q or E461Q). The final concentration of proteins was 2 mM. The treating object of A was *E. coli* XL1, B was *E. coli* BL21, C was *B. subtilis* PY79. The black bar represents control cells that were treated with strep elution buffer. The lattice bars represent cells that treated with LytCF5. The bar with lines inside represents cells that were treated with LytCF5 (E342Q). The empty white bar represents cells that were treated with LytC (E461Q).

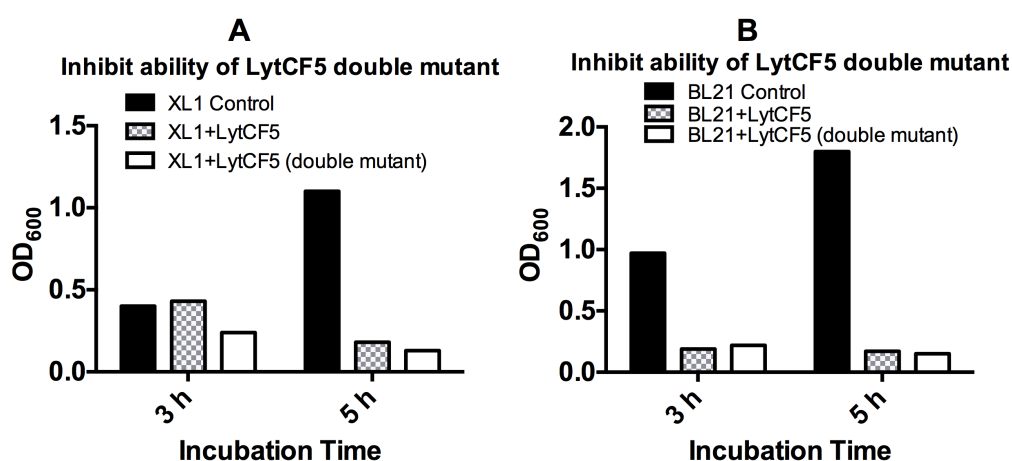


Figure 23. The inhibition ability test of LytCF5 double mutant. The final concentration was 1.8 mM. The black bars were *E. coli* control that treated with strep elution buffer, the lattice bars were treated with LytCF5 and the empty white bars were treated with LytCF5 (E342Q and E461Q) double mutants. All culture were treated with 300  $\mu$ l of sample.

### 3.2.2 Partial deletion of the functional region

The site-directed mutagenesis did not reduce the activity of LytCF5. Therefore, we performed another experiment in which we deleted 22 amino acids at the C-terminal of the functional region of LytC. LytCF2R2 (a.a. 220-470) has a molecular weight of about 34 kDa. The purified LytCF2R2 is shown in Figure 24 D and E. After we purified the partially deleted LytCF2R2, it was used to treat *E. coli* and *B. subtilis* to check if the lyse activity was lost. Data showed that the activity of LytCF2R2 was partially kept but dropped dramatically if compared to native LytCF2 (Figure 24 A, B and C). Hereby we confirmed the inhibition activity was from the functional region of LytC.

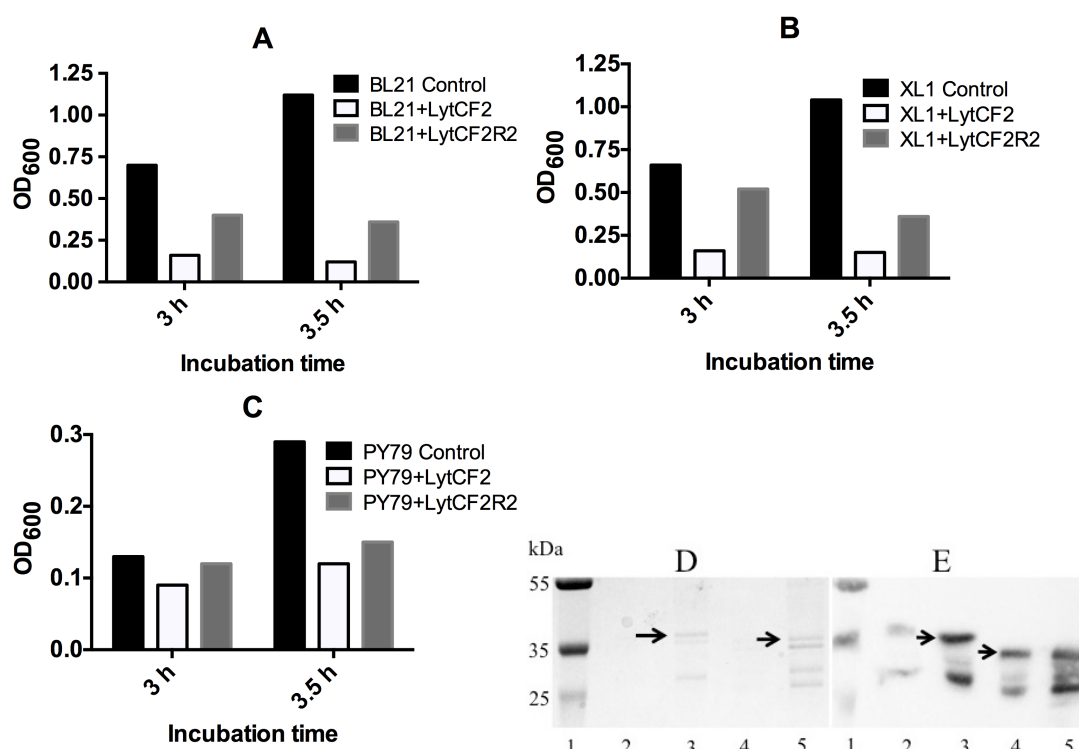


Figure 24. (A, B and C): all the original cultures were 500 µl, treated with 150 µl samples. The final concentration of both LytCF2 and LytCF2R2 was 11 mM. The black bars were control that cells treated with strep elution buffer. The empty bars represent cells treated with LytCF2 while the grey bars represent cells treated with partially deleted LytCF2R2. *E. coli* BL21 was used in A, *E. coli* XL1 was used in B, *B. subtilis* PY79 was used in C. (D and E): purified LytCF2R2. (D) SDS-PAGE image of purified LytC proteins. (E) Western-blot image (with strep antibody) of purified LytC proteins. Lane 1 represents prestained protein ladder (Thermo), 2 and 4 were loaded with 1 µl sample, 3 and 5 were loaded 5 µl sample, 2 and 3 represent LytCF2, 4 and 5 represent LytCF2R2. The black arrows show the position of desired proteins.

### 3.3 Microscopy evidence that LytC degrades the cell wall

To provide further evidence that LytC is capable of degrading the cell wall and thus inhibits the growth of *E. coli* and *B. subtilis*, we performed microscopy experiments after bacteria were treated with LytC. We chose LytCF5 to treat cells for microscopy evaluation because the inhibition results by using LytCF5 have been repeated several times and the purity of LytCF5 is the highest among all the constructs we made, which makes LytCF5 construct the most useful for potential industrial application.

Microscopy data showed that LytCF5 indeed inhibited the growth of *E. coli* and *B. subtilis* and further broke down the cell wall (Figure 25). The cell wall of XL1 can be lysed by LytCF5, and some cells lost their rod shape and acquired a spherical cell shape because of the lysed cell wall (Figure 25 C1 and D1). The cell wall of BL21 can be lysed and part of cells lost the rod cell shape and acquired the spherical cell shape (Figure 25 C2 and D2). LytCF5 also can cause Gram-positive bacteria *B. subtilis* (PY79) to lose the rod cell shape because of cell wall lysis. Since Gram-positive bacteria PY79 has thicker cell wall than the Gram-negative *E. coli*, the lysed PY79 were not as widely visualized as *E. coli* (Figure 25 F and H).

The same phenomenon was observed when we imaged the *E. coli* and *B. subtilis* that treated with purified LytCF6 (data not shown). Therefore, we confirmed that LytC can hydrolyze cell wall at microscopy single cell level. The attempt to track the process of bacterial cell wall breakdown and cell death under live time high resolution microscopy was not successful.



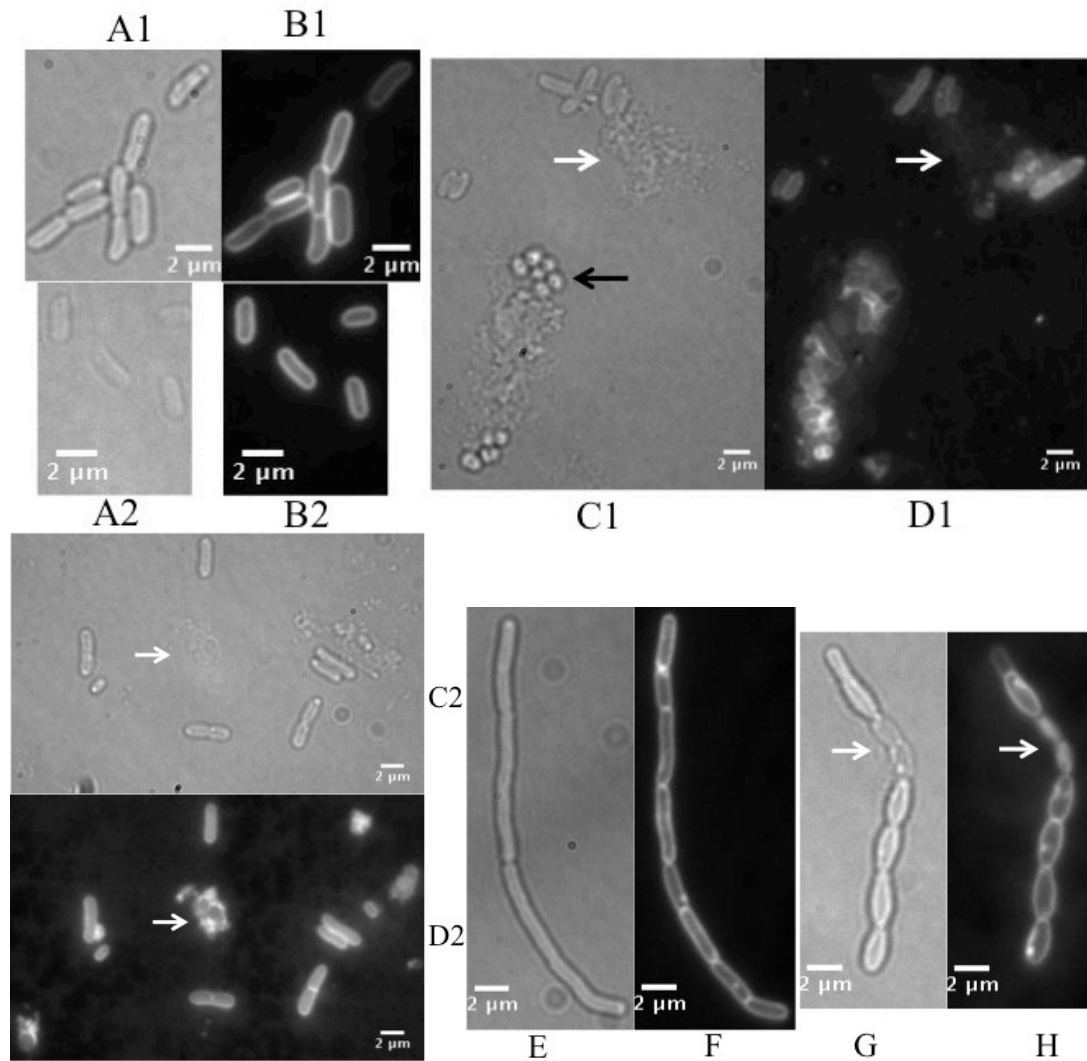


Figure 25. LytCF5 degrades the cell wall of Gram-negative *E. coli* (XL1-Blue and BL21) and Gram-positive bacteria *B. subtilis* (PY79) in their exponential growth, and *B. subtilis* cells grow as chains in their exponential growth. A and B are images of *E. coli* control that were treated with strep elution buffer, C and D are images after *E. coli* cells were treated by LytCF5. The white arrows in C1 and D1 show the example of lysed XL1 cells, the black arrow in C1 shows that XL1 cells lost the rod cell shape and acquired the spherical cell shape because of the lysed cell wall. The white arrows in C2 and D2 show the lysed BL21 and spherical cell shaped BL21. E and F are images of *B. subtilis* control; in G and H, PY79 cells were treated with LytCF5. White arrows show the lysed PY79. A, C, E and G are bright-field images, B, D, F and H are membrane stained images. The white bar is 2 μm.

### 3.4 Localization studies of MreB, MreC, MreD, PfkA, Pbp1A, RodZ and subunits of PDH complex *in vivo*

#### 3.4.1 Localization studies of MreB, MreC and MreD *in vivo*

In order to characterize the structure of MreB *in vivo*, a *yfp-mreB* fusion was integrated into the chromosomal of *B. subtilis* by a double cross-over with *amyE* gene. The correct transformants were first selected via Spec resistance, then screened by detecting for defective *amyE* and lack of starch degradation ability. *B. subtilis* transformants were streaked on LB agar plates with 0.5% (w/v) starch and incubated overnight in a 30°C incubator. The starch plates were stained with Lugol's iodine (solution of iodine and potassium iodide) to screen the colonies with stained halos (the negative colonies contain the no-stained halos). The colonies that have stained halos are positive transformants, in which the fusion genes were correctly integrated into the *amyE* site of the genomic chromosome. Fusions that were constructed into the pSG1164-NLMV and pHJDS vectors were used for the integration of genes into the original gene locus with a single cross-over in the *B. subtilis* chromosome.

*B. subtilis* and *E. coli* grown to exponential phase were used for the imaging of functional MreB. Fluorescently tagged YFP-MreB was visualized in *B. subtilis*. The fusion was integrated into the *amyE* gene locus under the xylose promoter as an additional copy to the native MreB from the original gene locus [92]. In order to further investigate the function and structure of MreB, the comparison of MreB localization in *B. subtilis* and *E. coli* strains were performed. We obtained two *E. coli* strains (kindly gifts from the laboratory of Jan Löwe, Cambridge, UK) with GFP-MreB, both were used to visualize the localization of MreB in *E. coli*. In one strain (PG3087), GFP-MreB was integrated into the chromosome of *E. coli*, in another strain (PG3088), GFP-MreB was cloned into pS2131 vector and transformed into *E. coli*. In both strains, GFP-MreB was under control of the T7 promoter. Only the localization results of GFP-MreB that was integrated into the chromosome of *E. coli* will be presented, because from both *E. coli* strains the localization patterns of GFP-MreB were the same. The attempt to perform single molecule microscopy of GFP-MreB in *E. coli* failed, since MreB is a high-copy protein. We could not manage to get single molecule level of MreB in *E. coli* even though the amount of IPTG we used in this study was under strict control. We tried gradient concentrations of IPTG for the

GFP-MreB *E. coli* strain, however, we either have over expressed MreB or weak illumination signal of GFP-MreB that was not strong enough to recognize the single molecules.

MreB filaments in *B. subtilis* localized as discontinuous filamentous structures that are located underneath the cell membrane (Figure 26 A), the same phenomenon was observed in *E. coli* (Figure 26 D). With the reduction of xylose induction, YFP-MreB localized in *B. subtilis* as a patchy structure (Figure 26 B). If we use no xylose for induction, traces of YFP-MreB fluorescence can still be visualized (Figure 26 C) because the xylose promoter is a leaky promoter.

The image of *B. subtilis* YFP-MreB epifluorescence microscopy showed that MreB localizes as extended but discontinuous filaments along the lateral membrane and MreB also has a patchy and short filamentous structure. Most of the filaments extend about the entire cell width (around 1.1  $\mu\text{m}$ ), some filaments even expand more than half of the cell circumference. Furthermore, a minor fraction of MreB formed short filaments [172]. From the microscopy image we concluded that the orientation of MreB filaments was extremely variable, and the distribution of MreB filaments was irregular, as was shown in previous studies [172]. TIRF microscopy could detect fluorescence within a focal plane of about 100 nm in depth, while the minimal radius for the rod shaped *B. subtilis* is 500 nm. So the TIRF microscopy could not be the best to visualize the MreB fluorescence structures that extend over the entire width of membrane. This could be also the reason why MreB has different localization types with different microscopy technology. In Gram-negative bacteria *E. coli*, MreB localized the same as in *B. subtilis* (Figure 26 A and D).

The proteins of MreC and MreD are colocalized with MreB. MreC and MreD were first tagged with GFP or YFP, then integrated into the amy locus of *B. subtilis* chromosome. The localization of GFP-MreC (Figure 26 E) and GFP-MreD (Figure 26 F) showed the same pattern of a membrane staining (Figure 25 F), which indicates that MreC and MreD might membrane proteins. In the constructs of YFP-MreC and YFP-MreD, they not only have a same localization as membrane staining, but also form some patchy spots within the cell (Figure 26 G and H).

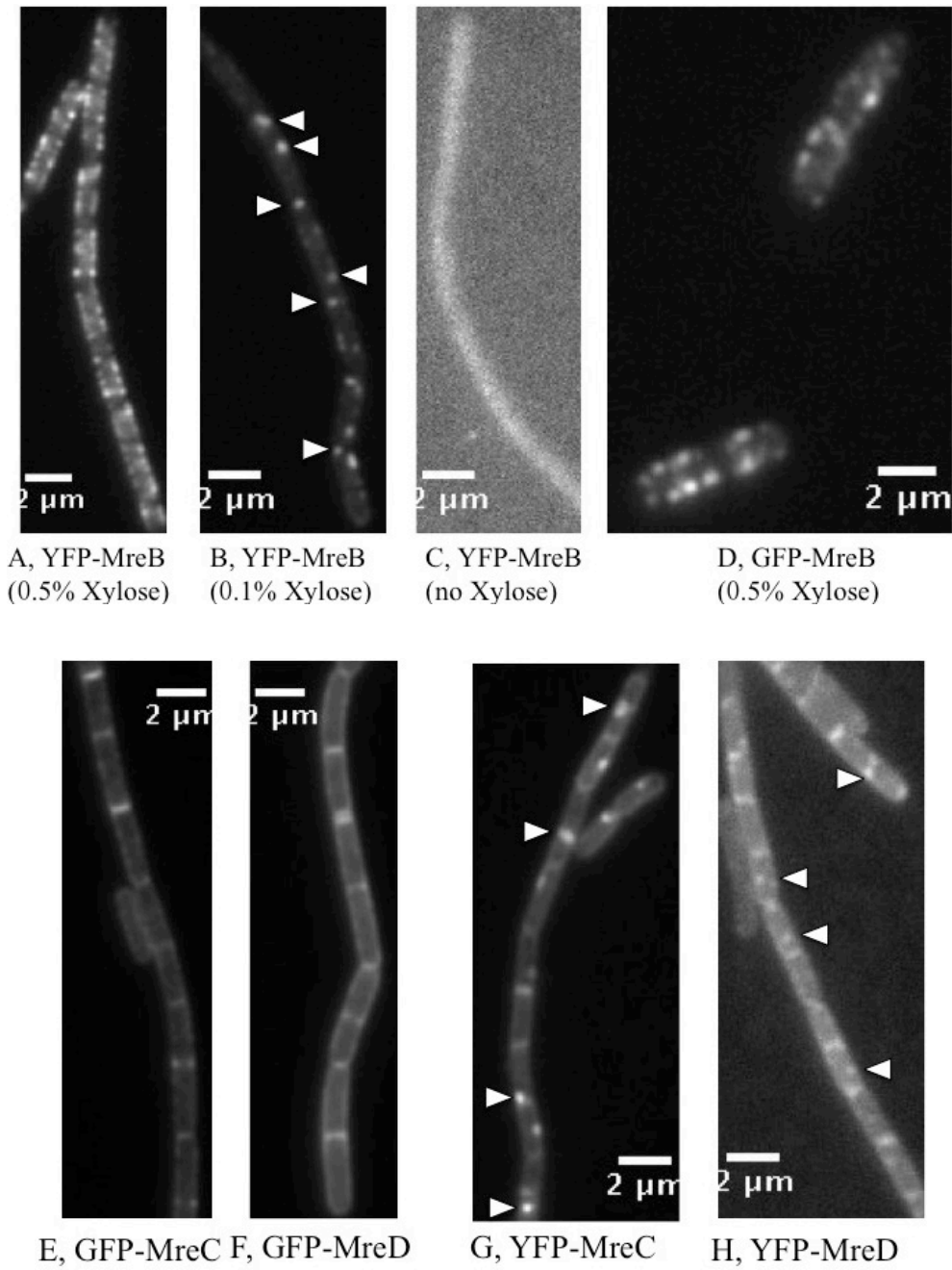


Figure 26. Localization study of MreB, MreC and MreD. (A) TIRF image of YFP-MreB::amy with full xylose (0.5%) induction. (B) TIRF image of YFP-MreB::amy with medium xylose (0.1%) induction. (C) TIRF image of YFP-MreB::amy without xylose induction. (D) TIRF image of GFP-MreB with IPTG full induction in *E. coli*. (E) TIRF image of GFP-MreC::amy with full xylose (0.5%) induction. (F) TIRF image of GFP-MreD::amy with full xylose induction. (G) TIRF image of GFP-MreC::amy with full xylose induction. (H) TIRF image of GFP-MreD::amy with full xylose induction. All the localization experiments were done in exponentially growing *B. subtilis* (grow as chains) or *E. coli*, the experiment of image D was performed in *E. coli*, the rest were performed in *B. subtilis*. White bar 2 μm.

### 3.4.2 Localization studies of PDH complex in *B. subtilis*

The pyruvate dehydrogenase (PDH) complex consists of four subunits: E1 (PdhA and PdhB), E2 (PdhC) and E3 (PdhD). Each genes (*pdhA*, *pdhB*, *pdhC*, *pdhD*) of PDH complex was fused with fluorescence protein gene *yfp* into pSG1164-NLMV vector by the C-terminal. These genes were integrated into the chromosome of *B. subtilis* with a single cross-over, so these genes are under the control of original *pdhABCD* promoter.

PdhA showed polar localization in exponential growth phase *B. subtilis*, and localized as foci at the cell pole with different intensity (Figure 27). The cells with bright foci, faint foci and no foci account for around one third of the total population for each type of localization. PdhB distributed uniformly under the lateral membrane and within the cytoplasm of the cell (Figure 27 B). PdhC also showed a uniform and diffuse pattern of localization, which is the same as PdhB (Figure 27 C). We detected two types of localization pattern for PdhD. One pattern showed PdhD might have a strong DNA affinity, because the illumination of PdhD is overlapped with DNA staining (Figure 27 D). The other pattern is the same as PdhB and PdhC, which uniformly distributed in the cytoplasm (Figure 27 D).

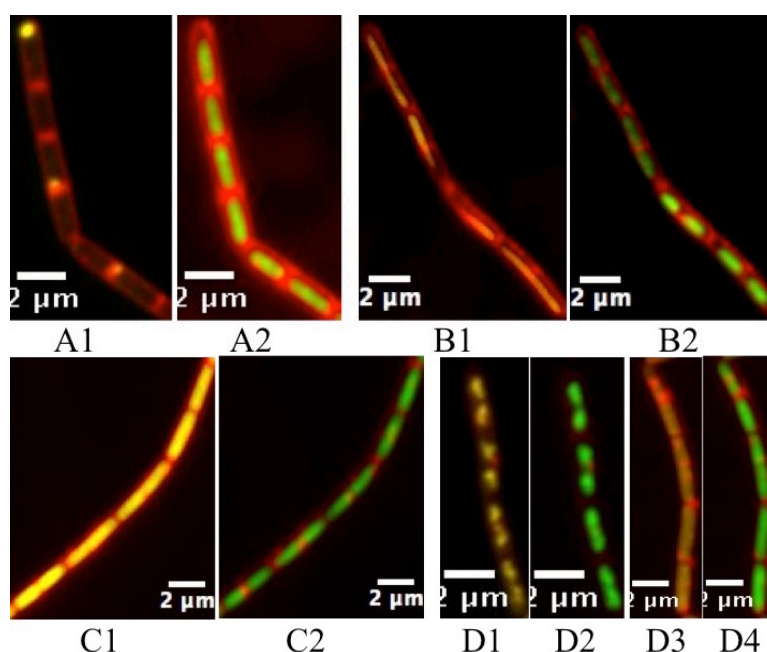


Figure 27. The localization study of PDH complex subunits was performed in chains of exponential growing *B. subtilis* cells. A, B, C and D represent the localizaiton study of PdhA, PdhB, PdhC and PdhD, respectively. Red: membrane staining. Yellow: YFP signal. Green: DAPI staining. White bar 2  $\mu$ m.

### 3.4.3 Localization study of RodZ, PfkA, Pbp1A, RecX and YfhH in *B. subtilis*

RodZ (or YmfM) is responsible for the cell shape determination and maintenance in *B. subtilis*, which is also a membrane protein and colocalizes with MreB [82]. The *rodZ* gene was fused with *yfp* into pSG1729 vector by its N-terminal or fused into pSG1164-NLMV vector by its C-terminal. The performed TIRF microscopy of YFP-RodZ in the exponential *B. subtilis* showed that it is localized as the membrane staining, the illumination density of YFP-RodZ is uniformly distributed on the membrane (Figure 28 A). RodZ-YFP in *B. subtilis* also localized on the membrane and uniformly distributed (Figure 28 B), which is the same as YFP-RodZ. These results indicate that RodZ is a membrane protein.

The localization of YFP-Pbp1A in *B. subtilis* has a same pattern as the membrane staining, which indicate Pbp1A is also a membrane protein (Figure 28 D). The fluorescence density of YFP-Pbp1A is lower if compared with the density of YFP-RodZ or RodZ-YFP, which indicate the copy number of Pbp1A is lower than RodZ in the exponential growth of *B. subtilis*.

The *pfkA* and *recX* gene was also fused with *yfp* by its C-terminal into pSG1164-NLMV vector. The experiment of PfkA-YFP epifluorescence microscopy in exponential growing *B. subtilis* showed that it is uniformly distributed in the cytoplasm of cell (Figure 28 C). This means that PfkA is probably a cytoplasmic protein.

RecX-YFP protein is mainly localized at the cell poles (Figure 28 E). *yfhH*, which was amplified with primers yfhHSalIF1/yfhHEcoRIR1-198, was fused with *yfp* by its N-terminal into pHJDS vector. The signal of YFP-YfhH is uniformly distributed within the cell (Figure 28 F), which is same as PfkA-YFP. Therefore, YfhH is probably also a cytoplasmic protein.

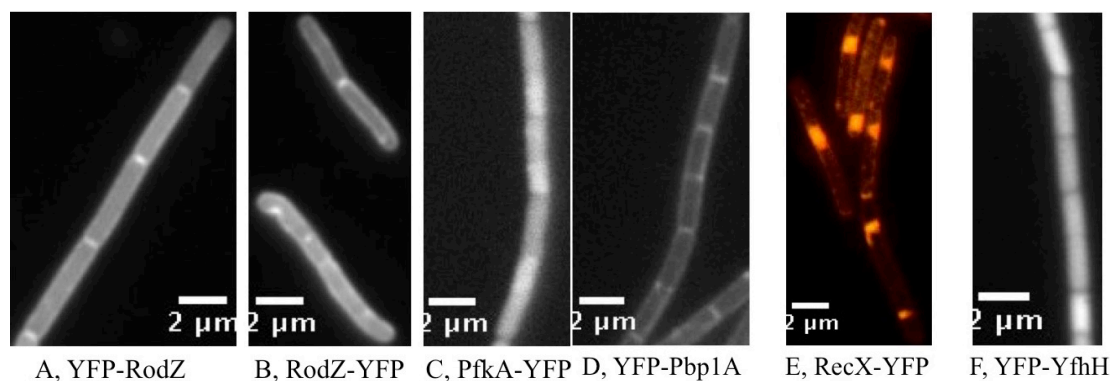


Figure 28. Localization study of RodZ, PfkA, Pbp1A, RecX and YfhH in the exponential growth *B. subtilis* (grow as chains). A, B, C, D, E and F represent the localization study of YFP-RodZ, RodZ-YFP, PfkA-YFP, YFP-Pbp1A, RecX-YFP and YFP-YfhH, respectively. The red color is the signal of membrane staining, the yellow color is the signal of RecX-YFP. White bar 2  $\mu$ m.

### 3.5 Single molecule microscopy

To gain further insights into the dynamics and movement of the single particles of MreB and other proteins, single molecule microscopy was performed. This technique uses fluorescent protein tags, a focused laser beam excites and bleaches the fluorescent protein fusions, and images are acquired in stream acquisition. High aperture objective and sensitive cameras make the stream acquisition of single GFP or YFP molecules in real-time available. All fused proteins except PfkA that used for single molecule experiments are expressed under the xylose promoter by genomic recombination with chromosome DNA at the *amy* site, all the proteins were fused to one of the GFP variants YFP. Because the single molecule microscopy is usually limited with low copy proteins, the expression level of high copy proteins needs to be repressed. We put the genes under xylose promoter without any xylose induction since *pxyl* is a leaky promoter so the single molecule level can be reached. Single molecule microscopy was performed to determine the dynamic behavior of proteins *in vivo*. The images were acquired with 10 ms exposure time and 10 ms time interval, the frames of each movie was adjusted accordingly, and the intensity of laser beam was used at 10 mW. The parameters (frame number, acquisition interval, voxel depth and pixel size) of each imaged movies were first calibrated by program 'Fiji ImageJ' and the brightness and contrast were adjusted properly. Then the movement of each single molecules was tracked by u-track with the program MATLAB, the data from

processed movies was analyzed by msd-analyzer and MicrobeTacker with MATLAB. The data I obtained was further analyzed by Dr. Thomas Rösch (University of Marburg).

### **3.5.1 Single molecule detection and identification**

In the first frame of the time lapse, fluorescence of all YFP fused proteins was detectable. YFPs bleach randomly in the following frames and in later frames there will be a few molecules left and they switch from the fluorescent state ('blink') to the state in which they lose the fluorescence [173]. Therefore, the single molecules can be detected and the intensities of the YFPs can be measured. Single molecules tracking were performed by using u-track of Matlab plugin, trajectories shorter than 5 frames were discarded. And most of the proteins that we analyzed contained two kinds of behavior, one kind is highly static and the other one is mobile.

The images below (Figure 29) showed the fluorescence of single molecules over time (each frame is 10 ms). The single molecule can be clearly visualized in frames, the ones that blinked can be recognized as one single molecule. The numbers 1, 2, 3, 4 in A and B stand for tracks, number 2 (yellow) track in image A is quite dynamic while the number 1 (red) and 3 (green) tracks in image A are quite static. The red circle in image C is a static single molecule. There are also some molecules that blink in one frame and disappear in the next frame and therefore cannot be tracked so they must be freely diffusing within the cell and out of the focus layer very fast. The PfkA-YFP fusion molecules were very difficult to track, because PfkA is under the original promoter and PfkA is over expressed. So it is very hard to distinguish the single molecules. Tracking of YFP-MreB molecules indicated that there are two fractions: one is immobile and the other one is mobile. Figure 29 gives examples of mobile spots that moved for a few frames and then photobleached, it also gives examples of static spots that are immobile for a few frames and then photobleached.



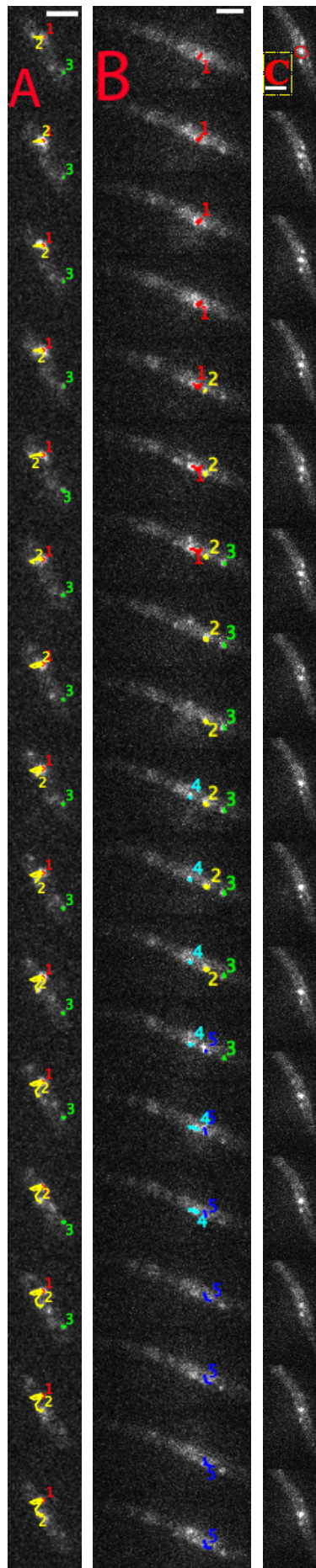


Figure 29. Single molecule detection and tracking in exponential growth *B. subtilis* cells. From left to right, they are YFP-MreB, YFP-MreC and YFP-MreD fusions, respectively. (A) Example tracks of YFP-MreB spots that are mobile and static before photobleaching. Number 1 (in red color) and 3 (in green color) are the dynamic spots and number 2 (in yellow color) is the static spot. (B) Mobile and static spots example of YFP-MreC. (C) Example of single molecule detection, the one in red circle is recognized as one molecule. Single molecule acquisition with time interval of 10 ms, each frame has an exposure time of 10 ms. There is more than one single molecule in one plane but some are photobleached and some others appear over time. The full set of pictures contain from 1000 to 5000 frames. Scale bars 2  $\mu$ m.

### 3.5.2 Tracking analysis of YFP-MreB and PfkA-YFP single molecules

*B. subtilis* with YFP-MreB or PfkA-YFP fusions were grown in S7<sub>50</sub> minimal medium without xylose induction. Because *pfkA* is driven by the original promoter, *mreB* is under the control of leaky xylose promoter, and the leaky level of expression is enough for us to visualize the single molecules. The dynamics of YFP-MreB and PfkA-YFP was investigated by stream acquisition of single molecule microscopy. To determine the movement speed of single mobile molecules, the diffusion coefficients were determined using msd-analyzer plugin together with MATLAB program. From the tracks that were analyzed by the U-track plugin of MATLAB, the mean square displacement (MSD) of each trajectory were calculated and the first 25% of a MSD versus time curve were fitted linearly. The diffusion coefficients were calculated from the slope of these fits. Actin accounts approximately 10-15% of total cell protein in the average eukaryotic cells. Actin can be divided into two categories: one is a free monomer called G-actin (globular), the other one is a linear polymer microfilament called F-actin (filamentous) [174]. Prokaryotes also contain proteins that are highly similar to actin monomers and polymers. The bacterial protein MreB polymerizes into filaments similar to F-actin [175, 176]. The crystalline structure of MreB is very similar to that of G-actin (three-dimensional conformation) [114]. In *B. subtilis*, there are approximately 8000 MreB molecules, which were calculated by using quantitative western-blot [174]. In some eukaryotic cells (e.g. Swiss 3T3 cells, *Asterias* or *Thyone* sperm), approximately 80% of actin is in the monomeric state (G-actin) [177-179].

A former study of our laboratory has shown that MreB filaments consist of two different populations, an exchangeable and a non-(or very slowly) exchangeable fraction. More than 50% of MreB molecules are associated with the polymerized

fraction. Thus, at least half of the MreB molecules are within filamentous structures and are not available for exchange [95]. Our results of single molecule tracking also showed that MreB molecules are composed of two populations. One is immobile which has a diffusion coefficient ( $D$ ,  $\mu\text{m}^2/\text{s}$ ) of 0.060 and account for 53.1% of the total population. Another one is the mobile population with a diffusion coefficient of 0.463 and account for 46.9% of the total population (Figure 30). Immobile (or static) MreB molecules (more than half of the total population) are within MreB filamentous structures, the remainder of MreB molecules (less than half of the total population) are mobile and freely diffusing within the cytoplasm. These results are in accordance with the former studies of our laboratory [95].

Single molecule tracking analysis of PfkA-YFP revealed that there are two populations (we can also see it as one moving population since one plot curve of Gaussian fit can also explain the movement well, Appendix Figure 36 D2) of moving fraction and no static molecules could be detected. One population is highly dynamic, which has a diffusion coefficient of 0.755 and accounts for 49.3% of total molecules. Another population is composed of slow moving molecules, which has a diffusion coefficient of 0.232 and accounts for 50.7% of total population (Figure 30). However, because a diffusion coefficient of 0.2 is still much higher than that of a static MreB molecule, there is likely only one dynamic PfkA population with a wide range of diffusion rates. Both the diffusion coefficient and proportion of highly dynamic YFP-MreB molecules are lower than those of PfkA-YFP.

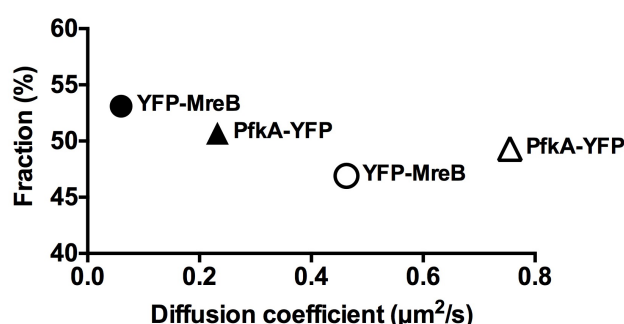
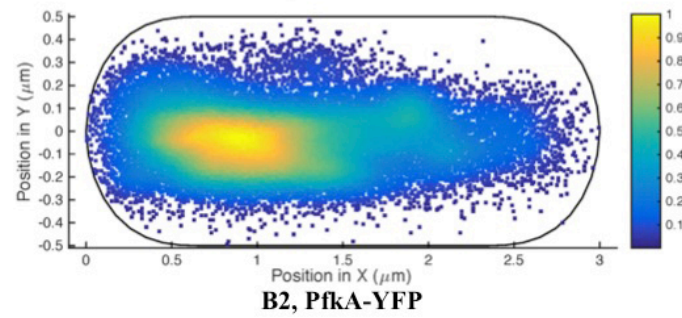
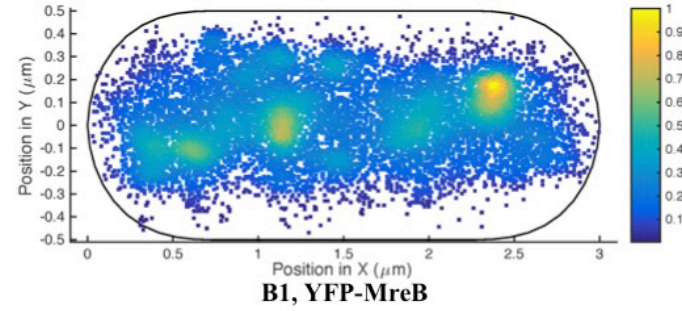
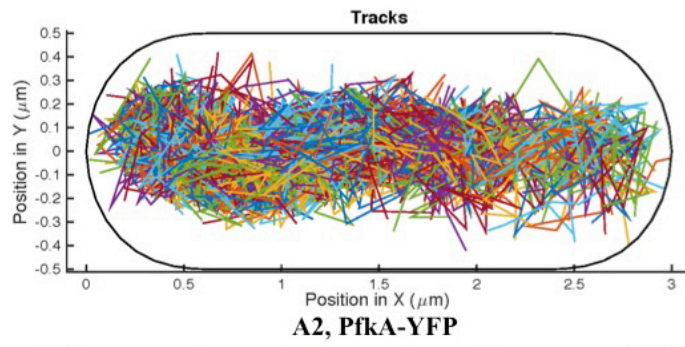
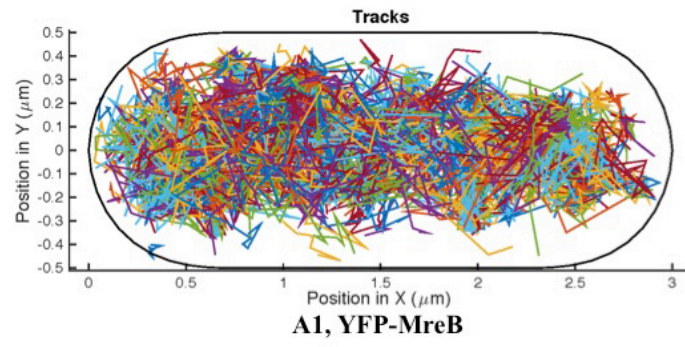


Figure 30. Diffusion coefficients. The mean diffusion coefficient of mobile and static YFP-MreB were 0.463 (with a fraction of 46.9%) and 0.060 (53.1%)  $\mu\text{m}^2/\text{s}$ , respectively. The mean diffusion coefficient of two PfkA-YFP mobile populations were 0.232 (50.7%) and 0.755 (49.3%)  $\mu\text{m}^2/\text{s}$ . The round circles represent the movement behavior of YFP-MreB. The triangles represent the movement behavior of PfkA-YFP. The X axis shows the diffusion coefficient of each population, the Y axis shows the fraction of each diffusion coefficient.

MreB has high membrane affinity, and localized underneath the lateral membrane. The focus plane was at the bottom of the cell during the slim-field movie capture. The localization of single molecule spots is denser in the middle of the cell than at the edge of cell from the horizontal direction (Figure 31 B1 and D1). This result is in accordance with our knowledge of MreB localization because MreB is a membrane protein so we lose the focus at the cell edges when we focus at the bottom of the cell. From the vertical direction, we observed the density of MreB spots is higher at some position than others, which indicates that MreB has some preferable localization place and formed the filaments structure, and the spots density at the cell poles is much lower than in the cell center (Figure 31 B1 and C1). These results are in accordance with the result that MreB forms filaments underneath the cell membrane (Figure 26 A). The cumulative density function (CDF) fitting of single molecule step size distribution was also used to determine the moving behavior of tracks. For YFP-MreB, the fitting curve with one mobile and one immobile population fitted very well with the experimental data (Appendix Figure 36 F1). For PfkA-YFP, the fit with two mobile populations explains very well of the experimental data (Appendix Figure 36 F2).

The bottom of the cells were focused when the single molecule microscopy was performed. The movement overlay and the spots density of YFP-MreB showed a pattern that similar to membrane staining (Figure 31 A1 and B1). This indicates that MreB is a membrane-associated protein. The movement of YFP-MreB and the density of spots were not or (at least) less observed along the cell edges and the cell poles, which further proved that MreB is a membrane associated protein. The localization of PfkA-YFP is more uniformly distributed within the cytoplasm of cell.



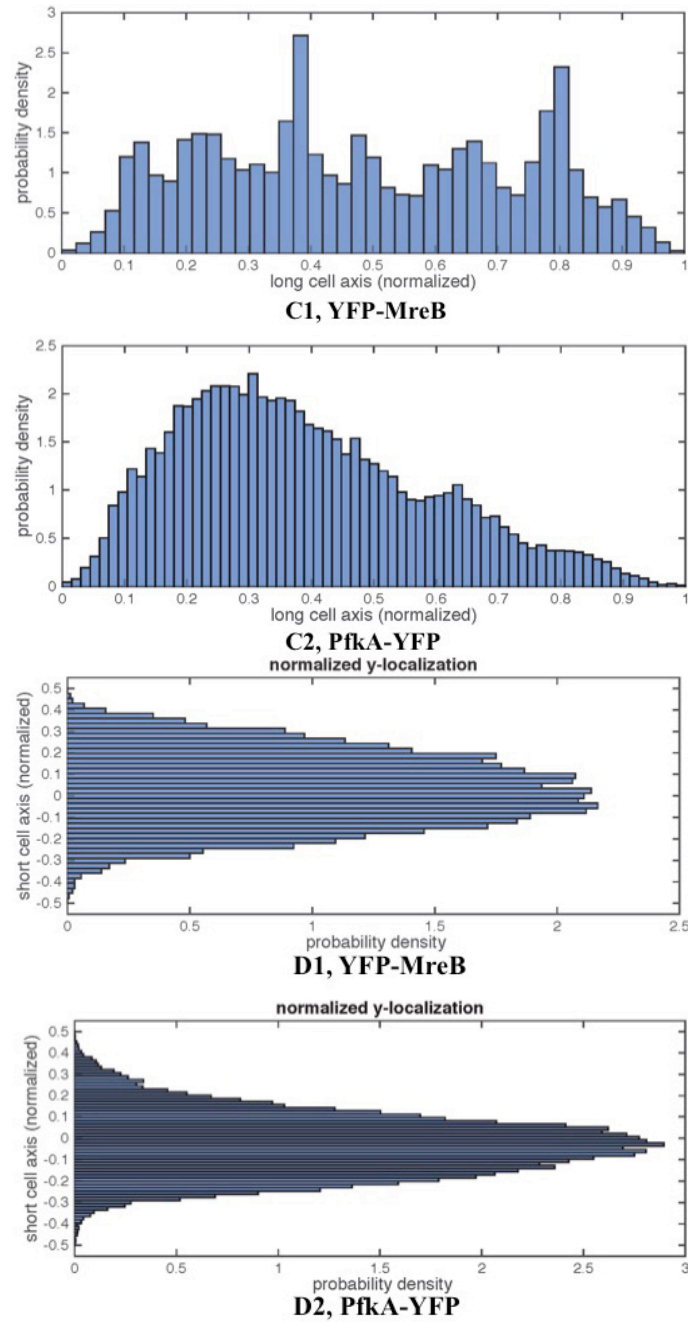


Figure 31. Single molecule tracking and spots localization study. (A) Overlay of single molecule tracking. A1 and A2 are overlays of single molecule trajectories of YFP-MreB and PfkA-YFP that obtained in exponentially growing *B. subtilis* cells. Trajectories longer than 5 frames were analyzed. In both A and B images, the X axis represents the cell length, the Y axis represents the cell width. (B) Heatmap of spots localization, which represents the density of single molecule spots. The gradient bar on the right side of each heatmap stands for the density of each color, from above (yellow) to bottom are gradient densities from 100% to 10%. (C) Normalized X-localization. The X axis represents the cell length; the Y axis represents the density of spots along the cell length. (D) Normalized Y-localization. The Y axis represents the cell width; the X axis represents the probability density of spots along the cell width. Images were created by Dr. Thomas Rösch.

### 3.5.3 Single molecule analysis of MreC, MreD, RodZ and Pbp1A

The data analysis from u-track and msd-analyzer of YFP-MreC, YFP-MreD, YFP-RodZ and YFP-Pbp1A showed that the movements of their single molecules consist of two populations. One is the static population, another one is the highly dynamic population. YFP-MreC and YFP-MreD (Figure 32) have the similar moving behavior as the YFP-MreB (Figure 30). The reason is that MreC and MreD are colocalize with MreB. YFP-RodZ, which is also an MreB-associated protein, has a similar moving behavior as the YFP-MreB. Pbp1A, which is a key enzyme of the cell wall biosynthesis machinesry and belong to the PBPs, has a mobile fraction with the highest diffusion coefficient ( $0.812 \mu\text{m}^2/\text{s}$ ). More than half of the total population of YFP-MreC, YFP-MreD and YFP-Pbp1A single molecules belong to the immobile fraction, while 42.1% of YFP-RodZ single molecules are static. The localization of MreC (Figure 26 E and G), MreD (Figure 26 F and H), RodZ (Figure 28 A and B), Pbp1A (Figure 28 D) shows they are membrane proteins as MreB.

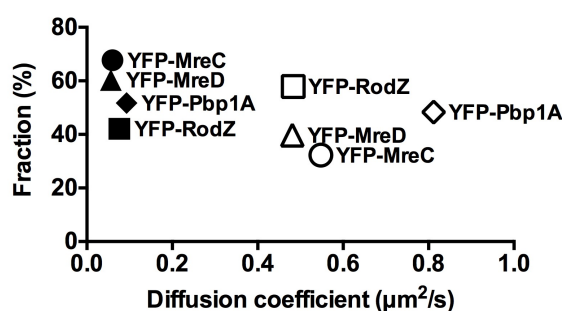
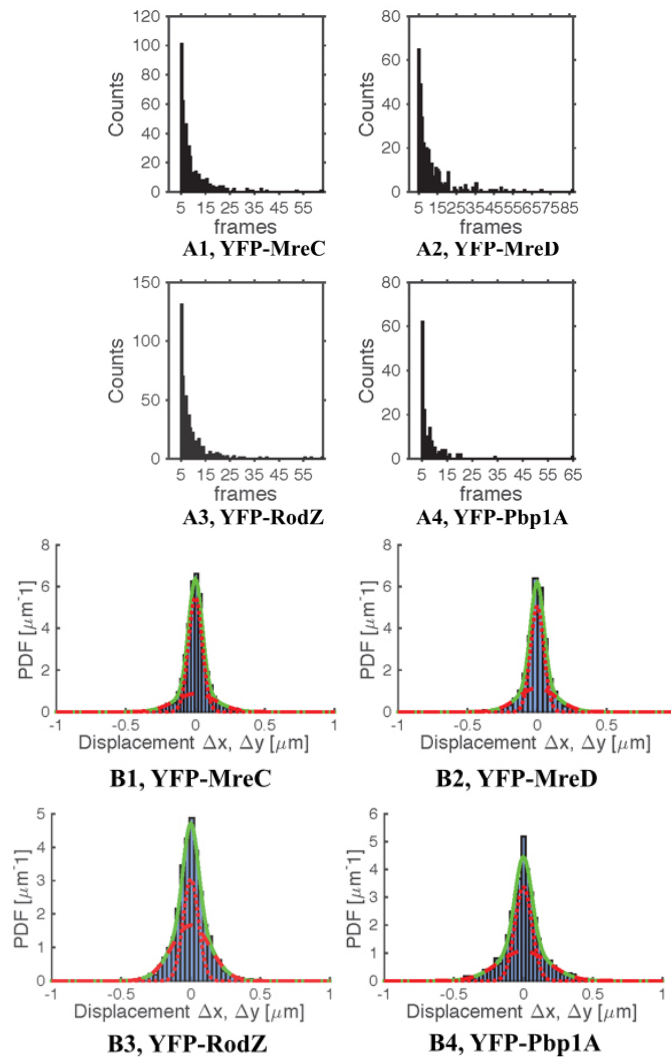


Figure 32. Diffusion coefficients. The mean diffusion coefficients of mobile and static YFP-MreC were  $0.548$  (32.3%) and  $0.060$  (67.7%)  $\mu\text{m}^2/\text{s}$ , respectively. The mean diffusion coefficients of mobile and static YFP-MreD were  $0.481$  (39.7%) and  $0.056$  (60.3%)  $\mu\text{m}^2/\text{s}$ . The mean diffusion coefficients of mobile and static YFP-RodZ were  $0.483$  (57.9%) and  $0.076$  (42.1%)  $\mu\text{m}^2/\text{s}$ . The mean diffusion coefficients of mobile and static YFP-Pbp1A were  $0.812$  (48.3%) and  $0.093$  (51.7%)  $\mu\text{m}^2/\text{s}$ . The round circles represent the movement behavior of YFP-MreC. The triangles represent the movement behavior of YFP-MreD. The squares represent the movement behavior of YFP-RodZ. The diamonds represent the movement behavior of YFP-Pbp1A. The X axis shows the diffusion coefficient of each population, the Y axis shows the fraction of each population.

The fit plot of Gaussian distribution (Figure 33 A) and CPD (cumulative probability density function, data not shown) of YFP-MreC, YFP-MreD, YFP-RodZ and YFP-



Pbp1A showed that the single molecules consist of two populations. One is the immobile population, the other one is the mobile population. The superposition plot curve of two populations fitted very well with the Gaussian distribution of our experimental data (Figure 33 B). The heatmap of spots localization of YFP-MreC and YFP-MreD showed that MreC and MreD are widely distributed within the cell, and they have some preferable localization place in the cytoplasm of cell (Figure 33 C1 and C2). The density of YFP-MreC and YFP-MreD single molecules is higher at some places, this result is in accordance with the localization study of YFP-MreC and YFP-MreD by using epifluorescence microscopy (Figure 26 G and H). YFP-RodZ and YFP-Pbp1A are widely distributed inside the cytoplasm (Figure 33 C3 and C4), RodZ and Pbp1A are membrane proteins (Figure 28 A and D). Since MreC, MreD, RodZ and Pbp1A are membrane proteins, their single molecule spots have similar localization patterns (Figure 33), but the movement speed of mobile Pbp1A single molecules is the highest among all of these membrane proteins.





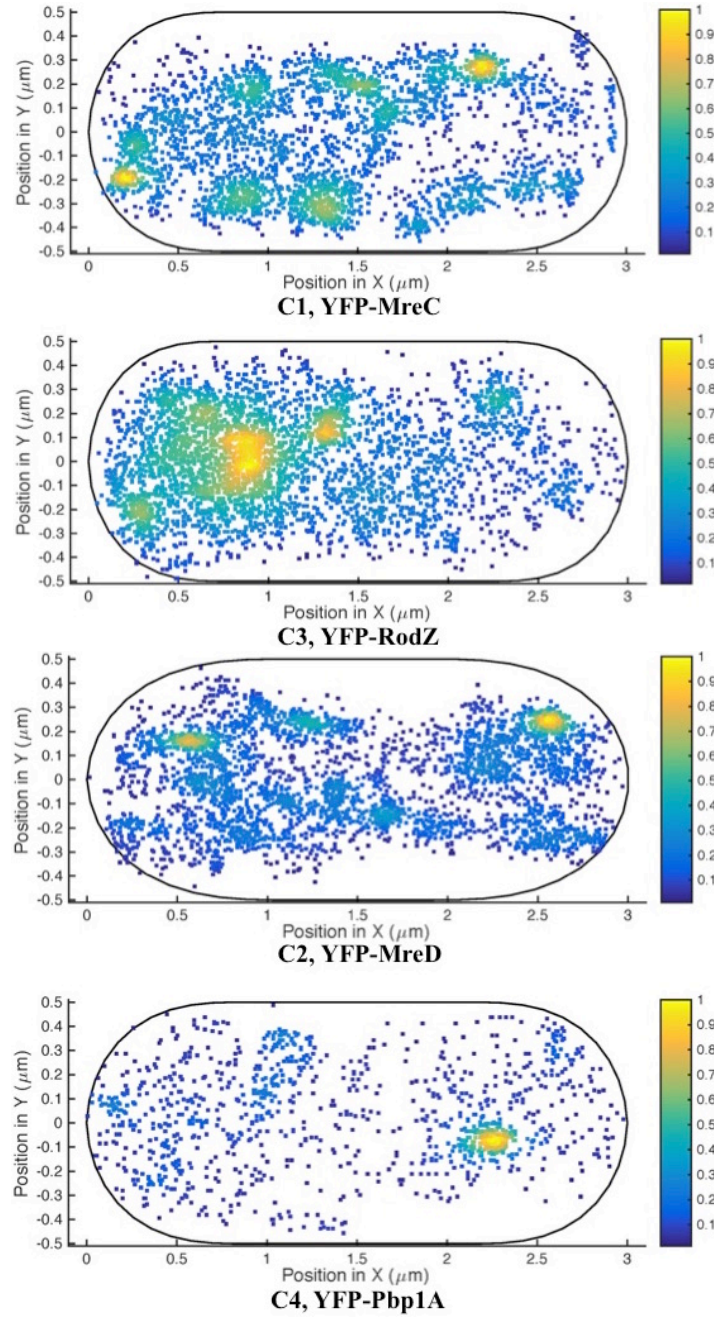


Figure 33. Single molecule tracking analysis and the study of spots localization. (A) Track lengths in frames. The X axis stands for the frame interval of each spot, the Y axis stands for the number of frame interval. (B) Two populations fit of Gaussian distribution. The X axis represents each moving behavior. The Y axis represents the density of each moving behavior. The green curve represents the superposition plot of two populations fit. The dotted red curve represents the Gaussian fit of the immobile population, the dashed red curve represents the Gaussian fit of mobile population. (C) Heatmap of single molecule spots localization. The X axis represents the cell length, the Y axis represents the cell width. The gradient bar on the right side of each heatmap stands for the density of each color, from above (yellow) to bottom there is a gradient density from 100% to 10%. Images were created by Dr. Thomas Rösch.

### 3.5.4 Single molecule analysis of pyruvate dehydrogenase (PDH) complex

The pyruvate dehydrogenase (PDH) complex catalyzes the conversion of pyruvate to acetyl-CoA and CO<sub>2</sub> [180]. PDH is a large complex, which contains multiple copies of three enzymatic components: pyruvate dehydrogenase (E1,  $\alpha$  and  $\beta$  subunits are PdhA and PdhB), dihydrolipoamide acetyltransferase (E2, PdhC) and lipoamide dehydrogenase (E3, PdhD). In Gram-negative bacteria, the central core of PDH complex contains 24 molecules of E2 (PdhC) [143]. Up to 24 copies of E1 (PdhA and PdhB) and 12 copies of E3 (PdhD) bind to the E2 core [181]. In Gram-positive bacteria and eukaryotes, the PDH complex consists of a central icosahedron core that is made up of 60 E2 (PdhC) molecules, and 30 E1 (PdhA and PdhB) and 6 E3 (PdhD) subunits bind to this core [142]. Eukaryotes contain 12 copies of an additional core protein, E3 binding protein (E3BP). In yeast, E3BP binds to each of the icosahedral faces [182].

The data analysis of PDH complex single molecule tracking showed that each subunit of PDH is composed of two populations. One is the mobile population, which is highly diffusing within the cell. The other one is the immobile population, which forms the PDH complex. We can distinguish which subunit of PDH is the core of the complex by analyzing the fraction and the diffusion coefficient of each population. From four PDH subunits, the E2 (PdhC) core has both the lowest fraction (27.0%) and the lowest diffusion coefficient ( $0.357 \mu\text{m}^2/\text{s}$ ) of the mobile population in comparison with the other 3 subunits (Figure 34). These results further prove that E2 is the core of PDH complex, because the other subunits need to bind to this core, which makes them more dynamic. Therefore, the core of the complex must be more static and the fraction (73.0%) of static molecules must be higher than in the other subunits of PDH. The E2 subunit is needed in bigger amounts than the E1 (PdhA and PdhB) and E3 (PdhD) subunits, therefore, the fraction of static E2 single molecules is higher than that of E1 and E3 subunits.

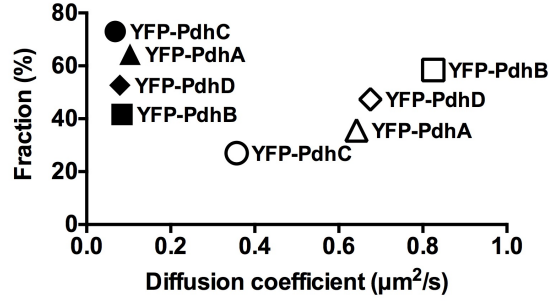


Figure 34. Diffusion coefficients. The mean diffusion coefficients of mobile and static YFP-PdhA were 0.642 (with a fraction of 35.6%) and 0.103 (with a fraction of 64.4%)  $\mu\text{m}^2/\text{s}$ . The mean diffusion coefficients of mobile and static YFP-PdhB were 0.825 (58.4%) and 0.084 (41.6%)  $\mu\text{m}^2/\text{s}$ . The mean diffusion coefficients of mobile and static YFP-PdhC were 0.357 (27.0%) and 0.068 (73.0%)  $\mu\text{m}^2/\text{s}$ . The mean diffusion coefficients of mobile and static YFP-PdhD were 0.675 (47.3%) and 0.079 (52.7%)  $\mu\text{m}^2/\text{s}$ . The round circle represents the movement behavior of YFP-PdhC. The triangle represents the movement behavior of YFP-PdhA. The square represents the movement behavior of YFP-PdhB. The diamond represents the movement behavior of YFP-PdhD. The X axis shows the diffusion coefficient of each population, the Y axis shows the fraction of each population.

The fit plot of Gaussian distribution (Figure 35 A) and CPD (cumulative probability density function, data not shown) of YFP-PdhABCD (each subunits of PDH) showed that their single molecules are make up of two populations. One is the immobile population, the other one is the mobile population. The superposition plot curve of two populations fitted very well with the Gaussian distribution of our experimental data (Figure 35 A). The heatmap of spots localization of YFP-PdhB, YFP-PdhC and YFP-PdhD showed that PdhB, PdhC and PdhD are widely and uniformly distributed within the cytoplasm of cell (Figure 35 B2 and B3). This result is in accordance with the localization study of PdhB and PdhC by using epifluorescence microscopy (Figure 27 B and C). The heatmap of YFP-PdhA single molecule spots localization showed that PdhA is localized at one cell pole, this result is also in accordance with our localization study of PdhA (Figure 27 A).

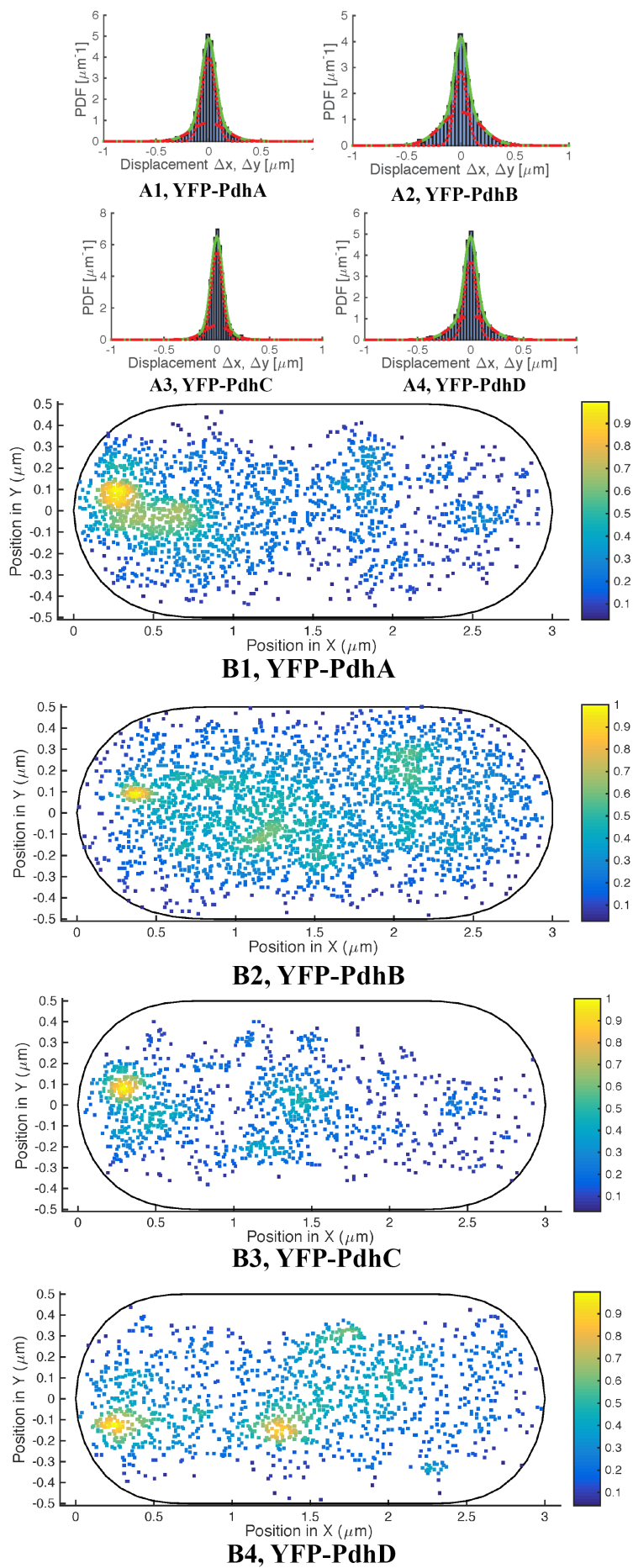


Figure 35. Single molecule tracking analysis and the spots localization study of PDH complex subunits. (A) Two populations fit of Gaussian distribution. The X axis represents each moving behavior. The Y axis represents the density of each moving behavior. Two red curves represent the plot of two populations. The green curve represents the superposition plot of two populations fit. The dotted red curve represents the fit of immobile population; the dashed red curve represents the fit of mobile population. (B) Heatmap of single molecule spots localization. The X axis represents the cell length, the Y axis represents the cell width. The gradient bar on the right side of each heatmap stands for the density of each color, from above (yellow) to bottom are gradient density from 100% to 10%. Number 1-4 represents the analysis of YFP-PdhA, YFP-PdhB, YFP-PdhC and YFP-PdhD, respectively. Images were created by Dr. Thomas Rösch.

### 3.6 Conclusion

Our results showed that the purified lytic enzyme LytC could inhibit the growth of Gram-negative *E. coli* and Gram-positive *B. subtilis*. LytC is moderately stable and not a monomeric protein. The use of BSA as control shows that the inhibition is caused by the LytC enzyme rather than any ordinary protein. The deletions of the trans-membrane domain, the CWB domain and the LCR domain do not affect the activity of LytC. The C-terminal construct of LytC with a strep-tag worked while the N-terminal fusion of GST-His tag to LytC failed. Site directed mutagenesis (a.a. 342 and 461) in functional region did not cause activity loss of LytC. The activity comparison between LytCF2 and LytCF2R2 (functional region partially deleted) shows that it is the functional region that determines the catalytic ability. The deletion of functional region could cause the loss of activity. We microscoped the cells that were treated with LytC to see the phenotype after cell growth inhibition. We observed that in the cells that were treated with LytC, some cells were dead because of the cell wall break down. In survived cells, the spherical or elliptical cell-shapes instead of the original rod-cell shape were observed.

We used PfkA-YFP as a control to compare the moving behavior of its single molecules with YFP-MreB. Diffusion coefficient and single molecule analysis of YFP-MreB showed that more than half of MreB molecules are static (Figure 30, Appendix Figure 36 E1 and F1). Less than half of rapid moving YFP-MreB molecules were also observed, these molecules are the ones that freely diffuse within

the cell. According to the Gaussian and CDF fit, YFP-MreB has a fraction of 53.1% of immobile molecules and 46.9% of mobile molecules. PfkA-YFP does not have static molecules, the highly dynamic population accounts for 49.3% with a diffusion coefficient of  $0.755 \mu\text{m}^2/\text{s}$ , the relatively slower dynamic population accounts for 53.1% with a diffusion coefficient of  $0.232 \mu\text{m}^2/\text{s}$ . We concluded that MreB is much more static and has more static fraction molecules than PfkA. The heatmap of MreB single molecule localization further proved that MreB is a membrane protein. The fraction and the movement speed of mobile MreC, MreD, Pbp1A and RodZ are in a similar pattern with the movement of MreB, because those proteins are membrane-associated proteins. The single molecule data analysis of PDH subunits showed that E2 (PdhC) has both the lowest fraction (27.0%) of mobile population and movement speed ( $0.357 \mu\text{m}^2/\text{s}$ ) of all four subunits. Thus, PdhC is the most static subunit of all four PDH subunits. These results suggest that E2 is the core of PDH *in vivo*.

## 4 Discussion

For many years people tried to explore the next generation of wide range antibiotics since ampicillin was first discovered, and a lot of effort was focused on discovering the ones that bind to cell wall biosynthesis machinery enzymes such as the PG biosynthesis machinery and PBPs. We provide a new idea to find the next generation antibiotics, we mainly focus on the cell wall degradation enzymes which can cause the break down of cell wall, furthermore, cell membrane breaks. And one advantage of these enzymes is they work on all the bacteria that have the cell wall, and they function in the periplasm and will not easily induce the antibiotic resistance. Our results showed the potential of a cell wall breakdown enzyme can be applied for industrial usage.

### **LytC kills host during incubation**

We already overexpressed several constructs successfully. *E. coli* BL21 (DE3) was used for protein overexpression. After induced by IPTG, cells started to lyse after 1 hour of incubation, so it is hard to harvest enough amount of pellets to continue the research. After we managed to obtain enough proteins, we wanted to know if those constructs can lyse cells (we used living organisms *E. coli* and *B. subtilis* as objects), we added purified protein into cell culture (strep elution buffer used as control) and discovered that purified LytC protein can greatly inhibit the growth of bacteria. With the aid of microscopy, we confirmed that the cell wall of *E. coli* and *B. subtilis* is indeed lysed after cells were treated with LytC. We used BSA as control to make sure that it is not just any ordinary protein that can lyse cell wall but the cell wall lyse protein LytC. Finally we found out that cells with BSA grow slightly better than the ones without BSA (we suppose that cells can use protein as one nutrition source).

### **LytC is not a monomer and is moderately stable**

Our proteins can keep activity over one week at 4°C or over 24 hours at room temperature, and can be stored at -20°C or -80°C and keep most activity after once frozen. However, two main problems exist. One is that during the overexpression step LytC kills the host cells so the production of LytC is not very high. The other one is chaperones were produced for some of our constructs (LytCF2, LytCF3 and LytCF4) probably because the protein was not correctly folded which causes the impurity of

the protein. When we concentrated the LytC proteins by ultrafiltration, we used columns that have much bigger molecular weight membrane (only the proteins have bigger MW can be concentrated, the rest small proteins will pass through the membrane). Yet the LytC proteins still blocked by the membrane (confirmed by western-blot of the pass through and membrane blocked parts). This indicates the LytC proteins are not monomer. Since the purified LytC was not monomer, it is not easy to separate the chaperones from the desired protein by gel filtration.

### **LytC keeps its function only by C-terminal fusion and kills bacteria during exponential growth**

We wanted to enhance protein production by fusing our constructs with GST-His tag since it is a widely used tag for protein overexpression. Unfortunately, some constructs did not work in the test expression step and some did not work in the purification step and some do not have the inhibition effect on bacterial growth. The only successful purified construct is GSH-His-LytCF6, but the results of this construct did not fulfill our expectations since it had a slight inhibition on the growth of *E. coli* (Figure 16 C), because the inhibition effect of this construct did not have any advantage in comparison with other C-terminal strep-tagged LytC constructs (e.g. LytCF6). The N-terminal fusion might caused the mis-folding of LytC.

Pneumococcal LytC can kill cells that are in early exponential phase maybe because the LytC from pneumococcus is only able to hydrolyze non-cross-linked PG chains so probably the same applied to the LytC of *B. subtilis* [63]. The attempt to track the process of bacterial cell wall breakdown and cell death under high resolution microscopy was not successful and the test digest of cells from plates did not work as we expected. We assume the reason should be that LytC only works for bacteria that are in exponential phase, or in other words that LytC can only inhibit cell growth but can not hydrolyze the cell wall that in stationary phase. Another reason is that bacteria need longer time for growing on plate than in liquid medium so that the LytC was probably already degraded by the proteases that secreted by the cells. The reason for the failure of live cell lysing visualization could be that when cells are attached with S7<sub>50</sub> agar, the cells start to absorb nutrition from S7<sub>50</sub> solid medium instead of liquid medium and the effective concentration of LytC decreased in comparison with in liquid culture.



### **Functional region rather other domains work as bacteria inhibitor**

We made 6 constructs of LytC (from LytCF1 to LytCF6) that fused with strep-tag at the C-terminal. Purification of LytCF1 failed (Figure 11 D). LytCF3 was not very pure after the strep-tag column purification and even after gel filtration, there is always a un-wanted band (Figure 11 A and C). The reason could be that the impurity chaperones have similar molecular weight as non-monomeric state LytCF3. The situation for LytCF4 was similar to LytCF3, the purity of LytCF4 is not high enough for precise analysis (Figure 12 A and B). The production of LytCF6 (Figure 12 C and D) is too low in comparison with LytCF2 and LytCF5, so the further usage of LytCF6 had to be limited. We mainly used the constructs of LytCF2 and LytCF5 for the study. Bacteria *E. coli* and *B. subtilis* were used for the inhibition test: the purified LytCF1 was not obtained so that the inhibition test was not performed; LytCF2 can greatly inhibit the growth of *E. coli* (Figure 15 A and B) and *B. subtilis* (Figure 15 C) with a final concentration of 7.6 mM and 17 mM, respectively. LytCF3 can inhibit the growth of *E. coli* with a final concentration of 3.1 mM (Figure 15 D). LytCF4 can inhibit the growth of *E. coli* BL21 with a final concentration of 10.2 mM (Figure 16 A). The purified LytCF5 protein can greatly inhibit the growth of *E. coli* and *B. subtilis* with a final concentration of 1.8 mM and 8.3 mM, respectively, and this have been proved by several repeats (Figure 17 and Figure 18). The purified LytCF6 protein proved again that LytC can inhibit the growth of *E. coli* with a final concentration of 1.3 mM. We proved that LytC can function without the trans-membrane region. LytC can function when „low complexity region“ (LCR) is partially deleted (LytCF3) or totally removed (LytCF2, LytCF5 and LytCF6). LytC can function when two cell wall binding (CWB) regions were removed (LytCF3 and LytCF2) and even all three CWB regions were removed (LytCF5 and LytCF6). LytC can function as long as the functional region is kept, LytC kept the lytic activity when only the functional region was kept (LytCF6). We conclude that the trans-membrane region, CWB regions and LCR are not necessary for the activity of LytC. Chaperones were formed in the constructs of LytCF2, LytCF3 and LytCF4. Therefore, in these constructs the LytC proteins could not be folded properly and this affected the purity and activity of LytC, which caused an imprecise calculation of LytC concentration.

### **Defect of LytC functional region causes activity loss**

To further prove it is the function region of LytC inhibit the growth of bacteria and degrad the cell wall, the site-directed mutagenesis and functional region partially deletion were performed. In the LytC mutation experiments, we chose the LytCF5 construct for producing site-directed mutants. The single site-directed mutation and double sites mutation results showed that the sites we mutated are not the key amino acid points for the function of LytCF5 (Figure 22 and Figure 23). LytCF2 construct was chosen for the partial deletion experiment, the activity of LytCF2R2 (partial deletion construct) was lost in almost half if compared to that of LytCF2 for *E. coli* (Figure 24 A and B), the activity of LytCF2R2 was also partially lost for *B. subtilis* (Figure 24 C). Therefore we proved it is the functional region of LytC protein that inhibits cell growth. Yet the evidence was not enough for us to conclude that LytC can break down the cell wall, we needed visual proof to see what happened to the cells after treated with LytC and what kind of damage LytC could cause. *E. coli* of XL1 and BL21 and *B. subtilis* PY79 that treated by LytCF5 and LytCF6 samples were used for microscopy. In the treated *E. coli* samples, we captured images of cells that were dead probably because of the degradation of cell wall (Figure 25). There were also some cells that still survived even after they lost the cell wall but those cells had a new spherical cell-shape instead of the normal rod-cell shape (Figure 25). In the treated *B. subtilis* samples, the dead cell images were not so widely captured as *E. coli* because the gram-positive bacteria *B. subtilis* have thicker cell wall than the gram-negative *E. coli*. Dead *B. subtilis* cells that loss their cell wall were also visualized (Figure 25). Even though most *B. subtilis* cells survived, the survived ones partly lost their cell wall and could not maintain the rod-cell shape. The new cell shape is neither like rod shape nor like spherical shape since part of the cell wall was still left surrounding the cell membrane (Figure 25).

### **Localization study of proteins *in vivo***

The localization study of YFP-MreB in exponential growth *B. subtilis* showed that MreB localized underneath the lateral membrane as a discontinuous filament structure. Some MreB filaments are long and can extend over the entire cell width and even more than half of the cell circumference, while some filaments are rather short. Patchy spots of MreB localization pattern were also observed (Figure 26 A). When the expression level of MreB was decreased, most of the long filament structure was

lost and the short filaments or spots localization started to appear (Figure 26 B). If we totally cut off the expression of YFP-MreB by removing xylose induction, very weak of MreB illumination signal was still recorded because of the leaky xylose promoter. We expressed the GFP-MreB in two *E. coli* strains, the *gfp-mreB* was integrated into the chromosome in one strain and *gfp-mreB* was cloned into a vector in other strain. The expression of GFP-MreB showed that MreB has the same localization pattern in Gram-negative bacteria *E. coli* as in Gram-positive bacteria *B. subtilis* (Figure 26 D, the localization of GFP-MreB in the vector-transformed strain was not shown since it is the same as in the case of chromosome recombination). GFP-MreC and GFP-MreD in exponential *B. subtilis* localized on the membrane, with the same localization pattern as membrane staining (Figure 26 E and F). YFP-MreC and YFP-MreD proteins showed a more defined localization pattern than the GFP-tagged ones, they also have patchy spots localization within the cell besides the localization pattern of membrane staining. These results showed that MreB, MreC and MreD are membrane proteins and they colocalized.

RodZ and Pbp1A also play a key role in the cell shape determination and maintenance, and RodZ also colocalized with MreB. YFP-RodZ and YFP-Pbp1A have the same localization pattern as membrane staining which is also similar to MreB, MreC and MreD localization. The illumination signal of MreC and Pbp1A is lower than that of MreB and RodZ, while the signal of MreD is the most moderate among those five proteins (Figure 28 A, B and D). These results indicate that the copy number of MreC and Pbp1A is lower than that of MreB and RodZ and the copy number of MreD is moderate. And the results also proved that those five proteins are membrane proteins. The epifluorescence signals of PfkA-YFP and YfhH-YFP are widely and uniformly distributed inside the cell cytoplasm (Figure 28 C and F), this demonstrates that PfkA and YfhH are cytoplasmic proteins. In the RecX-YFP constructed strain, we observed elongated cells and RecX is prone to localized at one cell pole in exponentially grown *B. subtilis* (Figure 28 E).

Two subunits of PDH complex, PdhB (E1  $\beta$ ) and PdhC (E2) have the same localization pattern, they are uniformly distributed under the lateral membrane and within the cytoplasm of the cell (Figure 27 B and C). PdhA (E1  $\alpha$ ) localized as foci at the cell pole with different fluorescence intensity. From our estimation, one third of

the cells have PdhA localized at the cell pole with high intensity, another one third of cells have PdhA localized at the cell pole with low intensity, the last one third of cells does not contain any PdhA foci. PdhD (E3) has two patterns of localization in *B. subtilis*. In one pattern, the localization of PdhD is overlapped with the illumination of DNA staining (Figure 27 D1), which indicates PdhD might have DNA affinity. In another pattern, PdhD localized uniformly within the cytoplasm of the cells (Figure 27 D3), which is the same pattern as PdhB and PdhC.

### **Two distinct fractions of YFP-MreB single molecules**

Single molecule microscopy of several proteins was performed in this study. The movement of these molecules was tracked both manually and automatically, the automatic tracking data were further modified manually and processed. The automatic tracking fit our experimental data well most of the time. But some tracks were not accurate since the spots disappeared (not only by photobleaching) in some frames because some molecules moved out of the focal plane. The single molecules are moving in a 3 dimensional space while the single molecules tracking were captured by camera in a 2 dimensional plane so there must be some missed tracks or error calculation. Another major error source is that the cells we microscoped were alive and their positions can be changed casually even the cells were fixed to the agarose. Therefore, if a spot moved out of the focus plane or it does not move strictly in the 2 dimensional plane or the cell changed its position, then the spots cannot be detected by the camera or the movement was misrecorded. The new blinked spots were not only from the bleached recovery but also from the places that were not in the focal plane. Single molecule experiments were performed in real time in living *B. subtilis* cells to investigate the dynamics of MreB. Single molecules of different proteins were microscoped in this study. The movement of these molecules was tracked automatically, and the automatic tracking followed the spots pretty well. Since the cells are alive and can change their position subtly, this will lead to the change of focal plane. Some spots could move out of the focal plane, therefore those spots cannot be detected or detected with less intensity. This will cause many short tracks and further reduce the precision of our data analysis, hence the tracks that were shorter than 5 frames were not included.

For most of the proteins we tracked, two categories of molecular movements could be visualized, a mobile one and a static one. The movement of PfkA-YFP can be divided into two mobile categories or one mobile category. The movement speed and fraction of each mobile population of proteins were calculated. The single molecules of each protein can switch their state between static and dynamic. For example, the freely diffusing MreB single molecules can bind to the existing MreB filament structure and form the static molecules. The MreB single molecules in filaments can also diffuse from the negative end and form the freely diffusing MreB. We used PfkA as the control of MreB since PfkA is a fast moving protein. The data analysis of MreB and PfkA single molecules showed that MreB is more static while PfkA is freely diffusing within the cytoplasm of the cell. Two fractions of YFP-MreB could be distinguished: a mobile and a static fraction of molecules. The evaluation revealed that more than half MreB molecules are static (53.1% with a  $D$  of  $0.060 \mu\text{m}^2/\text{s}$ ) and the rest is highly dynamic (46.9% with a  $D$  of  $0.463 \mu\text{m}^2/\text{s}$ ). To further elucidate that PfkA-YFP consists of two populations of molecules with different mobility, another approach based on the fitting of CDF on the distribution of single molecules step sizes was used. The fitting with two populations of molecules distribution fitted much better with the experimental data than with one mobile population.

The construct of YFP-MreB we used in this study was at the *amy* locus of *B. subtilis* and under control of the xylose promoter. MreB can be divided into two categories: one category is the native MreB under the original promoter, the other category is the constructed YFP-MreB under the xylose promoter. The co-expression of both source of proteins will lead to the slightly over expression of MreB proteins. The amount of MreB that cell needs to form filaments are static. Therefore, there are more MreB molecules in our constructed strain than the wild type *B. subtilis*. The excessive single molecules are freely diffusing within the cell. Those freely diffusing YFP-MreB have to compete with native MreB molecules to bind to the MreB filaments, therefore, the speed of single molecules movement might also be accelerated. The real diffusion coefficient and fraction of mobile MreB single molecules should be lower than our data. In reality, MreB single molecules should be more static and the fraction of immobile molecules should also be slightly higher than in our data. For the PfkA-YFP case, the construct *pfkA-yfp* replaced the original *pfkA* gene and was under control of its original promoter. Therefore, the single molecule data of PfkA we obtained in this

study should be the most accurate one in comparison with other proteins. The effort of using *E. coli* with GFP-MreB construct to perform the single molecule experiment to clarify the dynamics of MreB molecules in Gram-negative bacteria failed. It will be a good control to compare the MreB moving behavior between Gram-positive and Gram-negative bacteria if it succeeded.

### **The movement pattern and fraction of MreC, MreD, RodZ and Pbp1A are similar to MreB**

The dynamic fraction and movement pattern of MreC, MreD, Pbp1A and RodZ single molecules are similar to MreB. These five proteins are all membrane proteins and play a critical role in the determination and maintenance of bacterial cell shape. MreC, MreD and RodZ colocalize with MreB, RodZ also interacts with other cell shape proteins, Pbp1A also plays an important role in cell wall synthesis. All of these reasons make MreB, MreC, MreD, RodZ and Pbp1A single molecules have similar dynamic movement pattern and fraction. Since YFP-MreC, YFP-MreD, YFP-RodZ and YFP-Pbp1A are all at the amy locus and under the drive of xylose promoter. The single molecule data we obtained for those proteins are similar to MreB, they are not 100% precise. In reality, the fraction and the diffusion coefficient of mobile single molecules of those proteins should be lower than the data we obtained in this study.

### **Single molecule data analysis indicate PdhC is the core of PDH complex**

Single molecule experiments revealed that 73.0% of PdhC are immobile, which is a higher percentage than for the other components of PDH (pyruvate dehydrogenase) complex. Both the diffusion coefficient ( $0.357 \mu\text{m}^2/\text{s}$ ) and fraction (27.0%) of mobile PdhC molecules are lower than the rest components of the PDH complex. This further demonstrates that PdhC is the core of PDH complex. There is a core (E2) in the pyruvate dehydrogenase (PDH) complex, that is why PdhC single molecules are more static and move slower than other subunits of PDH complex. The other subunits are binding to this core so they need to be more dynamic. The E2 (PdhC) subunit is needed more than other subunits in PDH complex, the fraction of immobile PdhC single molecules is the highest. This result further proves that the E2 subunit is the core of PDH. All four subunits of PDH complex we constructed in this work are at the amy locus of *B. subtilis*, and under the drive of the xylose promoter. Therefore, in *B. subtilis* cells, there are two kinds of proteins for each of our constructs, one kind is the

native proteins of PDH complex, the other kind is the constructed YFP-PDH that is at the amy locus and under the drive of xylose promoter. The native E1 (PdhA and PdhB) and E3 (PdhD) subunits are competing with the constructed E1 and E3 to bind to the E2 (PdhC) core of the PDH complex. In some cases, if the native E1 and E3 single molecules are already bound to the E2 cores, the constructed YFP-PdhA, YFP-PdhB and YFP-PdhD need to move around to find the unbound cores. Therefore, more movement of PDH single molecules were recorded by the microscopy camera, and the fraction and the movement speed of mobile single molecules are higher than in reality. In the wild type *B. subtilis*, the native PDH single molecules are more static. We need the constructed proteins expressed in single molecule level because too much of epifluorescence molecules will interfere with the accuracy of our results, so the expression of constructed proteins was strictly controlled. Therefore, even though our results are not 100% precise to describe the reality, we are trying to get closer to it. The same situation applies to the movement of MreB, MreC, MreD, RodZ and Pbp1A.

We can obtain much information from the single molecule analysis data. For example, we can judge if a protein is a membrane protein (MreB) from the heatmap figure of single molecule spots localization. We can also tell if a protein is freely diffusing or forms filaments or localizes at some positions (e.g. PdhA localizes at cell poles). From the fit of Gaussain distribution and cumulative probability density (CPD), we can conclude how many of dynamic population exist for each protein single molecule. From the analysis of mean square displacement (MSD) of each single molecule, we can get the fraction of each protein population, we can also tell if the protein is bond or freely diffusing. From the comparison of diffusion coefficient, we found that MreC, MreD and RodZ are colocalized with MreB. We also conclude that PdhC (E2) is the core of PDH complex by comparing the diffusion coefficient and the fraction of mobile single molecules with other subunits of PDH complex. If we continue the research, we can get even more information from the data analysis of single molecules.

## 5 Prospects of future study

There are over 35 autolysins genes in *B. subtilis* and 3 of them are the mainly autolysins for the cell wall but we only studied the major one, LytC, so there is still a lot of work to do. For example, in the sporulation process, after the formation of spores the mother cell is lysed and the LytC is not responsible for this process so we need to figure out which autolysin or how many autolysins can degrade the cross-linked PG (e.g. LytD can hydrolyze the cross linked PG indicate lytic enzymes can also kill the bacteria at stationary phase). So together with LytC, these autolysins cannot only inhibit the growth of bacteria but also kill the ones that are in vegetative phase. This could bring us to a brighter future of using industrialized proteins as potential antibiotics or as ingredients of cosmetics.

All in all, we open a potential gate to access a new way of antibacterial factors (or antibiotics) search, not like the old-fashioned way that managed to find the antibiotics that bind to the cell wall biosynthesis machinery and therefore kill the bacteria. For these traditional antibiotics, bacteria can easily evolve a pathway that causes the antibiotic resistance. We are seeking the enzymes that can degrade cell wall components and therefore inhibit bacterial growth and furthermore kill bacteria. The advantage of using cell wall breakdown enzymes as the new antibiotics is that enzymes do not need to pass through the cell wall and membrane to function (LytC can pass through both since the gram-negative bacteria *E. coli* have the double layer cell membrane) which will reduce activity lost. The second reason is that bacteria are not prone to develop protein resistance as with the traditional antibiotics. However, to use LytC as a new antibiotics in industrial scale and for clinical usage, there is still a lot of work that needs to be done, such as the production of LytC must be highly enhanced to make sure the industrial usage is profitable. And the side effects also need to be checked in case the LytC enzyme causes harm to human beings (even though human cells do not have cell wall). Another disadvantage is that LytC can only hydrolyze non-cross-linked PG chains so the LytC can only be used to kill the growing bacteria. For example, cells that in early exponential phase, therefore we need to discover other autolysins that are able to hydrolyze cross-linked PG chains. There are over 35 autolysins in *B. subtilis* so there is a great chance to discover another autolysin candidate that can hydrolyze cross-linked PG chains, if combined



with LytC they can kill bacteria in all growth phases. We are optimistic that our discovery of LytC function can be applied as medicine, for example it can be used for some skin disease or used as external medicine. Another potential is that LytC can be used as an additive in the cosmetic industry, which could reduce the infection chance of skin disease.

We already obtained much information from the data analysis of single molecules, yet we could get even more data if we analyze further. For example, we can get the diameter of movement by analyzing the trajectory. We can study the localization of proteins with single molecule microscopy, the traditional epifluorescence microscopy will not be needed. However, there are also some disadvantages of single molecule microscopy. First of all, single molecules are moving rapidly in living cells, even the slightest change of cell position could cause great error in single molecule tracking. Secondly, the single molecule microscopy was performed in 2 dimensional. But in living cell, the molecules could move in a 3 dimensional space. At present, the single molecule microscopy is a good tool to study membrane proteins, there are still some adjustments need to do for studying cytoplasmic proteins precisely in single molecule level. The diameter of bacteria (usually in  $\mu\text{m}$  level) is rather shorter than eukaryotes, the objective of microscopy can only focus at a small specific region. The focusd region (in  $\mu\text{m}$  level) of eukaryotes can be treated as flat 2 dimensional layer. Yet for bacteria, we usually lose the focus of single molecules at the edges or the poles of cells. Therefore, to use the single molecule microscopy technique and the analyzed data more widely, more models need to be built and more correction needs to be done to obtain more accurate data.

In our case, there are two categories of protein single molecules in cells, for PDH subunits, MreBCD and RodZ constructs. One is the native proteins and another one is the constructed proteins. The co-expression of both kind of proteins will lead to the over expression of proteins. The proteins that cells needed, for example MreB to form the filaments, PdhC to form the core of PDH complex, are unchanged. This will result in an excess of protein single molecules in the cells, and the excessive single molecules are more likely to diffuse freely in the cells. This is the main source of error in our work. In the future, we plan to delete the native genes to make our experimental data more matched with the reality. The enzyme activity of each

subunits of PDH complex also needs to be tested because we have both the N-terminal and the C-terminal fusion and usually only one kind of fusion works, we need to illustrate which fusion could maintain the enzyme activity.

## References

1. Errington, J., *Bacterial morphogenesis and the enigmatic MreB helix*. Nature Reviews Microbiology, 2015. **13**(4): p. 241-248.
2. Höltje, J.-V., *Growth of the stress-bearing and shape-maintaining murein sacculus of Escherichia coli*. Microbiology and Molecular Biology Reviews, 1998. **62**(1): p. 181-203.
3. Lazar, K. and S. Walker, *Substrate analogues to study cell-wall biosynthesis and its inhibition*. Current opinion in chemical biology, 2002. **6**(6): p. 786-793.
4. Barreteau, H., et al., *Cytoplasmic steps of peptidoglycan biosynthesis*. FEMS microbiology reviews, 2008. **32**(2): p. 168-207.
5. Bouhss, A., et al., *The biosynthesis of peptidoglycan lipid-linked intermediates*. FEMS microbiology reviews, 2008. **32**(2): p. 208-233.
6. Sauvage, E., et al., *The penicillin-binding proteins: structure and role in peptidoglycan biosynthesis*. FEMS microbiology reviews, 2008. **32**(2): p. 234-258.
7. Van Dam, V., et al., *Transmembrane transport of peptidoglycan precursors across model and bacterial membranes*. Molecular microbiology, 2007. **64**(4): p. 1105-1114.
8. White, C.L. and J.W. Gober, *MreB: pilot or passenger of cell wall synthesis?* Trends in microbiology, 2012. **20**(2): p. 74-79.
9. Silhavy, T.J., D. Kahne, and S. Walker, *The bacterial cell envelope*. Cold Spring Harbor perspectives in biology, 2010. **2**(5): p. a000414.
10. Vollmer, W., D. Blanot, and M.A. De Pedro, *Peptidoglycan structure and architecture*. FEMS microbiology reviews, 2008. **32**(2): p. 149-167.
11. Van Heijenoort, J., *Recent advances in the formation of the bacterial peptidoglycan monomer unit*. Natural product reports, 2001. **18**(5): p. 503-519.
12. Dramsi, S., et al., *Surface proteins covalently attached to peptidoglycan: examples from both Gram-positive and Gram-negative bacteria*. FEMS Microbiol Rev, 2008.
13. Neuhaus, F.C. and J. Baddiley, *A continuum of anionic charge: structures and functions of D-alanyl-teichoic acids in gram-positive bacteria*. Microbiology and Molecular Biology Reviews, 2003. **67**(4): p. 686-723.
14. Schleifer, K.H. and O. Kandler, *Peptidoglycan types of bacterial cell walls and their taxonomic implications*. Bacteriological reviews, 1972. **36**(4): p. 407.
15. Hughes, R., *Autolysis of Bacillus cereus cell walls and isolation of structural components*. Biochem. J, 1971. **121**: p. 791-802.
16. Warth, A. and J. Strominger, *Structure of the peptidoglycan from vegetative cell walls of Bacillus subtilis*. Biochemistry, 1971. **10**(24): p. 4349-4358.
17. Ward, J.B., *The chain length of the glycans in bacterial cell walls*. Biochemical Journal, 1973. **133**(2): p. 395.
18. Tuomanen, E., et al., *Unusual composition of peptidoglycan in Bordetella pertussis*. Journal of Biological Chemistry, 1989. **264**(19): p. 11093-11098.
19. Quintela, J., M. Caparrós, and M.A. de Pedro, *Variability of peptidoglycan structural parameters in gram-negative bacteria*. FEMS microbiology letters, 1995. **125**(1): p. 95-100.
20. Quintela, J.C., et al., *Structure of peptidoglycan from Thermus thermophilus HB8*. Journal of bacteriology, 1995. **177**(17): p. 4947-4962.

21. Glauner, B., *Separation and quantification of muropeptides with high-performance liquid chromatography*. Analytical biochemistry, 1988. **172**(2): p. 451-464.
22. Murray, R., P. Steed, and H. Elson, *The location of the mucopeptide in sections of the cell wall of Escherichia coli and other gram-negative bacteria*. Canadian journal of microbiology, 1965. **11**(3): p. 547-560.
23. Hobot, J., et al., *Periplasmic gel: new concept resulting from the reinvestigation of bacterial cell envelope ultrastructure by new methods*. Journal of bacteriology, 1984. **160**(1): p. 143-152.
24. Leduc, M., C. Frehel, and J. Van Heijenoort, *Correlation between degradation and ultrastructure of peptidoglycan during autolysis of Escherichia coli*. Journal of bacteriology, 1985. **161**(2): p. 627-635.
25. Leduc, M., et al., *Multilayered distribution of peptidoglycan in the periplasmic space of Escherichia coli*. Journal of general microbiology, 1989. **135**(5): p. 1243-1254.
26. Beveridge, T.J., *Structures of gram-negative cell walls and their derived membrane vesicles*. Journal of bacteriology, 1999. **181**(16): p. 4725-4733.
27. Prats, R. and M. De Pedro, *Normal growth and division of Escherichia coli with a reduced amount of murein*. Journal of bacteriology, 1989. **171**(7): p. 3740-3745.
28. Nikolaidis, I., S. Favini-Stabile, and A. Dessen, *Resistance to antibiotics targeted to the bacterial cell wall*. Protein Science, 2014. **23**(3): p. 243-259.
29. Smith, T.J., S.A. Blackman, and S.J. Foster, *Autolysins of Bacillus subtilis: multiple enzymes with multiple functions*. Microbiology, 2000. **146**(2): p. 249-262.
30. Blackman, S.A., T.J. Smith, and S.J. Foster, *The role of autolysins during vegetative growth of Bacillus subtilis 168*. Microbiology, 1998. **144**(1): p. 73-82.
31. Margot, P., et al., *The lytE gene of Bacillus subtilis 168 encodes a cell wall hydrolase*. Journal of bacteriology, 1998. **180**(3): p. 749-752.
32. Ohnishi, R., S. Ishikawa, and J. Sekiguchi, *Peptidoglycan hydrolase LytF plays a role in cell separation with CwlF during vegetative growth of Bacillus subtilis*. Journal of bacteriology, 1999. **181**(10): p. 3178-3184.
33. Horsburgh, G.J., et al., *LytG of Bacillus subtilis is a novel peptidoglycan hydrolase: the major active glucosaminidase*. Biochemistry, 2003. **42**(2): p. 257-264.
34. Yamaguchi, H., et al., *Characterization of a new Bacillus subtilis peptidoglycan hydrolase gene, yvcE (named cwlO), and the enzymatic properties of its encoded protein*. Journal of bioscience and bioengineering, 2004. **98**(3): p. 174-181.
35. Fukushima, T., et al., *A new D, L-endopeptidase gene product, YojL (renamed CwlS), plays a role in cell separation with LytE and LytF in Bacillus subtilis*. Journal of bacteriology, 2006. **188**(15): p. 5541-5550.
36. Fukushima, T., et al., *Characterization of new L, D-endopeptidase gene product CwlK (previous YcdD) that hydrolyzes peptidoglycan in Bacillus subtilis*. Molecular Genetics and Genomics, 2007. **278**(4): p. 371-383.
37. Wang, Y., et al., *Deleting multiple lytic genes enhances biomass yield and production of recombinant proteins by Bacillus subtilis*. Microbial cell factories, 2014. **13**(1): p. 1-11.

38. Chen, R., et al., *Role of the  $\sigma$ D-dependent autolysins in Bacillus subtilis population heterogeneity*. Journal of bacteriology, 2009. **191**(18): p. 5775-5784.
39. Rashid, M.H., A. Kuroda, and J. Sekiguchi, *Bacillus subtilis mutant deficient in the major autolytic amidase and glucosaminidase is impaired in motility*. FEMS microbiology letters, 1993. **112**(2): p. 135-140.
40. Helmann, J.D., L.M. Márquez, and M.J. Chamberlin, *Cloning, sequencing, and disruption of the Bacillus subtilis sigma 28 gene*. Journal of bacteriology, 1988. **170**(4): p. 1568-1574.
41. Kuroda, A. and J. Sekiguchi, *Molecular cloning and sequencing of a major Bacillus subtilis autolysin gene*. Journal of bacteriology, 1991. **173**(22): p. 7304-7312.
42. Lazarevic, V., et al., *Sequencing and analysis of the Bacillus subtilis lytRABC divergon: a regulatory unit encompassing the structural genes of the N-acetylmuramoyl-L-alanine amidase and its modifier*. Journal of general microbiology, 1992. **138**(9): p. 1949-1961.
43. Margot, P., C. Mauël, and D. Karamata, *The gene of the N-acetylglucosaminidase, a Bacillus subtilis 168 cell wall hydrolase not involved in vegetative cell autolysis*. Molecular microbiology, 1994. **12**(4): p. 535-545.
44. Margot, P., M. Pagni, and D. Karamata, *Bacillus subtilis 168 gene lytF encodes a  $\gamma$ -D-glutamate-meso-diaminopimelate muropeptidase expressed by the alternative vegetative sigma factor,  $\sigma$ D*. Microbiology, 1999. **145**(1): p. 57-65.
45. Helmann, J.D. and C.P. Moran, *RNA polymerase and sigma factors*. 2002.
46. Britton, R.A., et al., *Genome-wide analysis of the stationary-phase sigma factor (sigma-H) regulon of Bacillus subtilis*. Journal of bacteriology, 2002. **184**(17): p. 4881-4890.
47. Serizawa, M., et al., *Systematic analysis of SigD-regulated genes in Bacillus subtilis by DNA microarray and Northern blotting analyses*. Gene, 2004. **329**: p. 125-136.
48. Márquez, L.M., et al., *Studies of sigma D-dependent functions in Bacillus subtilis*. Journal of bacteriology, 1990. **172**(6): p. 3435-3443.
49. Kearns, D.B. and R. Losick, *Swarming motility in undomesticated Bacillus subtilis*. Molecular microbiology, 2003. **49**(3): p. 581-590.
50. Dubnau, D. and R. Losick, *Bistability in bacteria*. Molecular microbiology, 2006. **61**(3): p. 564-572.
51. Mirel, D.B. and M.J. Chamberlin, *The Bacillus subtilis flagellin gene (hag) is transcribed by the sigma 28 form of RNA polymerase*. Journal of bacteriology, 1989. **171**(6): p. 3095-3101.
52. Rashid, M.H., M. Mori, and J. Sekiguchi, *Glucosaminidase of Bacillus subtilis: cloning, regulation, primary structure and biochemical characterization*. Microbiology, 1995. **141**(10): p. 2391-2404.
53. Yamamoto, H., S.-i. Kurosawa, and J. Sekiguchi, *Localization of the vegetative cell wall hydrolases LytC, LytE, and LytF on the Bacillus subtilis cell surface and stability of these enzymes to cell wall-bound or extracellular proteases*. Journal of bacteriology, 2003. **185**(22): p. 6666-6677.
54. Smith, T.J. and S.J. Foster, *Characterization of the involvement of two compensatory autolysins in mother cell lysis during sporulation of Bacillus subtilis 168*. Journal of bacteriology, 1995. **177**(13): p. 3855-3862.

55. Kabisch, J., et al., *Characterization and optimization of Bacillus subtilis ATCC 6051 as an expression host*. Journal of biotechnology, 2013. **163**(2): p. 97-104.
56. Kobayashi, G., et al., *Accumulation of an artificial cell wall-binding lipase by Bacillus subtilis wprA and/or sigD mutants*. FEMS microbiology letters, 2000. **188**(2): p. 165-169.
57. Kobayashi, G., et al., *Accumulation of a recombinant Aspergillus oryzae lipase artificially localized on the Bacillus subtilis cell surface*. Journal of bioscience and bioengineering, 2000. **90**(4): p. 422-425.
58. Tsuchiya, A., et al., *Production of a recombinant lipase artificially localized on the Bacillus subtilis cell surface*. FEMS microbiology letters, 1999. **176**(2): p. 373-378.
59. Bisicchia, P., et al., *The essential YycFG two-component system controls cell wall metabolism in Bacillus subtilis*. Molecular microbiology, 2007. **65**(1): p. 180-200.
60. Hashimoto, M., S. Ooiwa, and J. Sekiguchi, *Synthetic lethality of the lytE cwlO genotype in Bacillus subtilis is caused by lack of D, L-endopeptidase activity at the lateral cell wall*. Journal of bacteriology, 2012. **194**(4): p. 796-803.
61. Illing, N. and J. Errington, *Genetic regulation of morphogenesis in Bacillus subtilis: roles of sigma E and sigma F in prespore engulfment*. Journal of bacteriology, 1991. **173**(10): p. 3159-3169.
62. Kuroda, A., M.H. Rashid, and J. Sekiguchi, *Molecular cloning and sequencing of the upstream region of the major Bacillus subtilis autolysin gene: a modifier protein exhibiting sequence homology to the major autolysin and the spoIID product*. Journal of general microbiology, 1992. **138**(6): p. 1067-1076.
63. Pérez-Dorado, I., et al., *Insights into pneumococcal fratricide from the crystal structures of the modular killing factor LytC*. Nature structural & molecular biology, 2010. **17**(5): p. 576-581.
64. Lovering, A.L., S.S. Safadi, and N.C. Strynadka, *Structural perspective of peptidoglycan biosynthesis and assembly*. Annual review of biochemistry, 2012. **81**: p. 451-478.
65. Matteï, P.-J., D. Neves, and A. Dessen, *Bridging cell wall biosynthesis and bacterial morphogenesis*. Current opinion in structural biology, 2010. **20**(6): p. 749-755.
66. Hamilton, T.E. and P.J. Lawrence, *The formation of functional penicillin-binding proteins*. Journal of Biological Chemistry, 1975. **250**(16): p. 6578-6585.
67. Lupoli, T.J., et al., *Lipoprotein activators stimulate Escherichia coli penicillin-binding proteins by different mechanisms*. Journal of the American Chemical Society, 2013. **136**(1): p. 52-55.
68. Vashist, J., et al., *Analysis of penicillin-binding proteins (PBPs) in carbapenem resistant Acinetobacter baumannii*. The Indian journal of medical research, 2011. **133**(3): p. 332.
69. Malouin, F. and L. Bryan, *Modification of penicillin-binding proteins as mechanisms of beta-lactam resistance*. Antimicrobial agents and chemotherapy, 1986. **30**(1): p. 1.
70. Frère, J.-M. and M.G. Page, *Penicillin-binding proteins: evergreen drug targets*. Current opinion in pharmacology, 2014. **18**: p. 112-119.

71. Martin, H., *Composition of the mucopolymer in cell walls of the unstable and stable L-form of Proteus mirabilis*. Journal of general microbiology, 1964. **36**(3): p. 441-450.
72. Wise Jr, E.M. and J.T. Park, *Penicillin: its basic site of action as an inhibitor of a peptide cross-linking reaction in cell wall mucopeptide synthesis*. Proceedings of the National Academy of Sciences of the United States of America, 1965. **54**(1): p. 75.
73. Tipper, D.J. and J.L. Strominger, *Mechanism of action of penicillins: a proposal based on their structural similarity to acyl-D-alanyl-D-alanine*. Proceedings of the National Academy of Sciences of the United States of America, 1965. **54**(4): p. 1133.
74. Spratt, B.G., *Distinct penicillin binding proteins involved in the division, elongation, and shape of Escherichia coli K12*. Proceedings of the National Academy of Sciences, 1975. **72**(8): p. 2999-3003.
75. van Heijenoort, J., *Peptidoglycan hydrolases of Escherichia coli*. Microbiology and Molecular Biology Reviews, 2011. **75**(4): p. 636-663.
76. Banzhaf, M., et al., *Cooperativity of peptidoglycan synthases active in bacterial cell elongation*. Molecular microbiology, 2012. **85**(1): p. 179-194.
77. Bertsche, U., et al., *Interaction between two murein (peptidoglycan) synthases, PBP3 and PBP1B, in Escherichia coli*. Molecular microbiology, 2006. **61**(3): p. 675-690.
78. Goffin, C. and J.-M. Ghuysen, *Multimodular penicillin-binding proteins: an enigmatic family of orthologs and paralogs*. Microbiology and Molecular Biology Reviews, 1998. **62**(4): p. 1079-1093.
79. Zhu, Y., et al., *Structure, function, and fate of the BlaR signal transducer involved in induction of beta-lactamase in Bacillus licheniformis*. Journal of bacteriology, 1992. **174**(19): p. 6171-6178.
80. Van Den Ent, F., et al., *Dimeric structure of the cell shape protein MreC and its functional implications*. Molecular microbiology, 2006. **62**(6): p. 1631-1642.
81. Slovak, P.M., S.L. Porter, and J.P. Armitage, *Differential localization of Mre proteins with PBP2 in Rhodobacter sphaeroides*. Journal of bacteriology, 2006. **188**(5): p. 1691-1700.
82. van den Ent, F., et al., *Bacterial actin MreB assembles in complex with cell shape protein RodZ*. The EMBO journal, 2010. **29**(6): p. 1081-1090.
83. Scheffers, D.-J. and J. Errington, *PBP1 is a component of the Bacillus subtilis cell division machinery*. Journal of bacteriology, 2004. **186**(15): p. 5153-5156.
84. Guder, A., I. Wiedemann, and H.G. Sahl, *Posttranslationally modified bacteriocins—the lantibiotics*. Peptide Science, 2000. **55**(1): p. 62-73.
85. Brötz, H. and H.-G. Sahl, *New insights into the mechanism of action of lantibiotics—diverse biological effects by binding to the same molecular target*. Journal of Antimicrobial Chemotherapy, 2000. **46**(1): p. 1-6.
86. Domínguez-Escobar, J., et al., *Processive movement of MreB-associated cell wall biosynthetic complexes in bacteria*. Science, 2011. **333**(6039): p. 225-228.
87. Garner, E.C., et al., *Coupled, circumferential motions of the cell wall synthesis machinery and MreB filaments in B. subtilis*. Science, 2011. **333**(6039): p. 222-225.
88. Van Teeffelen, S., et al., *The bacterial actin MreB rotates, and rotation depends on cell-wall assembly*. Proceedings of the National Academy of Sciences, 2011. **108**(38): p. 15822-15827.

89. Soufo, H.J.D. and P.L. Graumann, *Dynamic movement of actin-like proteins within bacterial cells*. EMBO reports, 2004. **5**(8): p. 789-794.
90. Shih, Y.-L., T. Le, and L. Rothfield, *Division site selection in Escherichia coli involves dynamic redistribution of Min proteins within coiled structures that extend between the two cell poles*. Proceedings of the National Academy of Sciences, 2003. **100**(13): p. 7865-7870.
91. Gitai, Z., N. Dye, and L. Shapiro, *An actin-like gene can determine cell polarity in bacteria*. Proceedings of the National Academy of Sciences of the United States of America, 2004. **101**(23): p. 8643-8648.
92. Defeu Soufo, H.J. and P.L. Graumann, *Dynamic localization and interaction with other Bacillus subtilis actin-like proteins are important for the function of MreB*. Molecular microbiology, 2006. **62**(5): p. 1340-1356.
93. Jones, L.J., R. Carballido-López, and J. Errington, *Control of cell shape in bacteria: helical, actin-like filaments in Bacillus subtilis*. Cell, 2001. **104**(6): p. 913-922.
94. Daniel, R.A. and J. Errington, *Control of cell morphogenesis in bacteria: two distinct ways to make a rod-shaped cell*. Cell, 2003. **113**(6): p. 767-776.
95. Dempwolff, F., et al., *Bacillus subtilis MreB orthologs self-organize into filamentous structures underneath the cell membrane in a heterologous cell system*. PloS one, 2011. **6**(11): p. e27035.
96. Kawai, Y., R.A. Daniel, and J. Errington, *Regulation of cell wall morphogenesis in Bacillus subtilis by recruitment of PBPI to the MreB helix*. Molecular microbiology, 2009. **71**(5): p. 1131-1144.
97. Leaver, M. and J. Errington, *Roles for MreC and MreD proteins in helical growth of the cylindrical cell wall in Bacillus subtilis*. Molecular microbiology, 2005. **57**(5): p. 1196-1209.
98. Foulquier, E., et al., *The YvcK protein is required for morphogenesis via localization of PBPI under gluconeogenic growth conditions in Bacillus subtilis*. Molecular microbiology, 2011. **80**(2): p. 309-318.
99. Salje, J., et al., *Direct membrane binding by bacterial actin MreB*. Molecular cell, 2011. **43**(3): p. 478-487.
100. Soufo, H.J.D., et al., *Bacterial translation elongation factor EF-Tu interacts and colocalizes with actin-like MreB protein*. Proceedings of the National Academy of Sciences, 2010. **107**(7): p. 3163-3168.
101. Divakaruni, A.V., et al., *The cell-shape protein MreC interacts with extracytoplasmic proteins including cell wall assembly complexes in Caulobacter crescentus*. Proceedings of the National Academy of Sciences of the United States of America, 2005. **102**(51): p. 18602-18607.
102. Divakaruni, A.V., et al., *The cell shape proteins MreB and MreC control cell morphogenesis by positioning cell wall synthetic complexes*. Molecular microbiology, 2007. **66**(1): p. 174-188.
103. Kruse, T., J. Bork-Jensen, and K. Gerdes, *The morphogenetic MreBCD proteins of Escherichia coli form an essential membrane-bound complex*. Molecular microbiology, 2005. **55**(1): p. 78-89.
104. Soufo, H.J.D. and P.L. Graumann, *Bacillus subtilis actin-like protein MreB influences the positioning of the replication machinery and requires membrane proteins MreC/D and other actin-like proteins for proper localization*. BMC cell biology, 2005. **6**(1): p. 10.
105. Muchová, K., Z. Chromiková, and I. Barák, *Control of Bacillus subtilis cell shape by RodZ*. Environmental microbiology, 2013. **15**(12): p. 3259-3271.



106. Strahl, H., F. Bürmann, and L.W. Hamoen, *The actin homologue MreB organizes the bacterial cell membrane*. Nature communications, 2014. **5**.
107. Fenton, A.K. and K. Gerdes, *Direct interaction of FtsZ and MreB is required for septum synthesis and cell division in Escherichia coli*. The EMBO journal, 2013. **32**(13): p. 1953-1965.
108. Abhayawardhane, Y. and G.C. Stewart, *Bacillus subtilis possesses a second determinant with extensive sequence similarity to the Escherichia coli mreB morphogene*. Journal of bacteriology, 1995. **177**(3): p. 765-773.
109. Levin, P.A., et al., *Identification of Bacillus subtilis genes for septum placement and shape determination*. Journal of bacteriology, 1992. **174**(21): p. 6717-6728.
110. Carballido-López, R., et al., *Actin homolog MreBH governs cell morphogenesis by localization of the cell wall hydrolase LytE*. Developmental cell, 2006. **11**(3): p. 399-409.
111. Domínguez-Cuevas, P., et al., *Differentiated roles for MreB-actin isoforms and autolytic enzymes in Bacillus subtilis morphogenesis*. Molecular microbiology, 2013. **89**(6): p. 1084-1098.
112. Kawai, Y., K. Asai, and J. Errington, *Partial functional redundancy of MreB isoforms, MreB, Mbl and MreBH, in cell morphogenesis of Bacillus subtilis*. Molecular microbiology, 2009. **73**(4): p. 719-731.
113. Bork, P., C. Sander, and A. Valencia, *An ATPase domain common to prokaryotic cell cycle proteins, sugar kinases, actin, and hsp70 heat shock proteins*. Proceedings of the National Academy of Sciences, 1992. **89**(16): p. 7290-7294.
114. van den Ent, F., L.A. Amos, and J. Löwe, *Prokaryotic origin of the actin cytoskeleton*. Nature, 2001. **413**(6851): p. 39-44.
115. Esue, O., et al., *The assembly of MreB, a prokaryotic homolog of actin*. Journal of Biological Chemistry, 2005. **280**(4): p. 2628-2635.
116. Ursell, T.S., et al., *Rod-like bacterial shape is maintained by feedback between cell curvature and cytoskeletal localization*. Proceedings of the National Academy of Sciences, 2014. **111**(11): p. E1025-E1034.
117. Wang, S. and N.S. Wingreen, *Cell shape can mediate the spatial organization of the bacterial cytoskeleton*. Biophysical journal, 2013. **104**(3): p. 541-552.
118. Olshausen, P.v., et al., *Superresolution Imaging of Dynamic MreB Filaments in B. subtilis—A Multiple-Motor-Driven Transport?* Biophysical journal, 2013. **105**(5): p. 1171-1181.
119. Dye, N.A., et al., *Mutations in the nucleotide binding pocket of MreB can alter cell curvature and polar morphology in Caulobacter*. Molecular microbiology, 2011. **81**(2): p. 368-394.
120. Dye, N.A., et al., *Two independent spiral structures control cell shape in Caulobacter*. Proceedings of the National Academy of Sciences of the United States of America, 2005. **102**(51): p. 18608-18613.
121. Figge, R.M., A.V. Divakaruni, and J.W. Gober, *MreB, the cell shape-determining bacterial actin homologue, co-ordinates cell wall morphogenesis in Caulobacter crescentus*. Molecular microbiology, 2004. **51**(5): p. 1321-1332.
122. Carballido-López, R., *The bacterial actin-like cytoskeleton*. Microbiology and Molecular Biology Reviews, 2006. **70**(4): p. 888-909.

123. Tiyanont, K., et al., *Imaging peptidoglycan biosynthesis in Bacillus subtilis with fluorescent antibiotics*. Proceedings of the National Academy of Sciences, 2006. **103**(29): p. 11033-11038.
124. White, C.L., A. Kitich, and J.W. Gober, *Positioning cell wall synthetic complexes by the bacterial morphogenetic proteins MreB and MreD*. Molecular microbiology, 2010. **76**(3): p. 616-633.
125. Varma, A. and K.D. Young, *In Escherichia coli, MreB and FtsZ direct the synthesis of lateral cell wall via independent pathways that require PBP 2*. Journal of bacteriology, 2009. **191**(11): p. 3526-3533.
126. Mohammadi, T., et al., *The essential peptidoglycan glycosyltransferase MurG forms a complex with proteins involved in lateral envelope growth as well as with proteins involved in cell division in Escherichia coli*. Molecular microbiology, 2007. **65**(4): p. 1106-1121.
127. Vollmer, W., M. von Rechenberg, and J.-V. Hölte, *Demonstration of molecular interactions between the murein polymerase PBP1B, the lytic transglycosylase MltA, and the scaffolding protein MipA of Escherichia coli*. Journal of Biological Chemistry, 1999. **274**(10): p. 6726-6734.
128. Lovering, A.L. and N.C. Strynadka, *High-resolution structure of the major periplasmic domain from the cell shape-determining filament MreC*. Journal of molecular biology, 2007. **372**(4): p. 1034-1044.
129. Takacs, C.N., et al., *MreB drives de novo rod morphogenesis in Caulobacter crescentus via remodeling of the cell wall*. Journal of bacteriology, 2010. **192**(6): p. 1671-1684.
130. Alyahya, S.A., et al., *RodZ, a component of the bacterial core morphogenic apparatus*. Proceedings of the National Academy of Sciences, 2009. **106**(4): p. 1239-1244.
131. Bendezu, F.O., et al., *RodZ (YfgA) is required for proper assembly of the MreB actin cytoskeleton and cell shape in E. coli*. The EMBO journal, 2009. **28**(3): p. 193-204.
132. Shiomi, D., M. Sakai, and H. Niki, *Determination of bacterial rod shape by a novel cytoskeletal membrane protein*. The EMBO journal, 2008. **27**(23): p. 3081-3091.
133. Hellenga, H.W. and P.R. Evans, *Mutations in the active site of Escherichia coli phosphofructokinase*. Nature, 1987. **327**(6121): p. 437-439.
134. Wegener, G. and U. Krause, *Different modes of activating phosphofructokinase, a key regulatory enzyme of glycolysis, in working vertebrate muscle*. Biochemical Society Transactions, 2002. **30**(2): p. 264-269.
135. Raben, N., et al., *Functional expression of human mutant phosphofructokinase in yeast: genetic defects in French Canadian and Swiss patients with phosphofructokinase deficiency*. American journal of human genetics, 1995. **56**(1): p. 131.
136. Selwood, T. and E.K. Jaffe, *Dynamic dissociating homo-oligomers and the control of protein function*. Archives of biochemistry and biophysics, 2012. **519**(2): p. 131-143.
137. Shirakihara, Y. and P.R. Evans, *Crystal structure of the complex of phosphofructokinase from Escherichia coli with its reaction products*. Journal of molecular biology, 1988. **204**(4): p. 973-994.
138. Sonenshein, A.L., J.A. Hoch, and R. Losick, *Bacillus subtilis and its closest relatives: from genes to cells*. 2002: Asm Press.

139. Blencke, H.-M., et al., *Transcriptional profiling of gene expression in response to glucose in Bacillus subtilis: regulation of the central metabolic pathways*. Metabolic engineering, 2003. **5**(2): p. 133-149.
140. Schilling, O., et al., *Transcriptional and metabolic responses of Bacillus subtilis to the availability of organic acids: transcription regulation is important but not sufficient to account for metabolic adaptation*. Applied and environmental microbiology, 2007. **73**(2): p. 499-507.
141. Tojo, S., et al., *Heavy involvement of stringent transcription control depending on the adenine or guanine species of the transcription initiation site in glucose and pyruvate metabolism in Bacillus subtilis*. Journal of bacteriology, 2010. **192**(6): p. 1573-1585.
142. Gao, H., et al., *The E1 and E2 Subunits of the Bacillus subtilis Pyruvate Dehydrogenase Complex Are Involved in Regulation of Sporulation*. Journal of Bacteriology, 2002. **184**(10): p. 2780-2788.
143. Guest, J. and I. Creaghan, *Gene-protein relationships of the  $\alpha$ -keto acid dehydrogenase complexes of Escherichia coli K12: isolation and characterization of lipoamide dehydrogenase mutants*. Journal of general microbiology, 1973. **75**(1): p. 197-210.
144. Partridge, S. and J. Errington, *The importance of morphological events and intercellular interactions in the regulation of prespore-specific gene expression during sporulation in Bacillus subtilis*. Molecular microbiology, 1993. **8**(5): p. 945-955.
145. Youngman, P.J., J.B. Perkins, and R. Losick, *Genetic transposition and insertional mutagenesis in Bacillus subtilis with Streptococcus faecalis transposon Tn917*. Proceedings of the National Academy of Sciences, 1983. **80**(8): p. 2305-2309.
146. Dubnau, D. and R. Davidoff-Abelson, *Fate of transforming DNA following uptake by competent Bacillus subtilis: I. Formation and properties of the donor-recipient complex*. Journal of molecular biology, 1971. **56**(2): p. 209-221.
147. Dubnau, D., *Genetic competence in Bacillus subtilis*. Microbiological reviews, 1991. **55**(3): p. 395.
148. Laemmli, U.K., *Cleavage of structural proteins during the assembly of the head of bacteriophage T4*. nature, 1970. **227**(5259): p. 680-685.
149. Plank, M., G.H. Wadhams, and M.C. Leake, *Millisecond timescale slimfield imaging and automated quantification of single fluorescent protein molecules for use in probing complex biological processes*. Integrative Biology, 2009. **1**(10): p. 602-612.
150. Shimomura, O., F.H. Johnson, and Y. Saiga, *Extraction, purification and properties of aequorin, a bioluminescent protein from the luminous hydromedusan, Aequorea*. Journal of cellular and comparative physiology, 1962. **59**(3): p. 223-239.
151. Hale, G.M. and M.R. Querry, *Optical constants of water in the 200-nm to 200- $\mu$ m wavelength region*. Applied optics, 1973. **12**(3): p. 555-563.
152. Prasher, D.C., et al., *Primary structure of the Aequorea victoria green-fluorescent protein*. Gene, 1992. **111**(2): p. 229-233.
153. Chalfie, M., et al., *Green fluorescent protein as a marker for gene expression*. Science, 1994. **263**(5148): p. 802-805.

154. Inouye, S. and F.I. Tsuji, *Aequorea green fluorescent protein: Expression of the gene and fluorescence characteristics of the recombinant protein*. FEBS letters, 1994. **341**(2): p. 277-280.
155. Tsien, R.Y., *The green fluorescent protein*. Annual review of biochemistry, 1998. **67**(1): p. 509-544.
156. Chudakov, D.M., S. Lukyanov, and K.A. Lukyanov, *Fluorescent proteins as a toolkit for in vivo imaging*. Trends in biotechnology, 2005. **23**(12): p. 605-613.
157. Ghosh, I., A.D. Hamilton, and L. Regan, *Antiparallel leucine zipper-directed protein reassembly: application to the green fluorescent protein*. Journal of the American Chemical Society, 2000. **122**(23): p. 5658-5659.
158. Miyawaki, A., et al., *Fluorescent indicators for  $Ca^{2+}$ ; based on green fluorescent proteins and calmodulin*. Nature, 1997. **388**(6645): p. 882-887.
159. Leake, M.C., et al., *Stoichiometry and turnover in single, functioning membrane protein complexes*. Nature, 2006. **443**(7109): p. 355-358.
160. Leake, M.C., et al., *Variable stoichiometry of the TatA component of the twin-arginine protein transport system observed by in vivo single-molecule imaging*. Proceedings of the National Academy of Sciences, 2008. **105**(40): p. 15376-15381.
161. Lenn, T., M.C. Leake, and C.W. Mullineaux, *Clustering and dynamics of cytochrome *bd-I* complexes in the Escherichia coli plasma membrane in vivo*. Molecular microbiology, 2008. **70**(6): p. 1397-1407.
162. Wollman, A.J., et al., *Probing DNA interactions with proteins using a single-molecule toolbox: inside the cell, in a test tube, and in a computer*. arXiv preprint arXiv:1504.03488, 2015.
163. Yanagida, T., Y. Harada, and A. Ishijima, *Nano-manipulation of actomyosin molecular motors in vitro: a new working principle*. Trends in biochemical sciences, 1993. **18**(9): p. 319-324.
164. Sase, I., et al., *Real time imaging of single fluorophores on moving actin with an epifluorescence microscope*. Biophysical journal, 1995. **69**(2): p. 323.
165. Funatsu, T., et al., *Imaging of single fluorescent molecules and individual ATP turnovers by single myosin molecules in aqueous solution*. Nature, 1995. **374**(6522): p. 555-559.
166. Dickson, R.M., et al., *Three-dimensional imaging of single molecules solvated in pores of poly (acrylamide) gels*. Science, 1996. **274**(5289): p. 966.
167. Keller, H.E. and J. Pawley, *Handbook of biological confocal microscopy*. Plenum Press, New York, 1995: p. 77.
168. Minsky, M., *Memoir on inventing the confocal scanning microscope*. Scanning, 1988. **10**(4): p. 128-138.
169. Plakhotnik, T., et al., *Nonlinear spectroscopy on a single quantum system: two-photon absorption of a single molecule*. Science, 1996. **271**(5256): p. 1703.
170. Reyes-Lamothe, R., D.J. Sherratt, and M.C. Leake, *Stoichiometry and architecture of active DNA replication machinery in Escherichia coli*. Science, 2010. **328**(5977): p. 498-501.
171. Shida, T., et al., *Mutational analysis of catalytic sites of the cell wall lytic N-acetylmuramoyl-L-alanine amidases CwlC and CwlV*. Journal of Biological Chemistry, 2001. **276**(30): p. 28140-28146.
172. Reimold, C., et al., *Motion of variable-length MreB filaments at the bacterial cell membrane influences cell morphology*. Molecular biology of the cell, 2013. **24**(15): p. 2340-2349.

173. Dickson, R.M., et al., *On/off blinking and switching behaviour of single molecules of green fluorescent protein*. Nature, 1997. **388**(6640): p. 355-358.
174. Mayer, J.A., *Assembly Properties of the Bacillus Subtilis Actin Orthologues MreB, MreBH, and Mbl*. 2008: ProQuest.
175. Popp, D., et al., *Filament structure, organization, and dynamics in MreB sheets*. Journal of Biological Chemistry, 2010. **285**(21): p. 15858-15865.
176. Oda, T., et al., *The nature of the globular-to fibrous-actin transition*. Nature, 2009. **457**(7228): p. 441-445.
177. Tilney, L.G., et al., *The polymerization of actin: its role in the generation of the acrosomal process of certain echinoderm sperm*. The Journal of cell biology, 1973. **59**(1): p. 109-126.
178. Jongstra-Bilen, J., et al., *The lymphocyte-specific protein LSP1 binds to F-actin and to the cytoskeleton through its COOH-terminal basic domain*. The Journal of cell biology, 1992. **118**(6): p. 1443-1453.
179. Yassin, R., et al., *Effects of chemotactic factors and other agents on the amounts of actin and a 65,000-mol-wt protein associated with the cytoskeleton of rabbit and human neutrophils*. The Journal of cell biology, 1985. **101**(1): p. 182-188.
180. Peng, H., et al., *Molecular docking and three-dimensional quantitative structure-activity relationship studies on the binding modes of herbicidal 1-(substituted phenoxyacetoxy) alkylphosphonates to the E1 component of pyruvate dehydrogenase*. Journal of agricultural and food chemistry, 2007. **55**(5): p. 1871-1880.
181. Izard, T., et al., *Principles of quasi-equivalence and Euclidean geometry govern the assembly of cubic and dodecahedral cores of pyruvate dehydrogenase complexes*. Proceedings of the National Academy of Sciences, 1999. **96**(4): p. 1240-1245.
182. Stoops, J.K., et al., *On the unique structural organization of the Saccharomyces cerevisiae pyruvate dehydrogenase complex*. Journal of Biological Chemistry, 1997. **272**(9): p. 5757-5764.

## Acknowledgements

I would like to give my sincere gratitude to my supervisor Prof. Dr. Peter Graumann for providing me such a great opportunity to join his lab and work with his great team. I appreciate his supervision and I am grateful for the discussions about my projects and his encouragement. With the help of him and his team, I learned many useful and interesting techniques and skills. I also want to thank Prof. Dr. Peter Graumann for giving me the chance to attend an international conference in London, sponsor me after my scholarship ended and translate my abstract into German. I also want to thank the Chinese Scholarship Council (CSC) for sponsoring me 3 years, without the grant I cannot support to study and live in Germany.

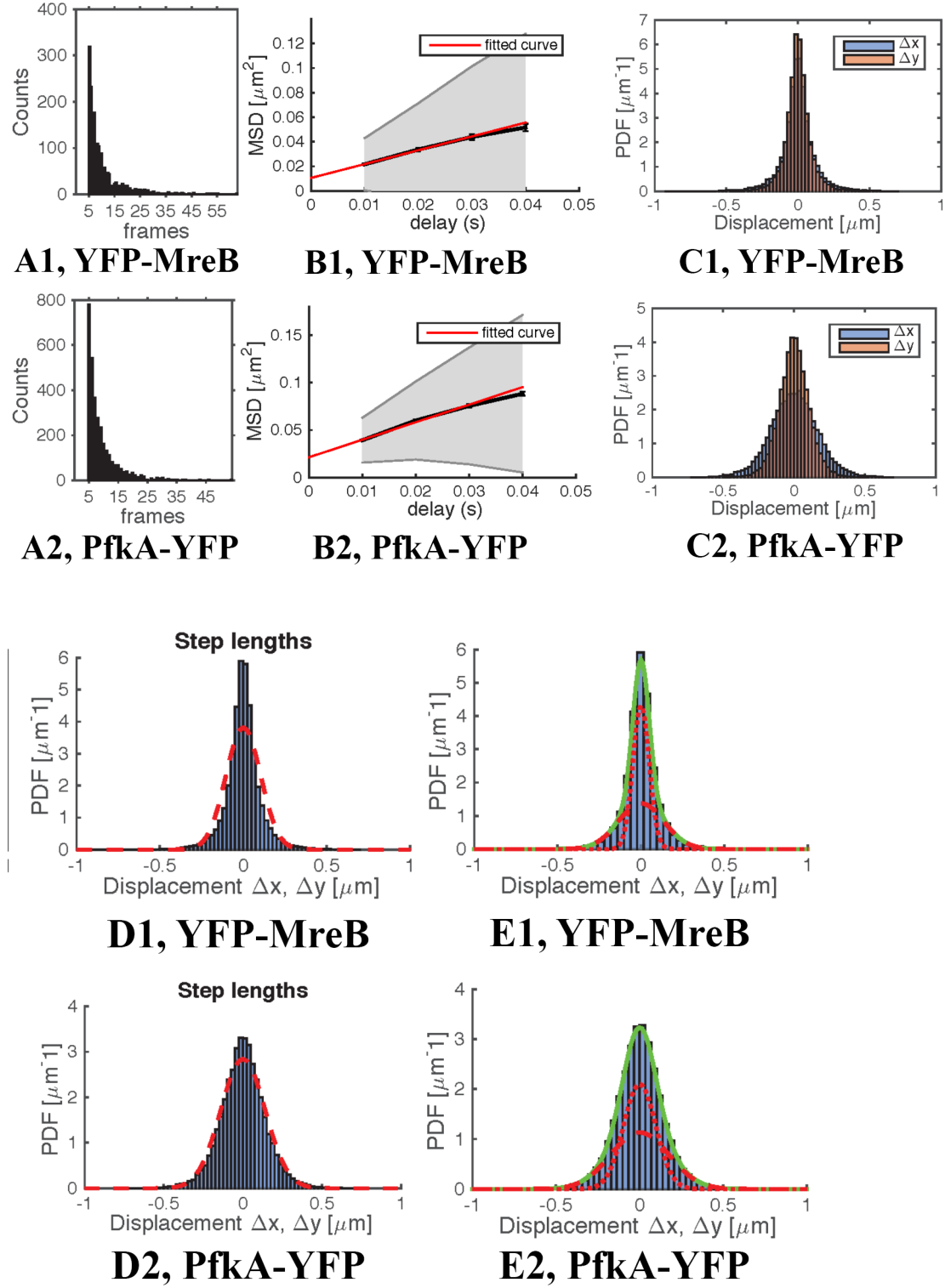
Thanks to Stephan Altenburger for introducing me the single molecule microscopy techniques and how to analyze my data with U-track, msd-analyzer and so on. Thanks to my colleague Nina Najjar for supervising me with the Riboflavin project and other helps. Nina introduced me from the beginning with cloning, Immunoblot and microscopy.

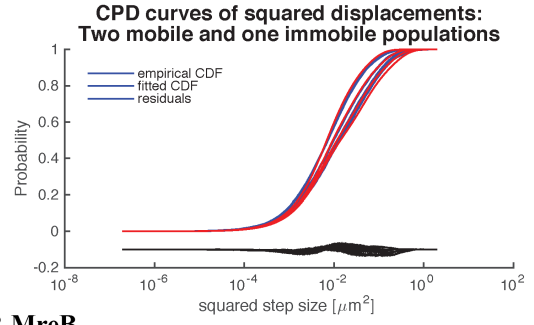
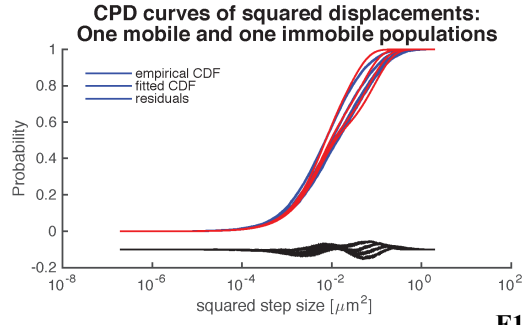
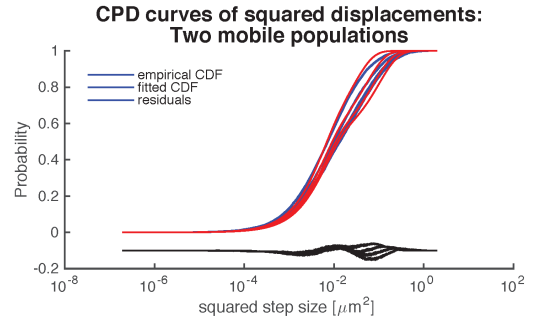
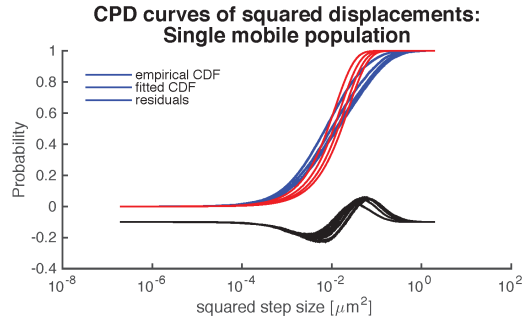
Many thanks to the back lab members, Dr. Ana Herva's Veguillas, Dr. Daniella Lucena, Dr. Jihad Andari, Dr. Christian Reimold, for supporting me get over with the obstacles in my experiments and correcting my thesis. Ana helped me with troubleshooting, Daniella helped me with my data analysis and Gibson Assembly. Christian showed me how to purify proteins. Jihad gave me with many useful advices and also many supports in my life in Marburg. Special thanks to Thomas Rösch for analyzing my U-track data of proteins single molecules.

Many thanks to the front lab members, Dr. Felix Dempwolff, Stephan Altenburger, Dr. Katrin Schenk, Patricia Bedrunka, Dr. Mara Specht, Sonja Schibany. And many thanks to our technicians, Dr. Barbara Waidner and secretary Julia Witsch. Special thanks to all the former and current Graumann lab members. I also want to express my appreciation to my parents and my friends for all the supporting.

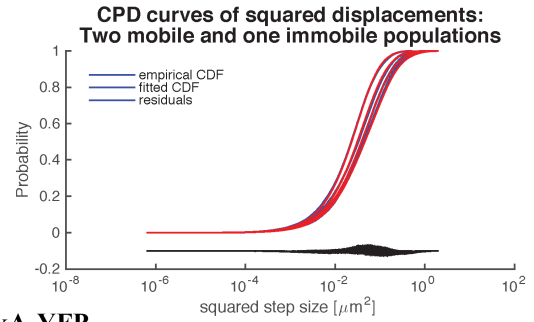
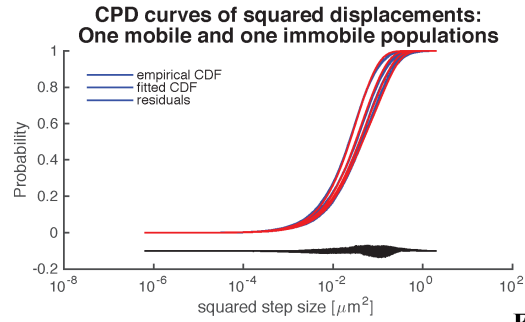
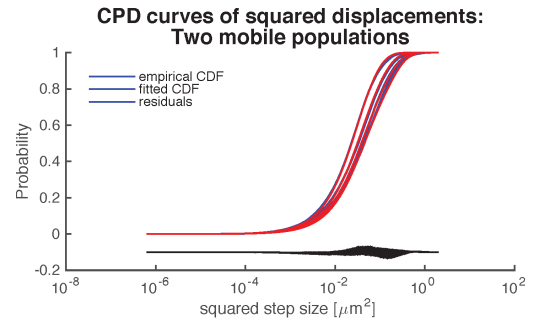
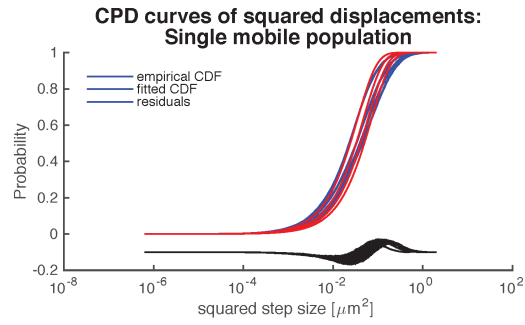
## Appendix

The single molecule tracking analysis of MreB and PfkA is shown in Figure 36.





**F1, YFP-MreB**



**F2, PfkA-YFP**



Figure 36. Single molecule tracking analysis. (A) Track lengths in frames. The X axis stands for the frame interval of each spot, the Y axis stands for the number of frame intervals (the shortest time interval is 5 frames). (B) Weighted average of all MSD curves. The red fitted curve is the superposition MSD curve of two Gaussian distributions. The slope of the red curve is the mean diffusion coefficients of two Gaussian distributions. (C) Probability density function (PDF) of all tracking displacement in X and Y directions. (D) One population fits of Gaussian distribution. (E) Two Gaussian distributions fits of single molecule moving behavior. The Y axis represents the density of each kind of moving behavior. The green curve stands for the superposition plot of two Gaussian distribution fits (dotted red curve and the dashed red curve). Two red curves represent the plot of two populations fit. In E1, the dotted red curve represents the immobile population of YFP-MreB, the dashed red curve represents the mobile population of YFP-MreB. In E2, two red curves represent two populations of mobile PfkA-YFP. (F) CPD (cumulative probability density function) curves of squared displacement. The blue curves represent experimental data, the red curve indicates the CPD fits data from blue curves, and the black curves represent the residuals between experimental data and the fits data. The X axis represents the displacement of spots movement in both X and Y direction. The Y axis represents the cumulative density of all displacements. In F1, one mobile and one immobile population fitted very well with the YFP-MreB results. In F2, two mobile populations fitted very well with the PfkA-YFP results. Images were created by Dr. Thomas Rösch.

## **Verzeichnis der akademischen Lehrer**

Meine akademischen Lehrer waren

in Marburg:

Prof. Dr. Peter Graumann

in Jinan:

Prof. Dr. Feng Huang

In Qingdao

Prof. Dr. Mo Xian